CD4$^+$ T cells are homeostatic regulators during *Mtb* reinfection

Joshua D. Bromley[1,2,3,4*], Sharie Keanne C. Ganchua[5,6*], Sarah K. Nyquist[1,2,3,8], Pauline Maiello[5], Michael Chao[1,9], H. Jacob Borish[5,6], Mark Rodgers[5,6], Jaime Tomko[5,6], Kara Kracinovsky[5,6], Douaa Mugahid[1,9], Son Nguyen[1,2,3], Dennis Wang[2], Jacob M. Rosenberg[1,9], Edwin C. Klein[7], Hannah P. Gideon[5,6], Roisin Floyd-O'Sullivan[1,2,3], Bonnie Berger[8], Charles A Scanga[5,6], Philana Ling Lin[6,10], Sarah M. Fortune[1,9,†,‡], Alex K. Shalek[1,2,3,11,12,†,‡], JoAnne L. Flynn[5,6,13,†,‡]

Affiliations

[1]Ragon Institute of MGH, MIT, and Harvard, Cambridge, MA, USA

[2]Institute for Medical Engineering and Science (IMES), Massachusetts Institute of Technology, Cambridge, MA, USA

[3]Broad Institute of MIT and Harvard, Cambridge, MA, USA

[4]Graduate Program in Microbiology, Massachusetts Institute of Technology, Cambridge, MA, USA

[5]Department of Microbiology and Molecular Genetics, University of Pittsburgh School of Medicine, Pittsburgh PA USA

[6]Center for Vaccine Research, University of Pittsburgh, Pittsburgh PA USA

[7]Division of Laboratory Animal Research, University of Pittsburgh, Pittsburgh, PA, USA

[8]Computer Science and Artificial Intelligence Laboratory, Massachusetts Institute of Technology, Cambridge, MA, USA

[9]Department of Immunology and Infectious Diseases, Harvard T.H. Chan School of Public Health, Boston, MA, USA

[10]Department of Pediatrics, UPMC Children's Hospital of Pittsburgh, University of Pittsburgh School of Medicine

[11]Department of Chemistry, Massachusetts Institute of Technology, Cambridge, MA, USA

[12]Koch Institute for Integrative Cancer Research, Massachusetts Institute of Technology, Cambridge, MA, USA

[13]Lead contact

*These authors contributed equally to this work

[†]These senior authors contributed equally to this work.

‡Correspondence: joanne@pitt.edu (J.L.F), shalek@mit.edu (A.K.S),
sfortune@hsph.harvard.edu (S.M.F)

ABSTRACT

Immunological priming – either in the context of prior infection or vaccination – elicits protective responses against subsequent *Mycobacterium tuberculosis* (*Mtb*) infection. However, the changes that occur in the lung cellular milieu post-primary *Mtb* infection and their contributions to protection upon reinfection remain poorly understood. Here, using clinical and microbiological endpoints in a non-human primate reinfection model, we demonstrate that prior *Mtb* infection elicits a long-lasting protective response against subsequent *Mtb* exposure and that the depletion of $CD4^+$ T cells prior to *Mtb* rechallenge significantly abrogates this protection. Leveraging microbiologic, PET-CT, flow cytometric, and single-cell RNA-seq data from primary infection, reinfection, and reinfection-$CD4^+$ T cell depleted granulomas, we identify differential cellular and microbial features of control. The data collectively demonstrate that the presence of $CD4^+$ T cells in the setting of reinfection results in a reduced inflammatory lung milieu characterized by reprogrammed $CD8^+$ T cell activity, reduced neutrophilia, and blunted type-1 immune signaling among myeloid cells, mitigating *Mtb* disease severity. These results open avenues for developing vaccines and therapeutics that not only target $CD4^+$ and $CD8^+$ T cells, but also modulate innate immune cells to limit *Mtb* disease.

INTRODUCTION

Management of the tuberculosis (TB) pandemic is limited by the lack of a robust vaccine that protects against *Mycobacterium tuberculosis (Mtb*) infection and disease progression. Bacillus Calmette–Guérin (BCG) remains the only licensed TB vaccine. BCG offers protection against ~70% of severe miliary and meningeal infections in pediatric TB; however, it fails to confer robust protection against infection or TB disease in adults (Lange et al., 2022). Regardless of BCG vaccination status, the majority (~90%) of infected individuals can control *Mtb* bacilli

naturally and experience asymptomatic infection (clinically classified as latent TB infection; LTBI). Only the minority (~5-10%) experience overt clinical manifestations of disease (Lawn and Zumla, 2011). In TB endemic regions – where people are likely repeatedly exposed – the incidence rate of recurrent TB disease, either by relapse or reinfection, after successful treatment with antibiotics was 18 (China) and 14.6 (Spain) times higher than the incidence rate of initial TB disease in the general population (J-P Millet et al., 2009; Shen et al., 2017; Verver et al., 2005). However, the effects of prior *Mtb* infection appear to be contextual: a retrospective epidemiological meta-analyses of healthcare professionals reported a 79% lower risk of developing active TB in LTBI individuals after re-exposure to *Mtb* compared to uninfected individuals (Andrews et al., 2012). This observation is further bolstered by findings from non-human primate (NHP) and murine models, which demonstrate that concomitant immunity (immunological memory conferred by concurrent *Mtb* infection) provides robust protection against *Mtb* reinfection, and that this protection persists to some extent after drug treatment (Cadena et al., 2018; Ganchua et al., 2023; Nemeth et al., 2020).

Several factors could explain variation in a host's ability to control TB following *Mtb* reinfection. Examples include intrinsic differences in host susceptibility, differences in the quality of the memory immune response, emergence of TB related structural lung disease, and pathogen characteristics (Abel et al., 2018; Cohen et al., 2022; Coscolla and Gagneux, 2014; Galagan, 2014). Since prior *Mtb* infection provides protection against reinfection in NHPs, we can use this model to dissect the roles that key immune cell subsets play in protection (Cadena et al., 2018). Here, we sought to define the roles and functions of $CD4^+$ T cells in the setting of reinfection.

The importance of $CD4^+$ T cells for protection from *Mtb* infection and TB disease has been established in humans by observing the devastating effects of HIV on TB disease burden worldwide. It is further supported by numerous studies in mice and NHPs, where loss of $CD4^+$ T cells leads to increased pathology, bacterial burden, and reactivation of disease (Kwan and Ernst, 2011; Lin et al., 2012b; Scanga et al., 2000). However, in NHPs as in humans, the outcome of *Mtb* infection varies significantly across sites of infection, such that there can be simultaneous sterilization and progression of disease in different granulomas within the same host (Gideon et al., 2022; Lin et al., 2014). Likewise, while $CD4^+$ T cell depletion in primary infection leads to worsened control on the whole, some lesions are fully sterilized and some animals do well –

observations which the current paradigm of protective immunity to *Mtb* cannot explain (Diedrich et al., 2020; Foreman et al., 2022; Larson et al., 2023; Lin et al., 2012b).

In this study, we sought to evaluate systematically long-lived immunological reprogramming in pulmonary granulomas after primary and secondary infection and to elucidate the role of $CD4^+$ T cells in protection against reinfection. Using *in vivo* perturbations (reinfection and $CD4^+$ T cell depletion) and a combination of clinical, microbiologic, and high-dimensional single-cell transcriptomic analyses, we characterized intra- and inter-cellular changes associated with disease outcomes within pulmonary granuloma in cynomolgus macaques. Our analysis helps to unravel the intricacies of host-pathogen dynamics in TB, providing foundational insights for advancing vaccine research and therapeutic modalities.

RESULTS

Experimental design

This study aimed to determine the role of $CD4^+$ T cells in establishing microbiologic, radiographic, and immunologic outcomes in the setting of *Mtb* reinfection in cynomolgus macaques. We used antibody-based depletion of $CD4^+$ T cells (hereafter, αCD4) immediately prior to reinfection to assess $CD4^+$ T cells effector functions rather than their roles in establishing adaptive responses to *Mtb* during primary infection. We compared the outcomes of *Mtb* reinfection in the setting of αCD4 (reinfection, $CD4^+$ T cell depletion, n=7) with those in animals which received an isotype control (reinfection, IgG antibody infusion, n=6). We also examined primary infection in naïve animals (primary infection only, n=6). Overall, this enabled us to compare the outcome of reinfection to primary infection (IgG vs naïve), and then assess the impact of $CD4^+$ T cell depletion (IgG vs αCD4) (**Figure 1A**).

We used *Mtb* Erdman for primary infection and reinfection. As previously described, these bacteria were differentially barcoded with a library of randomized tags, enabling us to track the infecting libraries (designated primary (P) and secondary (S)) and each unique founding bacterium within a library via deep sequencing (Martin et al., 2017). Specifically, the reinfection group was infected with ~10 CFU of *Mtb* Library P, and infection was allowed to progress for nine weeks before the animals received the standard four-drug TB treatment regimen (isoniazid, rifampin, pyrazinamide, ethambutol; HRZE) for four to five months, with the duration of treatment guided by the resolution of disease as defined by PET-CT imaging. For this study, the

animals were treated with drugs so that subsequent CD4 depletion would not result in overwhelming disease due to the primary infection. Our previous data support that drug treatment of primary infection has a modest effect on protection against reinfection (Ganchua et al., 2023). Subsequently, reinfection animals were randomized into the IgG or αCD4 cohorts. These groups began receiving weekly IgG or αCD4 antibody infusions starting one week before secondary infection with Library S and continuing until necropsy at four weeks post-infection. The naïve group was infected with ~10 CFU of barcoded *Mtb*-Erdman (Library S) at the same time as the reinfection macaques, and infection progressed for four weeks before necropsy. Assessment of total lung FDG activity pre- and post-HRZE indicated that the responses to treatment were similar in each of the two antibody treatment groups (**Figure S1A**). PET-CT was continued over the course of the experiment, enabling the identification of newly formed granulomas following *Mtb* re-challenge and antibody infusions (**Figure 1B**). At necropsy, individual PET-CT scan-matched granulomas and lymph nodes, as well as all lung lobes, were resected and dissociated into single-cell suspensions for flow cytometric, scRNA-seq, and/or microbiologic analyses.

Over the course of *Mtb* reinfection and antibody infusion, peripheral blood was sampled weekly to assess $CD4^+$ T cell depletion efficacy and to quantify cell type frequencies. $CD4^+$ T cells were significantly depleted post-infusion (10- to 1,000-fold compared to pre-infusion levels) in the blood of αCD4 animals up until necropsy, while no changes in $CD4^+$ T cell levels were observed in the naïve and IgG cohorts (**Figure 1C** and **S1B**). $CD4^+$ T cell depletion in macaques also reduced the number of $CD4^+$ T cells, but not $CD8^+$ T cells or B cells in tissues, including granulomas and lymph nodes, as compared to macaques that received IgG Ab infusion (**Figure 1D-G** and **S1C-F**).

Reinfection with *Mtb* reduces granuloma formation, as well as bacterial burden and dissemination in a $CD4^+$ T cell dependent manner

Analysis of PET-CT scans after secondary infection showed that a similar number of granulomas formed in animals receiving IgG as compared to naïve and αCD4 treated animals, although there was a trend ($p=0.0714$) towards lower numbers of new granulomas in IgG treated compared to naïve animals (**Figure 2A**). This was in contrast to our previous study of reinfection in non-drug treated animals, where fewer granulomas were established in animals with a

concurrent primary infection following reinfection (Cadena et al., 2018). Consistent with our prior data, granulomas in animals receiving IgG had significantly fewer viable bacteria than those in naïve animals, with $CD4^+$ T cell depletion partially abrogating protection against reinfection (**Figure 2B, E-G** and **S2A)**. While there was a trend towards lower cumulative bacterial burdens (chromosomal equivalents (CEQ); an estimate of total live and dead bacilli) in granulomas from NHPs receiving IgG infusion, these differences did not reach statistical significance (**Figure 2C** and **S2B**). The same was true for the CFU:CEQ ratio – a proxy for bacterial killing within a granuloma (**Figure 2D** and **S2C,D;** Lin et al., 2014). These data are most consistent with a model in which previous infection leads to an immune environment that restricts bacterial growth in a $CD4^+$ T cell dependent fashion but does not prevent establishment of infection or drive substantively increased bacterial killing.

Mtb barcode analysis of samples retrieved at necropsy revealed that previous infection provided enhanced protection against *Mtb* dissemination to lymph nodes and this protection was partially dependent on $CD4^+$ T cells (**Figure S2E-G**). We enumerated barcode dissemination and found a lower percentage of shared bacterial barcodes between tissues in the IgG animals as compared to both naïve and αCD4-treated animals, further suggesting that reinfection reduces bacterial dissemination in a $CD4^+$ T cell dependent manner (IgG vs naïve, $p<0.0001$; IgG vs αCD4, $p<0.0001$, Kruskal Wallis with Dunn's multiple comparison test; **Figure 2I**).

Cellular remodeling of the TB granuloma microenvironment following *Mtb* reinfection

To define the cellular features associated with protection in the setting of reinfection and the effects of $CD4^+$ T cell depletion, we performed Seq-Well S^3-based massively-parallel scRNA-seq on granulomas isolated from the three experimental groups (**Figures 2H, 3A;** Hughes et al., 2020). We analyzed 33 granulomas that were confirmed to arise from the second infection (Library S) (naïve=10, IgG=8, αCD4=15) from 7 cynomolgus macaques (naïve=2, IgG=3, αCD4=3), yielding a total of 88,360 high-quality transcriptomes. We annotated 16 clusters corresponding to distinct immune and non-immune cell types based on known marker genes and reference signatures (**Figure 3A** and **S3A;** Sikkema et al., 2023). While cellular frequencies varied among individual granulomas and experimental groups, each cluster was represented by multiple samples (**Figure S3B**).

We next sought to identify whether there were significant changes in cell type frequencies across granulomas. We implemented multivariate (scCODA), univariate (Mann-Whitney U test), and nonparametric (Fisher's exact test) tests to account for perturbation, cell type codependences, and low sample size, and considered a cell type differentially abundant if significant by at least two tests (Büttner et al., 2021; Smillie et al., 2019). We first assessed the global T cell composition of lesions from the three groups and observed a trend toward higher overall T, NK cell frequencies among IgG granulomas relative to naïve (**Figure 3B**). Given the trend toward increased T, NK cell frequencies among lesions formed in the setting of reinfection relative to naïve granulomas even in the setting of $CD4^+$ T cell depletion, we sought to identify whether prior infection promotes $CD4^+$ or $CD8^+$ T cell recruitment to the granuloma. Surprisingly, the total fraction of *CD4*+ and *CD8*+ T cells among *CD3D* expressors was significantly lower and higher in IgG granulomas relative to naïve granulomas, respectively ($p=0.0014$ and $p=0.0062$, respectively, Mann-Whitney U test, **Figure 3C,D**). The former is in line with flow cytometric data demonstrating a lower frequency of CD4+ T cells in IgG granulomas, relative to naïve granulomas (**Figure 1D**). There was no difference in the frequency of total T, NK cells between IgG and αCD4 granulomas, but the latter had significantly fewer $CD4^+$ T cells and significantly more $CD8^+$ T cells (**Figure 3C,D**).

IgG granulomas had lower frequencies of neutrophils relative to naïve granulomas, and depletion of $CD4^+$ T cells led to increased frequencies of neutrophils. IgG granulomas also had lower frequencies of cDC2s relative to both naïve and αCD4 granulomas. Finally, there were several differences between naïve and IgG granulomas that were not affected by $CD4^+$ T cell depletion. Mast cells were more frequent in IgG lesions compared to naïve granuloma, but this was not altered by $CD4^+$ T cell depletion. IgG granulomas also had lower frequencies of cDC1s, alveolar type 2 cells, ciliated cells, and pDCs as compared to naïve granulomas.

$CD4^+$ T cells regulate immune tone in granulomas formed after reinfection with *Mtb*

To better understand how reinfection and $CD4^+$ T cell depletion influence the structure of the overall T, NK cell cluster, we next classified all *CD3D,E, CD4, CD8A,B* T, NK cells into 11 major subpopulations based on gene signatures from external single-cell datasets (**Figure 4A** and **S3C** and **Table 1;** Almanzar et al., 2020; Zheng et al., 2021). The proportions of several of these T, NK cell subsets significantly differed among reinfection (IgG) granulomas, particularly the

CD8 enriched (GZMK^{hi} $T_{EM/PEX\text{-}like}$) and *CD8, CD4* co-expressing ($T_{EMRA\text{-}like}$) subsets. We found significant enrichment of immuno-modulatory and -regulatory *CD8* GZMK^{hi} $T_{EM/PEX\text{-}like}$ (*GZMK, EOMES, TOX, TIGIT, IL10*) (Mogilenko et al., 2021) cells in IgG granulomas relative to naïve ones; CD4-depletion significantly impaired either the localization or retention of these cells, suggesting CD4-dependence even after immune priming (**Figure 4B**).

We next investigated how infection status and immune perturbation altered global T, NK cell responses, as well as those of each cell subpopulation, by performing pairwise (IgG vs naïve; IgG vs αCD4) T, NK pseudobulk (i.e., all T, NK subsets aggregated) differential gene expression (DGE), and pairwise DGE analyses within T cell subpopulations. Pairwise analyses among the 11 identified T, NK cell subsets revealed a total of 1,542 DE genes (773 upregulated, 759 downregulated) in IgG vs naïve lesions and 1,263 DE genes (783 upregulated, 480 downregulated) in IgG vs αCD4 granuloma, demonstrating significant shifts in T cell circuitry in immunologically primed animals relative to naïve (IgG vs naïve) or CD4-depletion (IgG vs αCD4) animals (**Figure 4C,D** and **S3F**).

To examine the potential functional significance of these DE genes, we systematically queried cytokines canonically associated with protective anti-*Mtb* responses, including *TNF*, *IFNG*, and the pleiotropic cytokine *IL10*, while excluding *IL17* due to its low expression (**Figure 4C**). There were no significant differences in global (pseudobulk) *TNF* or *IFNG* expression among IgG vs naïve granulomas. We similarly found no significant differences in *IFNG* expression among T, NK subsets. We did observe significant induction of *IL10* expression in IgG compared to naïve granulomas, globally (**Figure 4C**). However, there was no one T, NK subset that was significantly enriched for *IL10* expression among IgG lesions; rather, *IL10* was expressed across several subsets. In addition to higher expression of *IL10*, IgG granulomas were characterized by greater global expression of immunoregulatory (*TIGIT*, *TOX*), costimulatory (*CD2*, *CD28*, *ICOS*), and negative regulators (*CD5*, *CD6*) of T cell activation (**Figure S3D**). Notably, the elevated expression of *TIGIT* and *TOX* was primarily associated with Treg and GZMK^{hi} $T_{EM/PEX\text{-}like}$ subsets. Relative to naïve granulomas, IgG granulomas had lower expression of most cytotoxic effector (*GZMA, GZMB, GZMH, PRF1*), hypoxia-induced factors (*HIF1A*, *BHLHE40*, *ENTPD1*), T1T17 transcription factors (TFs) (*RORA*, *RORC*) and interferon-stimulated genes (*ISG15, ISG20, IFI27*), across several T, NK subsets.

In the setting of $CD4^+$ T cell depletion, there was a global reduction in the abundance of *IL10*, *PDCD1*, *TIGIT,* and *TOX* gene expression (**Figure 4D**). In αCD4 vs IgG granulomas, there was higher expression levels of cytolytic effector molecules (*GZMA, GZMB, GZMH, PRF1*) and T1T17-associated TFs. There was also increased expression of the PD-1-repressor *SATB1* and *BHLHE40*, a putative negative regulator of *IL10* expression and hypoxia-induced factor (**Figure S3E**; Huynh et al., 2018; Stephen et al., 2017). Collectively, these changes suggest $CD8^+$ T cell reprogramming following *Mtb* reinfection and that acquisition of aspects of these terminally differentiated and immunoregulatory *$CD8^+$* T, NK cell gene programs are CD4-dependent.

Attenuated type-1 immunity among monocyte-derived transcriptomes in *Mtb* reinfection granulomas

Considering the established paradigm where $CD4^+$ T cells orchestrate pro-inflammatory myeloid cell responses primarily through IFN-γ and TNF-mediated pathways, we explored whether the observed increase in immunoregulatory T cell phenotypes among IgG granulomas was associated with altered myeloid cellularity and transcriptional programming in reinfection. Monocyte-derived cells partitioned into 6 subpopulations and exhibited varying degrees of expansion or contraction in naïve, IgG, and αCD4 granulomas (**Figure 5A-B, S4A**).

To identify global changes in myeloid gene programming following *Mtb* reinfection, we scored all monocyte-derived cells against Hallmark gene sets (**Figure 5C**). Specifically, all monocyte and macrophage subsets were grouped as "macrophages" and subject to gene set enrichment scoring. Our analyses demonstrated a global reduction in inflammatory responses, specifically IFNα-, IL6/JAK/STAT3, and IFNγ-responses, as well as significant enrichment of adipogenesis, fatty acid metabolism, Myc targets, and DNA repair signatures among monocyte-derived subsets in IgG relative to naïve granulomas. In contrast, in CD4-depletion granulomas the macrophages had increased IFNα-, IL6/JAK/STAT3, and IFNγ- inflammatory responses relative to IgG granulomas (**Figure 5D**).

Pairwise DGE analyses among monocyte-derived subpopulations revealed a total of 2,210 DE genes (1,236 upregulated, 974 downregulated) in IgG vs naïve lesions and 1,234 DE genes (777 upregulated, 457 downregulated) in IgG vs αCD4 granuloma (**Figure S4B**). Myeloid cells from naïve granulomas featured both significant global and subpopulation-specific increases in the expression of interferon-response genes (*ISG15*, *IRF7*), pro-inflammatory

mediators (*IL1A*, *ILB*), chemokines and cytokines including the CXCR3 ligands (*CXCL9, CXLC10, CXCL11*), fibrosis-related genes (*VEGFA*, *TGFB1*), and immunoregulatory molecules (*IDO1, CD274* (PD-L1), *IL10*) relative to macrophages in IgG granulomas (**Figure 5E-F** and **S4C)**. In the absence of $CD4^+$ T cells, a pseudobulk analysis indicated increased type-1 (e.g., *CXCL9-11*) immune signaling. A subpopulation-specific DE analysis of IgG vs αCD4 revealed various monocyte subsets significantly upregulated expression of CXCR3 ligands (*CXCL9, CXLC10, CXCL11*), and to a lesser featured upregulation of *IDO1* and *CD274* but not *IL10* in the αCD4 granulomas (**Figure 5F** and **S4D**).

Overall, naïve lesions showed enhanced type-1 immune signaling, while IgG granulomas displayed a significant reduction in these responses. The reversion of lesions toward a naïve-like state with $CD4^+$ T cell depletion indicates a regulatory role for $CD4^+$ T cells over the myeloid-driven inflammatory response during *Mtb* reinfection.

Neutrophil heterogeneity in the TB granuloma

Neutrophils play a crucial role as frontline defenders against microbial infections and are quickly recruited to sites of inflammation upon *Mtb* infection. However, their role in TB disease remains enigmatic, as they promote both *Mtb* sterilization and pathology (Ravesloot-Chávez et al., 2021). To evaluate how prior infection modulates neutrophil recruitment and phenotype upon reinfection and the role of $CD4^+$ T cells in that modulation, we quantified differences in cellular frequencies and gene expression following sub-clustering. Our analysis identified two neutrophil subpopulations: *ICAM1*^{hi}, *NBN*^{hi} neutrophils (*ICAM1*, *CD274*, *GADD45B, CCL3L1*) and *SORL1*^{hi}, *CFD*^{hi} neutrophils (*SORL1*, *CFD*, *CORO1A*, *PLBD1*) (**Figure 6A** and **S4E**; Montaldo et al., 2022). Both neutrophil subpopulations were significantly underrepresented among IgG lesions compared to naïve and αCD4 granulomas, suggesting that either bacterial burden and/or $CD4^+$ T cells regulate neutrophilic response and infiltration (**Figure 6B**).

To uncover potential differences in neutrophil transcriptional programming, we performed pairwise pseudobulk DGE analysis between these neutrophil subsets (*ICAM1*^{hi}, *NBN*^{hi} vs *SORL1*^{hi}, *CFD*^{hi} neutrophils) and pairwise DGE analyses across conditions (naïve vs IgG, and αCD4 vs IgG) between these neutrophil subsets. Comparisons of *ICAM1*^{hi}, *NBN*^{hi} to *SORL1*^{hi}, *CFD*^{hi} transcriptomes revealed *ICAM1*^{hi}, *NBN*^{hi} neutrophils upregulate type-1 immune chemokines (*CXCL10*, *CXCL11*) and cytokines (*CCL3*, *IL1A*), whereas *SORL1*^{hi}, *CFD*^{hi}

neutrophils upregulated molecules implicated in neutrophil trafficking (*CXCR1*, *CXCR2*) and netosis (*MGAM*, *MMP25*) (**Figure 6C;** Carmona-Rivera et al., 2015; Gasperini et al., 1999; Xie et al., 2020). Pairwise DE analyses (naïve vs IgG, and aCD4 vs IgG) revealed few significant differences in gene programming among *ICAM1*^{hi}, *NBN*^{hi} transcriptomes; however, *SORL1*^{hi}, *CFD*^{hi} neutrophils had significantly altered transcriptomes among IgG lesions relative to naïve, with naïve granulomas expressing significantly higher levels of inflammatory response genes (*STAT1, STAT3, CASP1)*, type-1 immune chemokines (*CXCL10*, *CXCL11*) and cytokines (*CCL3L1*, *TNF*, *IL1A*) (Ichikawa et al., 2013). CD4 depleted lesions, meanwhile, exhibited similar 'naïve-like' neutrophil gene programming compared to IgG lesions (**Figure 6D-E** and **S4F**). We further scored neutrophils against an IFN-inducible neutrophil gene signature previously shown to be upregulated in humans with active TB (**Figure 6F**; Berry et al., 2010). In line with our DE analyses, IgG neutrophils featured significant blunting of IFN-inducible genes.

Collectively, our data delineate the diversity among granuloma-localized neutrophils and demonstrate a significant reduction in neutrophilic responses among IgG lesions compared to naïve or αCD4, implying a potential regulatory role for $CD4^+$ T cells on neutrophil-driven immunity, pathophysiology, and TB disease progression. Furthermore, these data support the model that increased neutrophilic infiltration may contribute to the formation of *Mtb*-permissive niches, thus contributing to elevated bacillary loads among naïve and αCD4 lesions (Lovewell et al., 2021).

Differential cell-cell interactions in immunologically primed granulomas

To assess how the different aforementioned factors act together to modulate host immunity, we investigated differential cell-cell interaction networks among naïve, IgG, and αCD4 granulomas (i.e., IgG vs naïve, and IgG vs αCD4; Browaeys et al., 2023). First, we identified differences among coarse-level cell-cell interactions occurring in primary infection granulomas (naïve) vs those formed in a primed immune environment (IgG). Relative to IgG lesions, naïve cell-cell interaction networks were dominated by signaling from neutrophils, macrophage, and non-immune cells (endothelial cells, fibroblasts), and enriched for type-1 immune (*CXCL9-11, IL6 IL1B, TNF*) and type-1 IFNs (*IFNB1, IFNA1, IFNA2, IFNA16)* signaling – the latter implicated in TB pathogenesis and having been previously demonstrated to

contribute to neutrophil extracellular trap (NET) formation and subsequent *Mtb* proliferation (**Figure 7A,B** and **S5A-E**; Moreira-Teixeira et al., 2020).

To identify subpopulation-specific drivers of granuloma immune tone and cytokine flux, we quantified differential cell-cell interactions among all immune cell subpopulations (**Figure S5F,G**). This analysis identified several monocyte-derived subpopulations (*S100A4*^{hi}, *CFP*^{hi} monocytes, *FABP4*^{hi}, *MCEMP*^{hi} alveolar Mφ, *CXCL9*^{hi} *IDO1*^{hi} Mφ) "sending" the type-1 immune molecules *CXCL9-10*, and neutrophils (*ICAM1*^{hi}, *NBN*^{hi} neutrophils, *SORL1*^{hi}, *CFD*^{hi} neutrophils) "sending" *TNF, CSF1,* and *CXCL10,* which targeted both innate and adaptive (e.g., *CXCR3*$^{+}$ T1T17-like) cellular subpopulations (**Figure S5F**). In addition to the upregulated type-1 immune factors, our subpopulation-specific cell-cell interaction analysis identified prominent monocyte-derived (*THBS1* ^{hi}*, FCN1* ^{hi} Mφ; *LGALS3*^{hi}, *FN1*^{hi} Mφ; *FABP4*^{hi}, *MCEMP*^{hi} alveolar Mφ; *CXCL9*^{hi} *IDO1*^{hi} Mφ) *IL10* "senders" which targeted *ICAM1*^{hi}, *NBN*^{hi} neutrophils, and several monocyte-derived subpopulations as "receivers" (**Figure 7C** and **S5F,G**). Collectively, these data may suggest type-1 immune signaling networks may promote the recruitment of adaptive immune cells and induce a pro-inflammatory immune response to mount an early anti-microbial response, whereas *IL10*$^{+}$ monocyte-derived subpopulations attempt to mitigate this inflammatory response via self-reinforcing innate-innate immune cell circuits.

In contrast to naïve lesions, our analysis of coarse-level cell types in IgG granulomas revealed T, NK cells as the dominant "receiver" cell type, and macrophages as the most prolific "senders," communicating not only with T, NK cells, but also, strikingly, with mast cells (**Figure 7C,D** and **S5B,D,E)**. Outgoing macrophage-derived signaling was dominated by negative regulators of inflammatory response (*CD9, CD52, CDH1*), wound healing (*MMP14, S100A4*), and pro-angiogenic (*PDGFC*) signaling (Ackerman et al., 2019; Atkinson et al., 2007; Rashidi et al., 2018; Suzuki et al., 2009; **Figure S5B,E**). Outgoing mast cell signaling *IL7, TYROBP,*and *NECTIN2* largely targeted T, NK cell receivers expressing *TIGIT, IL7R, PECAM1, KLRD1,* suggesting immunoregulatory (*NECTIN2-TIGIT*) and homeostatic (*IL7-IL7R*) signaling axes among these cells. Our analysis also identified prominent B cell-macrophage communication via *TGFB1-SDC2* and *PTPRC-MRC1*, potentially suggesting that B cells contribute to macrophage polarization in the granuloma (Gong et al., 2012). Our subpopulation-specific cell-cell interaction analyses identified: (i) several monocyte-derived and mast cell subpopulations contributed to these wound-healing and anti-inflammatory signaling pathways and (ii) blunted

type-1 immune network topologies (**Figure S5F,G**). There was also T, NK signaling to T,NK cells; these circuits were characterized by *IL10-IL10RA* and *IL7-IL7R*, suggesting that reinfection granulomas and the associated cytokine milieu and cellular composition promote self-reinforcing immunosuppressive and homeostatic regulatory T cell interactions (**Figure S7D-E;** Sun et al., 2011). A subpopulation-specific query of these cells revealed that GZMK^{hi} $T_{EM/PEX\text{-}like}$ were one of the putative *IL10* "sender" populations and primarily targeted *IL10RA*$^{+}$ *S100A4*^{hi}, *CFP*^{hi} monocytes, Tc17-like, and T1T17-like cells. This analysis further defined a shift away from *IL10*$^{+}$ innate "sender" cellular subsets toward *IL10*$^{+}$ adaptive immune cell subpopulations: GZMK^{hi} $T_{EM/PEX\text{-}like}$ and NK-like cells, relative to naive granulomas, with these two T, NK cell subsets targeting several T, NK cells subsets (Tc17-like, T1T17-like, Tregs) (**Figure 7F**).

In the absence of CD4^{+} T cells, TB granulomas were again dominated by pro-inflammatory neutrophil-derived and type-1 IFN signaling (**Figure 7G,H** and **S5H**, **S5J-L**). Outgoing neutrophil-derived signaling was enriched for type-1 immune signaling (*TNF, IL1B, CXCL10*), targeting macrophages and T, NK cells. There was a relative loss of mast cell signaling, including *IL7* signaling to *IL7R* expressing T, NK cells, suggesting a loss of homeostatic cycling of memory T, NK cell subsets, compared to IgG (**Figure 7I,J** and **S5I**). CD4-depletion lesions were further characterized by a relative loss of T, NK-T, NK signaling circuits involving "sender" ligands (*IL7, IL10, CD40LG, CD28*) and corresponding "receiver" receptors (*CD4, IL10RA, IL10RB, B, IL7R, ITGB1-2*) on T, NK cells (**Figure 7H,I** and **S5K-L**). Given the enrichment of *IL10* among coarse-level T, NK cells, we systematically queried all immune cell subpopulations to identify the putative *IL10* sender subpopulation(s), which revealed two terminally differentiated (GZMK^{hi} $T_{EM/PEX\text{-}like}$, $T_{EMRA\text{-}like}$) and one innate-like (NK-like) T cell subpopulation, as well as two monocyte-derived subpopulations (*S100A4*^{hi}, *CFP*^{hi} monocytes, *FABP4*^{hi}, *MCEMP*^{hi} alveolar Mφ) which "targeted" nineteen immune cell subpopulations, including eight T, NK cell subpopulations, suggesting the presence of CD4^{+} T cells is necessary for *CD8* T, NK cell immunomodulation and regulation in the TB granuloma (**Figure 7K** and **S5M,N**). Strikingly, IgG granulomas also demonstrated robust B cell signaling compared to αCD4 lesions, which lacked B cell contributions, among the top 50 prioritized linkages, to the granuloma cell-cell interactome (**Figure 7H,I**). Compared to αCD4 granulomas, IgG B cell "sender" ligands (*B2M, CD40, CD72, RPS19, TGFB1*) targeted four cell types, with two (*CD40, CD72*) of the five top-ranked ligands targeting T, NK cell receptors (*CD40LG, CD5*)

– a potential consequence (direct or indirect) of $CD4^+$ T cell depletion (Crotty, 2011; Sangster et al., 2003).

In summary, our systematic examination of the TB granuloma microenvironment following *Mtb* reinfection delineated distinct cellular circuitries, presenting a spectrum of responses – from amplification to dampening of the host inflammatory response – and underscoring the intricate balance in immune regulation associated with enhanced TB control.

DISCUSSION

The TB granuloma represents a perturbed immunological niche where tissue resident and nascently recruited cells work together against microenvironmental stressors (e.g., *Mtb*, cellular enrichment/depletion, fibrosis, necrosis, inflammation, hypoxia) in an attempt to restore homeostasis. These responses can either promote bacterial control or dissemination, as well as tissue damage or preservation (Pagán and Ramakrishnan, 2018, 2015). In the present study, we leveraged PET-CT, microbiological assays, flow cytometry, and scRNA-seq of *Mtb* infected cynomolgus granulomas following primary *Mtb* infection and reinfection to identify the cellular features of protection that primary *Mtb* infection provides against *Mtb* reinfection and to examine how $CD4^+$ T cell depletion before reinfection modulates host immunity. Collectively, our multi-modal dataset reveals global shifts in cellular composition, gene programming, and *Mtb* dynamics in primary *Mtb* infection and reinfection and nominates mechanisms by which $CD4^+$ T cells contribute to a restrictive immunological niche. In doing so, our study yields new insights into the cellular, molecular, and niche features that support anti-*Mtb* activity or promote maladaptive immunity following natural infection – most critically, that $CD4^+$ T cells act as homeostatic regulators of inflammation. It also identifies tissue-level cellular response mechanisms that can be targeted in future investigations for the development of improved prophylactics and cures.

Our high-dimensional examination of TB reinfection granulomas revealed underlying mechanisms governing granuloma cellularity and cytokine flux, as well as putative cell-cell interactions, providing insights into their roles in modulating anti-mycobacterial immunity. Illustratively, IgG lesions featured robust upregulation of immuno-modulatory and -regulatory genes (*IL10, PDCD1, TOX, TIGIT*) among lymphocyte-derived transcriptomes relative to primary infection (naïve) granulomas, which appeared to be CD4-dependent. Strikingly,

cytokines canonically associated with protective TB immunity (*TNF*, *IFNG*) did not distinguish IgG granulomas from naïve or αCD4 lesions. These data corroborate our previous findings demonstrating that reinfection macaques concurrently infected with *Mtb* experienced significantly increased IL-10 secretion and relatively lower levels of TNF and IFNγ production (Cadena et al., 2018). Moreover, recent work assessing the efficacy of pulmonary mucosal BCG delivery identified IL-10^{+} T cells as the most robust correlate of protection (Dijkman et al., 2019). In both studies (Cadena et al., 2018; Dijkman et al., 2019), the source of IL-10 production among T cells was unknown. Our present work expands these findings, identifying several T, NK cell subpopulations, including terminally differentiated and cytotoxic *CD8*-enriched subpopulations as putative sources of *IL10* production in the TB granuloma. Altogether our data demonstrate a shift in reinfection granuloma cytokine flux, cellularity, and programming, with T, NK cells biasing towards *CD8*-enriched immunoregulatory phenotypes.

Our cell-cell interaction analyses further identified roles for the immunoregulatory molecules *IL10* and *TIGIT* – expressed among T, NK cells – following *Mtb* reinfection. Significantly, these molecules were absent among naïve and CD4-depleted signaling networks, suggesting that following immune priming, *CD8*$^{+}$ T, NK cells require CD4^{+} T cell help (direct or indirect) to engage in self- and non-self-immunoregulatory circuits. Critically, the immunoregulatory molecule PD-1 has been demonstrated to promote host-resistance to TB, with checkpoint inhibitors (PD-1 blockade) exacerbating TB disease and immunopathology via overproduction of IFNγ from CD4^{+} CXCR3^{+}, KLRG1^{-}, CX3CR1^{-} T cells and elevated infiltrates of pro-inflammatory CD8^{+} T cells (Kauffman et al., 2021; Sakai et al., 2016); this suggests that the immunoregulatory circuits we identified among reinfection T, NK cells may be attempting to balance granuloma equilibria and mitigate tissue damage. While PD-1, IL-10, TIGIT, and other immunosuppressive molecules may mitigate inflammatory pathophysiology associated with TB, they may also inadvertently foster an environment conducive to *Mtb* persistence (Redford et al., 2011, 2010; Wong et al., 2020); this highlights the importance of balanced interplay between IL-10, among other immunoregulatory molecules (e.g., TIGIT, PD-1), and type-1 immunity in anti-TB immunity (Gideon et al., 2015).

Our analyses revealed that the immunoregulatory molecules *TIGIT, IL10,* and *PDCD1* were upregulated in the *CD8*$^{+}$ GZMK^{hi} $T_{EM/PEX\text{-}like}$ T, NK cell subpopulation. A comparison of GZMK^{hi} $T_{EM/PEX\text{-}like}$ frequencies revealed that immunologically primed (IgG) animals experience

significantly elevated recruitment (or retention) of GZMK^{hi} $T_{EM/PEX-like}$ cells relative to naïve or αCD4 lesions, suggesting that GZMK^{hi} $T_{EM/PEX-like}$ localization is CD4^{+} T cell-dependent. Although GZMK^{hi} $T_{EM/PEX-like}$ cells were enriched in granuloma with dampened type-1 immune cellularity and inflammatory response, scRNA-seq analyses of disparate pathologies (e.g., rheumatoid arthritis, cancer, ulcerative colitis, viral infection) and tissues have suggested GZMK^{+} CD8^{+} T cells promote and potentiate inflammatory sequelae (Jonsson et al., 2022; Thomas et al., 2021; Zheng et al., 2021). Moreover, these scRNA-seq studies have demonstrated GZMK^{+} CD8^{+} TCRs are highly clonal and restricted to sites of inflammation, potentially suggesting that these cells differentiate at the site of disease or become differentiated before recruitment (Cai et al., 2022; Jonsson et al., 2022). An analysis of GZMK^{+} CD8^{+} transcriptomes and TCRs derived from TB pleural fluid showed that clonally expanded GZMK^{+} CD8^{+} cells were restricted to pleural fluid and absent in peripheral blood (Cai et al., 2022). Furthermore, *in vitro* experiments leveraging *Mtb*-infected macrophages demonstrated purified GZMK has both cytotoxic and anti-microbial effector functions. While the absence of TCR and PBMC sampling in our study precluded us from identifying the origin of GZMK^{+} CD8^{+} T cells, granuloma GZMK^{hi} $T_{EM/PEX-like}$ cells had only low expression of T cell migration factors (CCR7, *SELL*, *CXCR5*), and upregulated expression of genes canonically associated with chronic inflammation and immunoregulation potentially suggesting: (i) granuloma GZMK^{hi} $T_{EM/PEX-like}$ cells have intra-compartment/lesion migratory potential, and (ii) GZMK^{hi} $T_{EM/PEX-like}$ cells acquire a terminally differentiated phenotype at the site of infection. Collectively, these data suggest that GZMK^{hi} $T_{EM/PEX-like}$ recruitment (or retention), differentiation, and state may be CD4^{+} T cell-dependent, further supporting a critical role for CD4^{+} T cells in balancing pro- and anti-inflammatory immunity.

Upon *Mtb* exposure, myeloid-derived cells, namely alveolar macrophages, sense and phagocytose invading bacilli, activating cell-intrinsic anti-microbial and inflammatory pathways, thus deviating from homeostasis to clear infection (Cohen et al., 2018; Ravesloot-Chávez et al., 2021). Following failure to clear initial infection, bacilli disseminate to lymphoid tissues and persist in non-restrictive cellular niches (Ganchua et al., 2018). Indeed, in the absence of Th1 activation of myeloid-derived cells, microbial growth remains unrestricted; thus, the 'central dogma' of anti-mycobacterial immunity has placed significant weight on IFN-γ and TNF Th1 CD4^{+} T cell-mediated immunity (Nunes-Alves et al., 2014). In addition to CD4^{+} IFN-γ and TNF

production, T cells secrete the immunomodulatory cytokine IL-10 which dampens both adaptive and innate immunity, downregulating MHCs, reactive oxygen and nitrogen intermediates, and type-1 chemokines (e.g., CXCL10), as well as inhibiting phagosome maturation among innate cells (Kessler et al., 2017; O'Leary et al., 2011; Rene de Waal Malefy et al., 1991). In keeping with these findings, we observe reinfection (IgG) granulomas, enriched for *IL10* expressing T, NK cells, experienced significant blunting of type-1 inflammation and type-1 IFN signaling relative to primary infection (naïve) and αCD4 granulomas. Furthermore, our findings demonstrate IgG monocyte-derived transcriptomes downregulate type-1 chemokines (e.g., CXCL9-11), as well as the IFN-γ and TNF response pathways – potentially a nuanced mechanism wherein the host attempts to achieve an equilibrium between protective immunity and tissue preservation (Gazzinelli et al., 1996; Sun et al., 2009). This modulation, while potentially mitigating tissue damage, may inadvertently reduce the host's capacity to sterilize phagocytosed *Mtb*. Notably, however, our *Mtb* barcode data demonstrate reinfection (IgG) animals had significantly fewer tissues sharing *Mtb* barcodes, indicative of reduced bacterial dissemination compared to naïve granulomas, and that in the absence of $CD4^+$ T cells, reinfection macaques had significantly elevated sharing of bacterial barcodes, highlighting the pivotal role of $CD4^+$ T cells in modulating an effective host response that can mitigate bacterial establishment during reinfection and *Mtb* dissemination between compartments. The intricate host-pathogen dynamics in TB, as reflected by these findings, necessitate a comprehensive understanding not only of the evident immune markers but also of the broader roles that macrophages play within the inflammatory landscape.

Macrophage sensing and phagocytosis of *Mtb* during acute infection triggers the production of pro-inflammatory chemokines (CXCL1, CXCL2) and cytokines that promote vascular permeability, upregulation of adhesion molecules, and subsequent neutrophil recruitment (Cai et al., 2010; Phillipson and Kubes, 2011). Our scRNA-seq analyses uncovered previously unappreciated neutrophil heterogeneity – cell types that have been underrepresented in droplet-based single-cell profiling of TB (Esaulova et al., 2020; Pisu et al., 2021) – in the TB granuloma, including the identification of two neutrophil subsets (*ICAM1*^{hi}, *NBN*^{hi} neutrophils; *SORL1*^{hi}, *CFD*^{hi} neutrophils), with differential pathway activation and phenotypic signatures. Notably, our data demonstrate that hypoxia- and inflammatory-enriched naïve and αCD4 granulomas have significant neutrophilia, and significant induction of an IFN-responsive

module associated with active TB, which may contribute to tissue inflammation and lung structural damage and the formation of an *Mtb*-permissive niche (such as caseum), thus promoting *Mtb* growth and dissemination (Berry et al., 2010; Lovewell et al., 2021). Critically, our data demonstrate reinfection (IgG) granulomas – characterized by reduced neutrophilia – do not support the same level of bacterial growth or dissemination as naïve lesions. They also show that inhibition of *Mtb* outgrowth and dissemination post-reinfection is at least partially $CD4^+$ T cell-dependent and independent of $CD4^+$ T cell-mediated induction of myeloid IFNγ- and TNF-response pathways.

In line with our findings, which demonstrated that 4-week post-primary infection (i.e., naïve NHP cohort) granulomas feature robust type-1 immune induction (e.g., *IL1B, CXCL9-11*) and signaling, previous research has shown that the chemokines CXCL9-11 are enriched among 4 week primary granulomas and that those granulomas feature elevated $CXCR3^+$ T cell frequencies – putative sources of IFNγ and TNF (Gideon et al., 2022; Lin et al., 2006; Mehra et al., 2010). These findings highlight the critical role of CXCL9-11 during early *Mtb* infection (before immune priming), where they promote the recruitment of protective lymphocyte populations, such as $CXCR3^+$ T cells; however, their overexpression may drive TB sequelae via self-reinforcing pro-inflammatory myeloid (neutrophil, macrophage)-T, NK cell ($CXCR3^+$ IFN-γ^+ TNF^+ T1T17-like) circuits, thus potentiating pro-inflammatory response mechanisms and subsequent bacterial dissemination (Esaulova et al., 2020; Sakai et al., 2016). Indeed, the chemokines CXCL9-11 have been identified as potential biomarkers of TB severity, with overexpression reported in human study participants with active TB; however, the temporal dynamics of CXCL9-11 expression during active human TB are unclear as time of infection is frequently unknown (Bhattacharyya et al., 2018; Kumar et al., 2021; Lee et al., 2015; Nonghanphithak et al., 2017; Ruhwald et al., 2007). While there is substantial evidence suggesting that excessive CXCL9-11 may contribute to the early anti-*Mtb* immunity or immunopathology, other studies suggest that CXCL9-11 could serve as markers of trained immunity following BCG vaccination, potentially acting as an initial barrier against invading bacilli, as well as correlate of protection (Joosten et al., 2018). Nevertheless, the precise role of CXCL9-11 in immunity requires further exploration. Future work leveraging single-cell multi-omics data (e.g., scATAC-seq) in BCG-vaccinated and *Mtb*-infected macaques could help

550 determine whether, and possibly when, elevated type-1 immune signaling is indicative of innate
551 training or a correlate of TB pathophysiology and chronic inflammatory stimuli.
552 In summary, we provide the first in-depth characterization of primary infection,
553 reinfection, and CD4$^+$ T cell-depleted reinfection macaque granulomas, identifying potential
554 mechanisms by which CD4$^+$ T cells contribute to anti-mycobacterial immunity. Our high-
555 dimensional characterization of granuloma transcriptomes and multimodal analyses reveal
556 cellular networks in which CD4$^+$ T cells regulate pro- and anti-inflammatory gene programming
557 and cell-cell signaling networks to limit inflammatory sequelae, as well as bacterial
558 establishment, growth, and dissemination. These findings expand beyond the limited purview of
559 the TB 'central dogma,' demonstrating that CD4$^+$ T cells act not only as effectors secreting IFN-
560 γ and TNF but also as homeostatic regulators, orchestrating both pro- and anti-inflammatory
561 immunity, thus leading to a more nuanced understanding of protective immunity against TB
562 disease, and broader understanding of how CD4$^+$ T cells modulate the immune response in
563 reinfection events.
564
565 **Limitations of the study**
566 While our study provides pivotal insights into the role of CD4$^+$ T cells in the context of *Mtb*
567 reinfection, it is important to acknowledge several inherent limitations associated with our design
568 and experimental power, including: (i) the need to use a 4–5-month drug treatment to clear
569 primary infection; and, (ii) limited number of NHPs and granulomas for scRNA-seq.
570 Additionally, our study design does not enable us to compare the naïve and αCD4 groups
571 directly since we did not have sufficient numbers of animals or granulomas and cannot
572 disentangle shifts due to immunological priming from those due to CD4$^+$ T cell depletion.
573
574 **SUPPLEMENTAL INFORMATION**
575 Supplemental information can be found online.
576
577 **ACKNOWLEDGEMENTS**
578 We extend our appreciation to the technical and veterinary teams of the Flynn, Shalek, and
579 Fortune laboratories for their dedication and assistance. We are particularly indebted to the
580 University of Pittsburgh's Division of Laboratory Animal Research and the Unified Flow Core

for their animal husbandry and support. Moreover, we are grateful to the NIH Nonhuman Primate Reagent Resource for providing essential antibody reagents (the CD4 depleting mAb used in this study was developed and provided by the NIH Nonhuman Primate Reagent Resource (ORIP P40 OD028116, U24 AI126683) and their expert guidance on their application. This work was supported in part by the Bill and Melinda Gates Foundation (A.K.S.), NIH R01 AI114674 (Flynn and Fortune), and by NIH contract IMPAc-TB; 75N93019C00071 (Fortune, Flynn, Shalek).

AUTHOR CONTRIBUTIONS

Conceptualization, J.L.F, S.M.F., and A.K.S.; Data curation J.D.B., S.K.C.G., M.C., H.P.G., R.F.-O.; formal analysis J.D.B., S.K.C.G., S.K.N., P.M., M.C., D.W.; Investigation J.D.B., S.K.C.G., S.K.N., P.M., M.C., D.M., S.N., J.R., H.P.G.; Visualization J.D.B., P.M., M.C.; Funding acquisition J.L.F, S.M.F., and A.K.S; Supervision J.L.F, S.M.F., A.K.S., and B.B.; Writing – original draft J.D.B., D.M., J.L.F, S.M.F., and A.K.S.; Writing – review & editing J.D.B., S.K.C.G., S.K.N., M.C., D.M., S.N., J.R., J.L.F, S.M.F., and A.K.S.

DECLARATIONS OF INTERESTS

A.K.S. reports compensation for consulting and/or scientific advisory board membership from Honeycomb Biotechnologies, Cellarity, Ochre Bio, Relation Therapeutics, FL86, IntrECate Biotherapeutics, Bio-Rad Laboratories, Senda Biosciences and Dahlia Biosciences unrelated to this work. S.M.F. reports compensation for board of directors membership from Oxford Nanopore unrelated to this work.

REFERENCES

Abel, L., Fellay, J., Haas, D.W., Schurr, E., Srikrishna, G., Urbanowski, M., Chaturvedi, N., Srinivasan, S., Johnson, D.H., Bishai, W.R., 2018. Genetics of human susceptibility to active and latent tuberculosis: present knowledge and future perspectives. Lancet Infect. Dis. 18, e64–e75. https://doi.org/10.1016/S1473-3099(17)30623-0

Ackerman, J.E., Nichols, A.E., Studentsova, V., Best, K.T., Knapp, E., Loiselle, A.E., 2019. Cell non-autonomous functions of S100a4 drive fibrotic tendon healing. eLife 8, e45342. https://doi.org/10.7554/eLife.45342

Ahmed, A., Rakshit, S., Adiga, V., Dias, M., Dwarkanath, P., D'Souza, G., Vyakarnam, A., 2021. A century of BCG: Impact on tuberculosis control and beyond. Immunol. Rev. 301, 98–121. https://doi.org/10.1111/imr.12968

615 Ahrends, T., Spanjaard, A., Pilzecker, B., Bąbała, N., Bovens, A., Xiao, Y., Jacobs, H., Borst, J.,
616 2017. CD4+ T Cell Help Confers a Cytotoxic T Cell Effector Program Including
617 Coinhibitory Receptor Downregulation and Increased Tissue Invasiveness. Immunity 47,
618 848-861.e5. https://doi.org/10.1016/j.immuni.2017.10.009
619 Almanzar, N., Antony, J., Baghel, A.S., Bakerman, I., Bansal, I., Barres, B.A., Beachy, P.A.,
620 Berdnik, D., Bilen, B., Brownfield, D., Cain, C., Chan, C.K.F., Chen, M.B., Clarke, M.F.,
621 Conley, S.D., Darmanis, S., Demers, A., Demir, K., de Morree, A., Divita, T., du Bois,
622 H., Ebadi, H., Espinoza, F.H., Fish, M., Gan, Q., George, B.M., Gillich, A., Gòmez-
623 Sjöberg, R., Green, F., Genetiano, G., Gu, X., Gulati, G.S., Hahn, O., Haney, M.S., Hang,
624 Y., Harris, L., He, M., Hosseinzadeh, S., Huang, A., Huang, K.C., Iram, T., Isobe, T.,
625 Ives, F., Jones, R.C., Kao, K.S., Karkanias, J., Karnam, G., Keller, A., Kershner, A.M.,
626 Khoury, N., Kim, S.K., Kiss, B.M., Kong, W., Krasnow, M.A., Kumar, M.E., Kuo, C.S.,
627 Lam, J., Lee, D.P., Lee, S.E., Lehallier, B., Leventhal, O., Li, G., Li, Q., Liu, L., Lo, A.,
628 Lu, W.-J., Lugo-Fagundo, M.F., Manjunath, A., May, A.P., Maynard, A., McGeever, A.,
629 McKay, M., McNerney, M.W., Merrill, B., Metzger, R.J., Mignardi, M., Min, D.,
630 Nabhan, A.N., Neff, N.F., Ng, K.M., Nguyen, P.K., Noh, J., Nusse, R., Pálovics, R.,
631 Patkar, R., Peng, W.C., Penland, L., Pisco, A.O., Pollard, K., Puccinelli, R., Qi, Z.,
632 Quake, S.R., Rando, T.A., Rulifson, E.J., Schaum, N., Segal, J.M., Sikandar, S.S., Sinha,
633 R., Sit, R.V., Sonnenburg, J., Staehli, D., Szade, K., Tan, M., Tan, W., Tato, C., Tellez,
634 K., Dulgeroff, L.B.T., Travaglini, K.J., Tropini, C., Tsui, M., Waldburger, L., Wang,
635 B.M., van Weele, L.J., Weinberg, K., Weissman, I.L., Wosczyna, M.N., Wu, S.M.,
636 Wyss-Coray, T., Xiang, J., Xue, S., Yamauchi, K.A., Yang, A.C., Yerra, L.P.,
637 Youngyunpipatkul, J., Yu, B., Zanini, F., Zardeneta, M.E., Zee, A., Zhao, C., Zhang, F.,
638 Zhang, H., Zhang, M.J., Zhou, L., Zou, J., The Tabula Muris Consortium, 2020. A single-
639 cell transcriptomic atlas characterizes ageing tissues in the mouse. Nature 583, 590–595.
640 https://doi.org/10.1038/s41586-020-2496-1
641 Andreatta, M., Tjitropranoto, A., Sherman, Z., Kelly, M.C., Ciucci, T., Carmona, S.J., 2022. A
642 CD4+ T cell reference map delineates subtype-specific adaptation during acute and
643 chronic viral infections. eLife 11, e76339. https://doi.org/10.7554/eLife.76339
644 Andrews, J.R., Noubary, F., Walensky, R.P., Cerda, R., Losina, E., Horsburgh, C.R., 2012. Risk
645 of Progression to Active Tuberculosis Following Reinfection With Mycobacterium
646 tuberculosis. Clin. Infect. Dis. 54, 784–791. https://doi.org/10.1093/cid/cir951
647 Atkinson, J.J., Toennies, H.M., Holmbeck, K., Senior, R.M., 2007. Membrane type 1 matrix
648 metalloproteinase is necessary for distal airway epithelial repair and keratinocyte growth
649 factor receptor expression after acute injury. Am. J. Physiol.-Lung Cell. Mol. Physiol.
650 293, L600–L610. https://doi.org/10.1152/ajplung.00028.2007
651 Berry, M.P.R., Graham, C.M., McNab, F.W., Xu, Z., Bloch, S.A.A., Oni, T., Wilkinson, K.A.,
652 Banchereau, R., Skinner, J., Wilkinson, R.J., Quinn, C., Blankenship, D., Dhawan, R.,
653 Cush, J.J., Mejias, A., Ramilo, O., Kon, O.M., Pascual, V., Banchereau, J., Chaussabel,
654 D., O'Garra, A., 2010. An interferon-inducible neutrophil-driven blood transcriptional
655 signature in human tuberculosis. Nature 466, 973–977.
656 https://doi.org/10.1038/nature09247
657 Bertholet, S., Ireton, G.C., Ordway, D.J., Windish, H.P., Pine, S.O., Kahn, M., Phan, T., Orme,
658 I.M., Vedvick, T.S., Baldwin, S.L., Coler, R.N., Reed, S.G., 2010. A Defined
659 Tuberculosis Vaccine Candidate Boosts BCG and Protects Against Multidrug-Resistant

660 Mycobacterium tuberculosis. Sci. Transl. Med. 2, 53ra74-53ra74.
661 https://doi.org/10.1126/scitranslmed.3001094
662 Bhattacharyya, C., Majumder, P.P., Pandit, B., 2018. CXCL10 is overexpressed in active
663 tuberculosis patients compared to M. tuberculosis-exposed household contacts.
664 Tuberculosis 109, 8–16. https://doi.org/10.1016/j.tube.2018.01.005
665 Bourgeois, C., 2002. A Role for CD40 Expression on CD8+ T Cells in the Generation of CD8+
666 T Cell Memory. Science 297, 2060–2063. https://doi.org/10.1126/science.1072615
667 Browaeys, R., Gilis, J., Sang-Aram, C., De Bleser, P., Hoste, L., Tavernier, S., Lambrechts, D.,
668 Seurinck, R., Saeys, Y., 2023. MultiNicheNet: a flexible framework for differential cell-
669 cell communication analysis from multi-sample multi-condition single-cell
670 transcriptomics data (preprint). Bioinformatics.
671 https://doi.org/10.1101/2023.06.13.544751
672 Büttner, M., Ostner, J., Müller, C.L., Theis, F.J., Schubert, B., 2021. scCODA is a Bayesian
673 model for compositional single-cell data analysis. Nat. Commun. 12, 6876.
674 https://doi.org/10.1038/s41467-021-27150-6
675 Cadena, A.M., Hopkins, F.F., Maiello, P., Carey, A.F., Wong, E.A., Martin, C.J., Gideon, H.P.,
676 DiFazio, R.M., Andersen, P., Lin, P.L., Fortune, S.M., Flynn, J.L., 2018. Concurrent
677 infection with Mycobacterium tuberculosis confers robust protection against secondary
678 infection in macaques. PLOS Pathog. 14, e1007305.
679 https://doi.org/10.1371/journal.ppat.1007305
680 Cai, S., Batra, S., Lira, S.A., Kolls, J.K., Jeyaseelan, S., 2010. CXCL1 Regulates Pulmonary
681 Host Defense to *Klebsiella* Infection via CXCL2, CXCL5, NF-κB, and MAPKs. J.
682 Immunol. 185, 6214–6225. https://doi.org/10.4049/jimmunol.0903843
683 Cai, Y., Wang, Y., Shi, C., Dai, Y., Li, F., Xu, Y., Zhang, P., Kong, F., Deng, G., Wen, Z., Zhou,
684 Q., Kang, B.C., Singhal, A., Yang, Q., Feng, C.G., Chen, X., 2022. Single-cell immune
685 profiling reveals functional diversity of T cells in tuberculous pleural effusion. J. Exp.
686 Med. 219, e20211777. https://doi.org/10.1084/jem.20211777
687 Capuano, S.V., Croix, D.A., Pawar, S., Zinovik, A., Myers, A., Lin, P.L., Bissel, S., Fuhrman,
688 C., Klein, E., Flynn, J.L., 2003. Experimental *Mycobacterium tuberculosis* Infection of
689 Cynomolgus Macaques Closely Resembles the Various Manifestations of Human *M.*
690 *tuberculosis* Infection. Infect. Immun. 71, 5831–5844.
691 https://doi.org/10.1128/IAI.71.10.5831-5844.2003
692 Carmona-Rivera, C., Zhao, W., Yalavarthi, S., Kaplan, M.J., 2015. Neutrophil extracellular traps
693 induce endothelial dysfunction in systemic lupus erythematosus through the activation of
694 matrix metalloproteinase-2. Ann. Rheum. Dis. 74, 1417–1424.
695 https://doi.org/10.1136/annrheumdis-2013-204837
696 Chakravarty, S.D., Xu, J., Lu, B., Gerard, C., Flynn, J., Chan, J., 2007. The Chemokine Receptor
697 CXCR3 Attenuates the Control of Chronic *Mycobacterium tuberculosis* Infection in
698 BALB/c Mice. J. Immunol. 178, 1723–1735.
699 https://doi.org/10.4049/jimmunol.178.3.1723
700 Chen, C.Y., Huang, D., Wang, R.C., Shen, L., Zeng, G., Yao, S., Shen, Y., Halliday, L.,
701 Fortman, J., McAllister, M., Estep, J., Hunt, R., Vasconcelos, D., Du, G., Porcelli, S.A.,
702 Larsen, M.H., Jacobs, W.R., Haynes, B.F., Letvin, N.L., Chen, Z.W., 2009. A Critical
703 Role for CD8 T Cells in a Nonhuman Primate Model of Tuberculosis. PLoS Pathog. 5,
704 e1000392. https://doi.org/10.1371/journal.ppat.1000392

Cohen, S.B., Gern, B.H., Delahaye, J.L., Adams, K.N., Plumlee, C.R., Winkler, J.K., Sherman, D.R., Gerner, M.Y., Urdahl, K.B., 2018. Alveolar Macrophages Provide an Early Mycobacterium tuberculosis Niche and Initiate Dissemination. Cell Host Microbe 24, 439-446.e4. https://doi.org/10.1016/j.chom.2018.08.001

Cohen, S.B., Gern, B.H., Urdahl, K.B., 2022. The Tuberculous Granuloma and Preexisting Immunity. Annu. Rev. Immunol. 40, 589–614. https://doi.org/10.1146/annurev-immunol-093019-125148

Coleman, M.T., Chen, R.Y., Lee, M., Lin, P.L., Dodd, L.E., Maiello, P., Via, L.E., Kim, Y., Marriner, G., Dartois, V., Scanga, C., Janssen, C., Wang, J., Klein, E., Cho, S.N., Barry, C.E., Flynn, J.L., 2014a. PET/CT imaging reveals a therapeutic response to oxazolidinones in macaques and humans with tuberculosis. Sci. Transl. Med. 6. https://doi.org/10.1126/scitranslmed.3009500

Coleman, M.T., Maiello, P., Tomko, J., Frye, L.J., Fillmore, D., Janssen, C., Klein, E., Lin, P.L., 2014b. Early Changes by ^{18} Fluorodeoxyglucose Positron Emission Tomography Coregistered with Computed Tomography Predict Outcome after Mycobacterium tuberculosis Infection in Cynomolgus Macaques. Infect. Immun. 82, 2400–2404. https://doi.org/10.1128/IAI.01599-13

Coscolla, M., Gagneux, S., 2014. Consequences of genomic diversity in Mycobacterium tuberculosis. Semin. Immunol. 26, 431–444. https://doi.org/10.1016/j.smim.2014.09.012

Crotty, S., 2011. Follicular Helper CD4 T Cells (T_{FH}). Annu. Rev. Immunol. 29, 621–663. https://doi.org/10.1146/annurev-immunol-031210-101400

Darrah, P.A., Patel, D.T., De Luca, P.M., Lindsay, R.W.B., Davey, D.F., Flynn, B.J., Hoff, S.T., Andersen, P., Reed, S.G., Morris, S.L., Roederer, M., Seder, R.A., 2007. Multifunctional TH1 cells define a correlate of vaccine-mediated protection against Leishmania major. Nat. Med. 13, 843–850. https://doi.org/10.1038/nm1592

Darrah, P.A., Zeppa, J.J., Maiello, P., Hackney, J.A., Wadsworth, M.H., Hughes, T.K., Pokkali, S., Swanson, P.A., Grant, N.L., Rodgers, M.A., Kamath, M., Causgrove, C.M., Laddy, D.J., Bonavia, A., Casimiro, D., Lin, P.L., Klein, E., White, A.G., Scanga, C.A., Shalek, A.K., Roederer, M., Flynn, J.L., Seder, R.A., 2020. Prevention of tuberculosis in macaques after intravenous BCG immunization. Nature 577, 95–102. https://doi.org/10.1038/s41586-019-1817-8

Darrah, P.A., Zeppa, J.J., Wang, C., Irvine, E.B., Bucsan, A.N., Rodgers, M.A., Pokkali, S., Hackney, J.A., Kamath, M., White, A.G., Borish, H.J., Frye, L.J., Tomko, J., Kracinovsky, K., Lin, P.L., Klein, E., Scanga, C.A., Alter, G., Fortune, S.M., Lauffenburger, D.A., Flynn, J.L., Seder, R.A., Maiello, P., Roederer, M., 2023. Airway T cells are a correlate of i.v. Bacille Calmette-Guerin-mediated protection against tuberculosis in rhesus macaques. Cell Host Microbe 31, 962-977.e8. https://doi.org/10.1016/j.chom.2023.05.006

Desvignes, L., Ernst, J.D., 2009. Interferon-γ-Responsive Nonhematopoietic Cells Regulate the Immune Response to Mycobacterium tuberculosis. Immunity 31, 974–985. https://doi.org/10.1016/j.immuni.2009.10.007

Diedrich, C.R., Rutledge, T., Maiello, P., Baranowski, T.M., White, A.G., Borish, H.J., Karell, P., Hopkins, F., Brown, J., Fortune, S.M., Flynn, J.L., Ambrose, Z., Lin, P.L., 2020. SIV and Mycobacterium tuberculosis synergy within the granuloma accelerates the reactivation pattern of latent tuberculosis. PLOS Pathog. 16, e1008413. https://doi.org/10.1371/journal.ppat.1008413

751 Dijkman, K., Sombroek, C.C., Vervenne, R.A.W., Hofman, S.O., Boot, C., Remarque, E.J.,
752 Kocken, C.H.M., Ottenhoff, T.H.M., Kondova, I., Khayum, M.A., Haanstra, K.G.,
753 Vierboom, M.P.M., Verreck, F.A.W., 2019. Prevention of tuberculosis infection and
754 disease by local BCG in repeatedly exposed rhesus macaques. Nat. Med. 25, 255–262.
755 https://doi.org/10.1038/s41591-018-0319-9
756 DiToro, D., Harbour, S.N., Bando, J.K., Benavides, G., Witte, S., Laufer, V.A., Moseley, C.,
757 Singer, J.R., Frey, B., Turner, H., Bruning, J., Darley-Usmar, V., Gao, M., Conover, C.,
758 Hatton, R.D., Frank, S., Colonna, M., Weaver, C.T., 2020. Insulin-Like Growth Factors
759 Are Key Regulators of T Helper 17 Regulatory T Cell Balance in Autoimmunity.
760 Immunity 52, 650-667.e10. https://doi.org/10.1016/j.immuni.2020.03.013
761 Dwyer, D.F., Ordovas-Montanes, J., Allon, S.J., Buchheit, K.M., Vukovic, M., Derakhshan, T.,
762 Feng, C., Lai, J., Hughes, T.K., Nyquist, S.K., Giannetti, M.P., Berger, B.,
763 Bhattacharyya, N., Roditi, R.E., Katz, H.R., Nawijn, M.C., Berg, M., Van Den Berge, M.,
764 Laidlaw, T.M., Shalek, A.K., Barrett, N.A., Boyce, J.A., 2021. Human airway mast cells
765 proliferate and acquire distinct inflammation-driven phenotypes during type 2
766 inflammation. Sci. Immunol. 6, eabb7221. https://doi.org/10.1126/sciimmunol.abb7221
767 Ellis, R.D., Hatherill, M., Tait, D., Snowden, M., Churchyard, G., Hanekom, W., Evans, T.,
768 Ginsberg, A.M., 2015. Innovative clinical trial designs to rationalize TB vaccine
769 development. Tuberculosis 95, 352–357. https://doi.org/10.1016/j.tube.2015.02.036
770 Esaulova, E., Das, S., Singh, D.K., Choreño-Parra, J.A., Swain, A., Arthur, L., Rangel-Moreno,
771 J., Ahmed, M., Singh, B., Gupta, A., Fernández-López, L.A., de la Luz Garcia-
772 Hernandez, M., Bucsan, A., Moodley, C., Mehra, S., García-Latorre, E., Zuniga, J.,
773 Atkinson, J., Kaushal, D., Artyomov, M.N., Khader, S.A., 2020. The immune landscape
774 in tuberculosis reveals populations linked to disease and latency. Cell Host Microbe
775 S1931312820306351. https://doi.org/10.1016/j.chom.2020.11.013
776 Esmail, H., Riou, C., Du Bruyn, E., Lai, R.P.-J., Harley, Y.X.R., Meintjes, G., Wilkinson, K.A.,
777 Wilkinson, R.J., 2018. The Immune Response to *Mycobacterium tuberculosis* in HIV-1-
778 Coinfected Persons. Annu. Rev. Immunol. 36, 603–638. https://doi.org/10.1146/annurev-
779 immunol-042617-053420
780 Feau, S., Arens, R., Togher, S., Schoenberger, S.P., 2011. Autocrine IL-2 is required for
781 secondary population expansion of CD8+ memory T cells. Nat. Immunol. 12, 908–913.
782 https://doi.org/10.1038/ni.2079
783 Finak, G., McDavid, A., Yajima, M., Deng, J., Gersuk, V., Shalek, A.K., Slichter, C.K., Miller,
784 H.W., McElrath, M.J., Prlic, M., Linsley, P.S., Gottardo, R., 2015. MAST: a flexible
785 statistical framework for assessing transcriptional changes and characterizing
786 heterogeneity in single-cell RNA sequencing data. Genome Biol. 16, 278.
787 https://doi.org/10.1186/s13059-015-0844-5
788 Flynn, J.L., Chan, J., 2022. Immune cell interactions in tuberculosis. Cell 185, 4682–4702.
789 https://doi.org/10.1016/j.cell.2022.10.025
790 Flynn, J.L., Gideon, H.P., Mattila, J.T., Lin, P.L., 2015. Immunology studies in non-human
791 primate models of tuberculosis. Immunol. Rev. 264, 60–73.
792 https://doi.org/10.1111/imr.12258
793 Foreman, T.W., Mehra, S., LoBato, D.N., Malek, A., Alvarez, X., Golden, N.A., Bucşan, A.N.,
794 Didier, P.J., Doyle-Meyers, L.A., Russell-Lodrigue, K.E., Roy, C.J., Blanchard, J.,
795 Kuroda, M.J., Lackner, A.A., Chan, J., Khader, S.A., Jacobs, W.R., Kaushal, D., 2016.
796 CD4 $^{+}$ T-cell–independent mechanisms suppress reactivation of latent tuberculosis in a

macaque model of HIV coinfection. Proc. Natl. Acad. Sci. 113. https://doi.org/10.1073/pnas.1611987113

Foreman, T.W., Nelson, C.E., Kauffman, K.D., Lora, N.E., Vinhaes, C.L., Dorosky, D.E., Sakai, S., Gomez, F., Fleegle, J.D., Parham, M., Perera, S.R., Lindestam Arlehamn, C.S., Sette, A., Brenchley, J.M., Queiroz, A.T.L., Andrade, B.B., Kabat, J., Via, L.E., Barber, D.L., 2022. CD4 T cells are rapidly depleted from tuberculosis granulomas following acute SIV co-infection. Cell Rep. 39, 110896. https://doi.org/10.1016/j.celrep.2022.110896

Galagan, J.E., 2014. Genomic insights into tuberculosis. Nat. Rev. Genet. 15, 307–320. https://doi.org/10.1038/nrg3664

Galletti, G., De Simone, G., Mazza, E.M.C., Puccio, S., Mezzanotte, C., Bi, T.M., Davydov, A.N., Metsger, M., Scamardella, E., Alvisi, G., De Paoli, F., Zanon, V., Scarpa, A., Camisa, B., Colombo, F.S., Anselmo, A., Peano, C., Polletti, S., Mavilio, D., Gattinoni, L., Boi, S.K., Youngblood, B.A., Jones, R.E., Baird, D.M., Gostick, E., Llewellyn-Lacey, S., Ladell, K., Price, D.A., Chudakov, D.M., Newell, E.W., Casucci, M., Lugli, E., 2020a. Two subsets of stem-like CD8+ memory T cell progenitors with distinct fate commitments in humans. Nat. Immunol. 21, 1552–1562. https://doi.org/10.1038/s41590-020-0791-5

Galletti, G., De Simone, G., Mazza, E.M.C., Puccio, S., Mezzanotte, C., Bi, T.M., Davydov, A.N., Metsger, M., Scamardella, E., Alvisi, G., De Paoli, F., Zanon, V., Scarpa, A., Camisa, B., Colombo, F.S., Anselmo, A., Peano, C., Polletti, S., Mavilio, D., Gattinoni, L., Boi, S.K., Youngblood, B.A., Jones, R.E., Baird, D.M., Gostick, E., Llewellyn-Lacey, S., Ladell, K., Price, D.A., Chudakov, D.M., Newell, E.W., Casucci, M., Lugli, E., 2020b. Two subsets of stem-like CD8+ memory T cell progenitors with distinct fate commitments in humans. Nat. Immunol. 21, 1552–1562. https://doi.org/10.1038/s41590-020-0791-5

Ganchua, S.K.C., Cadena, A.M., Maiello, P., Gideon, H.P., Myers, A.J., Junecko, B.F., Klein, E.C., Lin, P.L., Mattila, J.T., Flynn, J.L., 2018. Lymph nodes are sites of prolonged bacterial persistence during Mycobacterium tuberculosis infection in macaques. PLOS Pathog. 14, e1007337. https://doi.org/10.1371/journal.ppat.1007337

Gasperini, S., Marchi, M., Calzetti, F., Laudanna, C., Vicentini, L., Olsen, H., Murphy, M., Liao, F., Farber, J., Cassatella, M.A., 1999. Gene Expression and Production of the Monokine Induced by IFN-γ (MIG), IFN-Inducible T Cell α Chemoattractant (I-TAC), and IFN-γ-Inducible Protein-10 (IP-10) Chemokines by Human Neutrophils. J. Immunol. 162, 4928–4937. https://doi.org/10.4049/jimmunol.162.8.4928

Gazzinelli, R.T., Wysocka, M., Hieny, S., Scharton-Kersten, T., Cheever, A., Kühn, R., Müller, W., Trinchieri, G., Sher, A., 1996. In the absence of endogenous IL-10, mice acutely infected with Toxoplasma gondii succumb to a lethal immune response dependent on CD4+ T cells and accompanied by overproduction of IL-12, IFN-gamma and TNF-alpha. J. Immunol. 157, 798–805. https://doi.org/10.4049/jimmunol.157.2.798

Giacomini, E., Sotolongo, A., Iona, E., Severa, M., Remoli, M.E., Gafa, V., Lande, R., Fattorini, L., Smith, I., Manganelli, R., Coccia, E.M., 2006. Infection of Human Dendritic Cells with a *Mycobacterium tuberculosis sigE* Mutant Stimulates Production of High Levels of Interleukin-10 but Low Levels of CXCL10: Impact on the T-Cell Response. Infect. Immun. 74, 3296–3304. https://doi.org/10.1128/IAI.01687-05

Gideon, H.P., Hughes, T.K., Tzouanas, C.N., Wadsworth, M.H., Tu, A.A., Gierahn, T.M., Peters, J.M., Hopkins, F.F., Wei, J.-R., Kummerlowe, C., Grant, N.L., Nargan, K., Phuah,

J.Y., Borish, H.J., Maiello, P., White, A.G., Winchell, C.G., Nyquist, S.K., Ganchua, S.K.C., Myers, A., Patel, K.V., Ameel, C.L., Cochran, C.T., Ibrahim, S., Tomko, J.A., Frye, L.J., Rosenberg, J.M., Shih, A., Chao, M., Klein, E., Scanga, C.A., Ordovas-Montanes, J., Berger, B., Mattila, J.T., Madansein, R., Love, J.C., Lin, P.L., Leslie, A., Behar, S.M., Bryson, B., Flynn, J.L., Fortune, S.M., Shalek, A.K., 2022. Multimodal profiling of lung granulomas in macaques reveals cellular correlates of tuberculosis control. Immunity 55, 827-846.e10. https://doi.org/10.1016/j.immuni.2022.04.004

Gideon, H.P., Phuah, J., Junecko, B.A., Mattila, J.T., 2019. Neutrophils express pro- and anti-inflammatory cytokines in granulomas from Mycobacterium tuberculosis-infected cynomolgus macaques. Mucosal Immunol. 12, 1370–1381. https://doi.org/10.1038/s41385-019-0195-8

Gideon, H.P., Phuah, J., Myers, A.J., Bryson, B.D., Rodgers, M.A., Coleman, M.T., Maiello, P., Rutledge, T., Marino, S., Fortune, S.M., Kirschner, D.E., Lin, P.L., Flynn, J.L., 2015. Variability in Tuberculosis Granuloma T Cell Responses Exists, but a Balance of Pro- and Anti-inflammatory Cytokines Is Associated with Sterilization. PLOS Pathog. 11, e1004603. https://doi.org/10.1371/journal.ppat.1004603

Gierahn, T.M., Wadsworth, M.H., Hughes, T.K., Bryson, B.D., Butler, A., Satija, R., Fortune, S., Love, J.C., Shalek, A.K., 2017. Seq-Well: portable, low-cost RNA sequencing of single cells at high throughput. Nat. Methods 14, 395–398. https://doi.org/10.1038/nmeth.4179

Gong, D., Shi, W., Yi, S., Chen, H., Groffen, J., Heisterkamp, N., 2012. TGFβ signaling plays a critical role in promoting alternative macrophage activation. BMC Immunol. 13, 31. https://doi.org/10.1186/1471-2172-13-31

Gopal, R., Monin, L., Torres, D., Slight, S., Mehra, S., McKenna, K.C., Fallert Junecko, B.A., Reinhart, T.A., Kolls, J., Báez-Saldaña, R., Cruz-Lagunas, A., Rodríguez-Reyna, T.S., Kumar, N.P., Tessier, P., Roth, J., Selman, M., Becerril-Villanueva, E., Baquera-Heredia, J., Cumming, B., Kasprowicz, V.O., Steyn, A.J.C., Babu, S., Kaushal, D., Zúñiga, J., Vogl, T., Rangel-Moreno, J., Khader, S.A., 2013. S100A8/A9 Proteins Mediate Neutrophilic Inflammation and Lung Pathology during Tuberculosis. Am. J. Respir. Crit. Care Med. 188, 1137–1146. https://doi.org/10.1164/rccm.201304-0803OC

Grant, N.L., Maiello, P., Klein, E., Lin, P.L., Borish, H.J., Tomko, J., Frye, L.J., White, A.G., Kirschner, D.E., Mattila, J.T., Flynn, J.L., 2022. T cell transcription factor expression evolves over time in granulomas from Mycobacterium tuberculosis-infected cynomolgus macaques. Cell Rep. 39, 110826. https://doi.org/10.1016/j.celrep.2022.110826

Green, A.M., DiFazio, R., Flynn, J.L., 2013. IFN-γ from CD4 T Cells Is Essential for Host Survival and Enhances CD8 T Cell Function during *Mycobacterium tuberculosis* Infection. J. Immunol. 190, 270–277. https://doi.org/10.4049/jimmunol.1200061

Gupta, A., Wood, R., Kaplan, R., Bekker, L.-G., Lawn, S.D., 2012. Tuberculosis Incidence Rates during 8 Years of Follow-Up of an Antiretroviral Treatment Cohort in South Africa: Comparison with Rates in the Community. PLoS ONE 7, e34156. https://doi.org/10.1371/journal.pone.0034156

Hamilton, S.E., Prlic, M., Jameson, S.C., 2004. Environmental conservation: bystander CD4 T cells keep CD8 memories fresh. Nat. Immunol. 5, 873–874. https://doi.org/10.1038/ni0904-873

Hansen, S.G., Zak, D.E., Xu, G., Ford, J.C., Marshall, E.E., Malouli, D., Gilbride, R.M., Hughes, C.M., Ventura, A.B., Ainslie, E., Randall, K.T., Selseth, A.N., Rundstrom, P., Herlache, L., Lewis, M.S., Park, H., Planer, S.L., Turner, J.M., Fischer, M., Armstrong, C., Zweig,

R.C., Valvo, J., Braun, J.M., Shankar, S., Lu, L., Sylwester, A.W., Legasse, A.W., Messerle, M., Jarvis, M.A., Amon, L.M., Aderem, A., Alter, G., Laddy, D.J., Stone, M., Bonavia, A., Evans, T.G., Axthelm, M.K., Früh, K., Edlefsen, P.T., Picker, L.J., 2018. Prevention of tuberculosis in rhesus macaques by a cytomegalovirus-based vaccine. Nat. Med. 24, 130–143. https://doi.org/10.1038/nm.4473

Hughes, T.K., Wadsworth, M.H., Gierahn, T.M., Do, T., Weiss, D., Andrade, P.R., Ma, F., De Andrade Silva, B.J., Shao, S., Tsoi, L.C., Ordovas-Montanes, J., Gudjonsson, J.E., Modlin, R.L., Love, J.C., Shalek, A.K., 2020. Second-Strand Synthesis-Based Massively Parallel scRNA-Seq Reveals Cellular States and Molecular Features of Human Inflammatory Skin Pathologies. Immunity 53, 878-894.e7. https://doi.org/10.1016/j.immuni.2020.09.015

Huynh, J.P., Lin, C.-C., Kimmey, J.M., Jarjour, N.N., Schwarzkopf, E.A., Bradstreet, T.R., Shchukina, I., Shpynov, O., Weaver, C.T., Taneja, R., Artyomov, M.N., Edelson, B.T., Stallings, C.L., 2018. Bhlhe40 is an essential repressor of IL-10 during *Mycobacterium tuberculosis* infection. J. Exp. Med. 215, 1823–1838. https://doi.org/10.1084/jem.20171704

Ichikawa, A., Kuba, K., Morita, M., Chida, S., Tezuka, H., Hara, H., Sasaki, T., Ohteki, T., Ranieri, V.M., Dos Santos, C.C., Kawaoka, Y., Akira, S., Luster, A.D., Lu, B., Penninger, J.M., Uhlig, S., Slutsky, A.S., Imai, Y., 2013. CXCL10-CXCR3 Enhances the Development of Neutrophil-mediated Fulminant Lung Injury of Viral and Nonviral Origin. Am. J. Respir. Crit. Care Med. 187, 65–77. https://doi.org/10.1164/rccm.201203-0508OC

Jonsson, A.H., Zhang, F., Dunlap, G., Gomez-Rivas, E., Watts, G.F.M., Faust, H.J., Rupani, K.V., Mears, J.R., Meednu, N., Wang, R., Keras, G., Coblyn, J.S., Massarotti, E.M., Todd, D.J., Anolik, J.H., McDavid, A., Accelerating Medicines Partnership RA/SLE Network, Wei, K., Rao, D.A., Raychaudhuri, S., Brenner, M.B., 2022. Granzyme K $^{+}$ CD8 T cells form a core population in inflamed human tissue. Sci. Transl. Med. 14, eabo0686. https://doi.org/10.1126/scitranslmed.abo0686

Joosten, S.A., Van Meijgaarden, K.E., Arend, S.M., Prins, C., Oftung, F., Korsvold, G.E., Kik, S.V., Arts, R.J.W., Van Crevel, R., Netea, M.G., Ottenhoff, T.H.M., 2018. Mycobacterial growth inhibition is associated with trained innate immunity. J. Clin. Invest. 128, 1837–1851. https://doi.org/10.1172/JCI97508

J-P Millet, À Orcau, P García de Olalla, M Casals, C Rius, J A Caylà, 2009. Tuberculosis recurrence and its associated risk factors among successfully treated patients. J. Epidemiol. Community Health 63, 799. https://doi.org/10.1136/jech.2008.077560

Kauffman, K.D., Sakai, S., Lora, N.E., Namasivayam, S., Baker, P.J., Kamenyeva, O., Foreman, T.W., Nelson, C.E., Oliveira-de-Souza, D., Vinhaes, C.L., Yaniv, Z., Lindestam Arleham, C.S., Sette, A., Freeman, G.J., Moore, R., NIAID/DIR Tuberculosis Imaging Program, Sher, A., Mayer-Barber, K.D., Andrade, B.B., Kabat, J., Via, L.E., Barber, D.L., 2021. PD-1 blockade exacerbates *Mycobacterium tuberculosis* infection in rhesus macaques. Sci. Immunol. 6, eabf3861. https://doi.org/10.1126/sciimmunol.abf3861

Kessler, B., Rinchai, D., Kewcharoenwong, C., Nithichanon, A., Biggart, R., Hawrylowicz, C.M., Bancroft, G.J., Lertmemongkolchai, G., 2017. Interleukin 10 inhibits pro-inflammatory cytokine responses and killing of Burkholderia pseudomallei. Sci. Rep. 7, 42791. https://doi.org/10.1038/srep42791

Khader, S.A., Bell, G.K., Pearl, J.E., Fountain, J.J., Rangel-Moreno, J., Cilley, G.E., Shen, F., Eaton, S.M., Gaffen, S.L., Swain, S.L., Locksley, R.M., Haynes, L., Randall, T.D., Cooper, A.M., 2007. IL-23 and IL-17 in the establishment of protective pulmonary CD4+ T cell responses after vaccination and during Mycobacterium tuberculosis challenge. Nat. Immunol. 8, 369–377. https://doi.org/10.1038/ni1449

Kotliar, D., Lin, A.E., Logue, J., Hughes, T.K., Khoury, N.M., Raju, S.S., Wadsworth, M.H., Chen, H., Kurtz, J.R., Dighero-Kemp, B., Bjornson, Z.B., Mukherjee, N., Sellers, B.A., Tran, N., Bauer, M.R., Adams, G.C., Adams, R., Rinn, J.L., Melé, M., Schaffner, S.F., Nolan, G.P., Barnes, K.G., Hensley, L.E., McIlwain, D.R., Shalek, A.K., Sabeti, P.C., Bennett, R.S., 2020. Single-Cell Profiling of Ebola Virus Disease In Vivo Reveals Viral and Host Dynamics. Cell 183, 1383-1401.e19. https://doi.org/10.1016/j.cell.2020.10.002

Kumar, N.P., Hissar, S., Thiruvengadam, K., Banurekha, V.V., Balaji, S., Elilarasi, S., Gomathi, N.S., Ganesh, J., Aravind, M.A., Baskaran, D., Tripathy, S., Swaminathan, S., Babu, S., 2021. Plasma chemokines as immune biomarkers for diagnosis of pediatric tuberculosis. BMC Infect. Dis. 21, 1055. https://doi.org/10.1186/s12879-021-06749-6

Kwan, C.K., Ernst, J.D., 2011. HIV and Tuberculosis: a Deadly Human Syndemic. Clin. Microbiol. Rev. 24, 351–376. https://doi.org/10.1128/CMR.00042-10

Laidlaw, B.J., Craft, J.E., Kaech, S.M., 2016. The multifaceted role of CD4+ T cells in CD8+ T cell memory. Nat. Rev. Immunol. 16, 102–111. https://doi.org/10.1038/nri.2015.10

Lange, C., Aaby, P., Behr, M.A., Donald, P.R., Kaufmann, S.H.E., Netea, M.G., Mandalakas, A.M., 2022. 100 years of Mycobacterium bovis bacille Calmette-Guérin. Lancet Infect. Dis. 22, e2–e12. https://doi.org/10.1016/S1473-3099(21)00403-5

Larson, E.C., Ellis-Connell, A.L., Rodgers, M.A., Gubernat, A.K., Gleim, J.L., Moriarty, R.V., Balgeman, A.J., Ameel, C.L., Jauro, S., Tomko, J.A., Kracinovsky, K.B., Maiello, P., Borish, H.J., White, A.G., Klein, E., Bucsan, A.N., Darrah, P.A., Seder, R.A., Roederer, M., Lin, P.L., Flynn, J.L., O'Connor, S.L., Scanga, C.A., 2023. Intravenous Bacille Calmette–Guérin vaccination protects simian immunodeficiency virus-infected macaques from tuberculosis. Nat. Microbiol. 8, 2080–2092. https://doi.org/10.1038/s41564-023-01503-x

Lawn, S.D., Zumla, A.I., 2011. Tuberculosis. The Lancet 378, 57–72. https://doi.org/10.1016/S0140-6736(10)62173-3

Lee, K., Chung, W., Jung, Y., Kim, Y., Park, J., Sheen, S., Park, K., 2015. CXCR3 ligands as clinical markers for pulmonary tuberculosis. Int. J. Tuberc. Lung Dis. 19, 191–199. https://doi.org/10.5588/ijtld.14.0525

Lin, P.L., Dartois, V., Johnston, P.J., Janssen, C., Via, L., Goodwin, M.B., Klein, E., Barry, C.E., Flynn, J.L., 2012a. Metronidazole prevents reactivation of latent *Mycobacterium tuberculosis* infection in macaques. Proc. Natl. Acad. Sci. 109, 14188–14193. https://doi.org/10.1073/pnas.1121497109

Lin, P.L., Ford, C.B., Coleman, M.T., Myers, A.J., Gawande, R., Ioerger, T., Sacchettini, J., Fortune, S.M., Flynn, J.L., 2014. Sterilization of granulomas is common in active and latent tuberculosis despite within-host variability in bacterial killing. Nat. Med. 20, 75–79. https://doi.org/10.1038/nm.3412

Lin, P.L., Pawar, S., Myers, A., Pegu, A., Fuhrman, C., Reinhart, T.A., Capuano, S.V., Klein, E., Flynn, J.L., 2006. Early Events in *Mycobacterium tuberculosis* Infection in Cynomolgus Macaques. Infect. Immun. 74, 3790–3803. https://doi.org/10.1128/IAI.00064-06

Lin, P.L., Rodgers, M., Smith, L., Bigbee, M., Myers, A., Bigbee, C., Chiosea, I., Capuano, S.V., Fuhrman, C., Klein, E., Flynn, J.L., 2009. Quantitative Comparison of Active and Latent Tuberculosis in the Cynomolgus Macaque Model. Infect. Immun. 77, 4631–4642. https://doi.org/10.1128/IAI.00592-09

Lin, P.L., Rutledge, T., Green, A.M., Bigbee, M., Fuhrman, C., Klein, E., Flynn, J.L., 2012b. CD4 T Cell Depletion Exacerbates Acute *Mycobacterium tuberculosis* While Reactivation of Latent Infection Is Dependent on Severity of Tissue Depletion in Cynomolgus Macaques. AIDS Res. Hum. Retroviruses 28, 1693–1702. https://doi.org/10.1089/aid.2012.0028

Loebbermann, J., Schnoeller, C., Thornton, H., Durant, L., Sweeney, N.P., Schuijs, M., O'Garra, A., Johansson, C., Openshaw, P.J., 2012. IL-10 Regulates Viral Lung Immunopathology during Acute Respiratory Syncytial Virus Infection in Mice. PLoS ONE 7, e32371. https://doi.org/10.1371/journal.pone.0032371

Love, M.I., Huber, W., Anders, S., 2014. Moderated estimation of fold change and dispersion for RNA-seq data with DESeq2. Genome Biol. 15, 550. https://doi.org/10.1186/s13059-014-0550-8

Lovewell, R.R., Baer, C.E., Mishra, B.B., Smith, C.M., Sassetti, C.M., 2021. Granulocytes act as a niche for Mycobacterium tuberculosis growth. Mucosal Immunol. 14, 229–241. https://doi.org/10.1038/s41385-020-0300-z

Lu, Y.-J., Barreira-Silva, P., Boyce, S., Powers, J., Cavallo, K., Behar, S.M., 2021. CD4 T cell help prevents CD8 T cell exhaustion and promotes control of Mycobacterium tuberculosis infection. Cell Rep. 36, 109696. https://doi.org/10.1016/j.celrep.2021.109696

Lückel, C., Picard, Felix.S.R., Huber, M., 2020. Tc17 biology and function: Novel concepts. Eur. J. Immunol. 50, 1257–1267. https://doi.org/10.1002/eji.202048627

Lyadova, I.V., Panteleev, A.V., 2015. Th1 and Th17 Cells in Tuberculosis: Protection, Pathology, and Biomarkers. Mediators Inflamm. 2015, 1–13. https://doi.org/10.1155/2015/854507

Martin, C.J., Cadena, A.M., Leung, V.W., Lin, P.L., Maiello, P., Hicks, N., Chase, M.R., Flynn, J.L., Fortune, S.M., 2017. Digitally Barcoding *Mycobacterium tuberculosis* Reveals *In Vivo* Infection Dynamics in the Macaque Model of Tuberculosis. mBio 8, e00312-17. https://doi.org/10.1128/mBio.00312-17

McCaffrey, E.F., Donato, M., Keren, L., Chen, Z., Delmastro, A., Fitzpatrick, M.B., Gupta, S., Greenwald, N.F., Baranski, A., Graf, W., Kumar, R., Bosse, M., Fullaway, C.C., Ramdial, P.K., Forgó, E., Jojic, V., Van Valen, D., Mehra, S., Khader, S.A., Bendall, S.C., Van De Rijn, M., Kalman, D., Kaushal, D., Hunter, R.L., Banaei, N., Steyn, A.J.C., Khatri, P., Angelo, M., 2022. The immunoregulatory landscape of human tuberculosis granulomas. Nat. Immunol. 23, 318–329. https://doi.org/10.1038/s41590-021-01121-x

Mehra, S., Pahar, B., Dutta, N.K., Conerly, C.N., Philippi-Falkenstein, K., Alvarez, X., Kaushal, D., 2010. Transcriptional Reprogramming in Nonhuman Primate (Rhesus Macaque) Tuberculosis Granulomas. PLoS ONE 5, e12266. https://doi.org/10.1371/journal.pone.0012266

Micheni, L.N., Kassaza, K., Kinyi, H., Ntulume, I., Bazira, J., 2022. Detection of Mycobacterium tuberculosis multiple strains in sputum samples from patients with pulmonary tuberculosis in south western Uganda using MIRU-VNTR. Sci. Rep. 12, 1656. https://doi.org/10.1038/s41598-022-05591-3

1025 Milner, J.J., Toma, C., He, Z., Kurd, N.S., Nguyen, Q.P., McDonald, B., Quezada, L., Widjaja,
1026 C.E., Witherden, D.A., Crowl, J.T., Shaw, L.A., Yeo, G.W., Chang, J.T., Omilusik, K.D.,
1027 Goldrath, A.W., 2020. Heterogenous Populations of Tissue-Resident CD8+ T Cells Are
1028 Generated in Response to Infection and Malignancy. Immunity 52, 808-824.e7.
1029 https://doi.org/10.1016/j.immuni.2020.04.007
1030 Miyamoto, M., Prause, O., Sjöstrand, M., Laan, M., Lötvall, J., Lindén, A., 2003. Endogenous
1031 IL-17 as a Mediator of Neutrophil Recruitment Caused by Endotoxin Exposure in Mouse
1032 Airways. J. Immunol. 170, 4665–4672. https://doi.org/10.4049/jimmunol.170.9.4665
1033 Mogilenko, D.A., Shpynov, O., Andhey, P.S., Arthur, L., Swain, A., Esaulova, E., Brioschi, S.,
1034 Shchukina, I., Kerndl, M., Bambouskova, M., Yao, Z., Laha, A., Zaitsev, K., Burdess, S.,
1035 Gillfilan, S., Stewart, S.A., Colonna, M., Artyomov, M.N., 2021. Comprehensive
1036 Profiling of an Aging Immune System Reveals Clonal GZMK+ CD8+ T Cells as
1037 Conserved Hallmark of Inflammaging. Immunity 54, 99-115.e12.
1038 https://doi.org/10.1016/j.immuni.2020.11.005
1039 Moguche, A.O., Musvosvi, M., Penn-Nicholson, A., Plumlee, C.R., Mearns, H., Geldenhuys, H.,
1040 Smit, E., Abrahams, D., Rozot, V., Dintwe, O., Hoff, S.T., Kromann, I., Ruhwald, M.,
1041 Bang, P., Larson, R.P., Shafiani, S., Ma, S., Sherman, D.R., Sette, A., Lindestam
1042 Arlehamn, C.S., McKinney, D.M., Maecker, H., Hanekom, W.A., Hatherill, M.,
1043 Andersen, P., Scriba, T.J., Urdahl, K.B., 2017. Antigen Availability Shapes T Cell
1044 Differentiation and Function during Tuberculosis. Cell Host Microbe 21, 695-706.e5.
1045 https://doi.org/10.1016/j.chom.2017.05.012
1046 Montaldo, E., Lusito, E., Bianchessi, V., Caronni, N., Scala, S., Basso-Ricci, L., Cantaffa, C.,
1047 Masserdotti, A., Barilaro, M., Barresi, S., Genua, M., Vittoria, F.M., Barbiera, G.,
1048 Lazarevic, D., Messina, C., Xue, E., Marktel, S., Tresoldi, C., Milani, R., Ronchi, P.,
1049 Gattillo, S., Santoleri, L., Di Micco, R., Ditadi, A., Belfiori, G., Aleotti, F., Naldini,
1050 M.M., Gentner, B., Gardiman, E., Tamassia, N., Cassatella, M.A., Hidalgo, A., Kwok, I.,
1051 Ng, L.G., Crippa, S., Falconi, M., Pettinella, F., Scapini, P., Naldini, L., Ciceri, F., Aiuti,
1052 A., Ostuni, R., 2022. Cellular and transcriptional dynamics of human neutrophils at
1053 steady state and upon stress. Nat. Immunol. 23, 1470–1483.
1054 https://doi.org/10.1038/s41590-022-01311-1
1055 Moreira-Teixeira, L., Stimpson, P.J., Stavropoulos, E., Hadebe, S., Chakravarty, P., Ioannou, M.,
1056 Aramburu, I.V., Herbert, E., Priestnall, S.L., Suarez-Bonnet, A., Sousa, J., Fonseca, K.L.,
1057 Wang, Q., Vashakidze, S., Rodríguez-Martínez, P., Vilaplana, C., Saraiva, M.,
1058 Papayannopoulos, V., O'Garra, A., 2020. Type I IFN exacerbates disease in tuberculosis-
1059 susceptible mice by inducing neutrophil-mediated lung inflammation and NETosis. Nat.
1060 Commun. 11, 5566. https://doi.org/10.1038/s41467-020-19412-6
1061 Moss, A.R., Hahn, J.A., Tulsky, J.P., Daley, C.L., Small, P.M., Hopewell, P.C., 2000.
1062 Tuberculosis in the Homeless: A Prospective Study. Am. J. Respir. Crit. Care Med. 162,
1063 460–464. https://doi.org/10.1164/ajrccm.162.2.9910055
1064 Muñoz-Elías, E.J., Timm, J., Botha, T., Chan, W.-T., Gomez, J.E., McKinney, J.D., 2005a.
1065 Replication Dynamics of *Mycobacterium tuberculosis* in Chronically Infected Mice.
1066 Infect. Immun. 73, 546–551. https://doi.org/10.1128/IAI.73.1.546-551.2005
1067 Muñoz-Elías, E.J., Timm, J., Botha, T., Chan, W.-T., Gomez, J.E., McKinney, J.D., 2005b.
1068 Replication Dynamics of *Mycobacterium tuberculosis* in Chronically Infected Mice.
1069 Infect. Immun. 73, 546–551. https://doi.org/10.1128/IAI.73.1.546-551.2005

1070 Nemeth, J., Olson, G.S., Rothchild, A.C., Jahn, A.N., Mai, D., Duffy, F.J., Delahaye, J.L.,
1071 Srivatsan, S., Plumlee, C.R., Urdahl, K.B., Gold, E.S., Aderem, A., Diercks, A.H., 2020.
1072 Contained Mycobacterium tuberculosis infection induces concomitant and heterologous
1073 protection. PLOS Pathog. 16, e1008655. https://doi.org/10.1371/journal.ppat.1008655
1074 Nonghanphithak, D., Reechaipichitkul, W., Namwat, W., Naranbhai, V., Faksri, K., 2017.
1075 Chemokines additional to IFN-γ can be used to differentiate among Mycobacterium
1076 tuberculosis infection possibilities and provide evidence of an early clearance phenotype.
1077 Tuberculosis 105, 28–34. https://doi.org/10.1016/j.tube.2017.04.005
1078 Nunes-Alves, C., Booty, M.G., Carpenter, S.M., Jayaraman, P., Rothchild, A.C., Behar, S.M.,
1079 2014. In search of a new paradigm for protective immunity to TB. Nat. Rev. Microbiol.
1080 12, 289–299. https://doi.org/10.1038/nrmicro3230
1081 O'Leary, S., O'Sullivan, M.P., Keane, J., 2011. IL-10 Blocks Phagosome Maturation in
1082 *Mycobacterium tuberculosis*– Infected Human Macrophages. Am. J. Respir. Cell Mol.
1083 Biol. 45, 172–180. https://doi.org/10.1165/rcmb.2010-0319OC
1084 Oliveira, G., Stromhaug, K., Klaeger, S., Kula, T., Frederick, D.T., Le, P.M., Forman, J., Huang,
1085 T., Li, S., Zhang, W., Xu, Q., Cieri, N., Clauser, K.R., Shukla, S.A., Neuberg, D.,
1086 Justesen, S., MacBeath, G., Carr, S.A., Fritsch, E.F., Hacohen, N., Sade-Feldman, M.,
1087 Livak, K.J., Boland, G.M., Ott, P.A., Keskin, D.B., Wu, C.J., 2021. Phenotype,
1088 specificity and avidity of antitumour CD8+ T cells in melanoma. Nature 596, 119–125.
1089 https://doi.org/10.1038/s41586-021-03704-y
1090 Ong, C.W.M., Fox, K., Ettorre, A., Elkington, P.T., Friedland, J.S., 2018. Hypoxia increases
1091 neutrophil-driven matrix destruction after exposure to Mycobacterium tuberculosis. Sci.
1092 Rep. 8, 11475. https://doi.org/10.1038/s41598-018-29659-1
1093 Pagán, A.J., Ramakrishnan, L., 2018. The Formation and Function of Granulomas. Annu. Rev.
1094 Immunol. 36, 639–665. https://doi.org/10.1146/annurev-immunol-032712-100022
1095 Pagán, A.J., Ramakrishnan, L., 2015. Immunity and Immunopathology in the Tuberculous
1096 Granuloma. Cold Spring Harb. Perspect. Med. 5, a018499.
1097 https://doi.org/10.1101/cshperspect.a018499
1098 Pelletier, M., Maggi, L., Micheletti, A., Lazzeri, E., Tamassia, N., Costantini, C., Cosmi, L.,
1099 Lunardi, C., Annunziato, F., Romagnani, S., Cassatella, M.A., 2010. Evidence for a
1100 cross-talk between human neutrophils and Th17 cells. Blood 115, 335–343.
1101 https://doi.org/10.1182/blood-2009-04-216085
1102 Phillipson, M., Kubes, P., 2011. The neutrophil in vascular inflammation. Nat. Med. 17, 1381–
1103 1390. https://doi.org/10.1038/nm.2514
1104 Pisu, D., Huang, L., Narang, V., Theriault, M., Lê-Bury, G., Lee, B., Lakudzala, A.E., Mzinza,
1105 D.T., Mhango, D.V., Mitini-Nkhoma, S.C., Jambo, K.C., Singhal, A., Mwandumba,
1106 H.C., Russell, D.G., 2021. Single cell analysis of *M. tuberculosis* phenotype and
1107 macrophage lineages in the infected lung. J. Exp. Med. 218, e20210615.
1108 https://doi.org/10.1084/jem.20210615
1109 Poon, M.M.L., Caron, D.P., Wang, Z., Wells, S.B., Chen, D., Meng, W., Szabo, P.A., Lam, N.,
1110 Kubota, M., Matsumoto, R., Rahman, A., Luning Prak, E.T., Shen, Y., Sims, P.A.,
1111 Farber, D.L., 2023. Tissue adaptation and clonal segregation of human memory T cells in
1112 barrier sites. Nat. Immunol. 24, 309–319. https://doi.org/10.1038/s41590-022-01395-9
1113 Rashidi, M., Bandala-Sanchez, E., Lawlor, K.E., Zhang, Y., Neale, A.M., Vijayaraj, S.L.,
1114 O'Donoghue, R., Wentworth, J.M., Adams, T.E., Vince, J.E., Harrison, L.C., 2018.

CD52 inhibits Toll-like receptor activation of NF-κB and triggers apoptosis to suppress inflammation. Cell Death Differ. 25, 392–405. https://doi.org/10.1038/cdd.2017.173

Ravesloot-Chávez, M.M., Van Dis, E., Stanley, S.A., 2021. The Innate Immune Response to *Mycobacterium tuberculosis* Infection. Annu. Rev. Immunol. 39, 611–637. https://doi.org/10.1146/annurev-immunol-093019-010426

Redford, P.S., Boonstra, A., Read, S., Pitt, J., Graham, C., Stavropoulos, E., Bancroft, G.J., O'Garra, A., 2010. Enhanced protection to Mycobacterium tuberculosis infection in IL-10-deficient mice is accompanied by early and enhanced Th1 responses in the lung. Eur. J. Immunol. 40, 2200–2210. https://doi.org/10.1002/eji.201040433

Redford, P.S., Murray, P.J., O'Garra, A., 2011. The role of IL-10 in immune regulation during M. tuberculosis infection. Mucosal Immunol. 4, 261–270. https://doi.org/10.1038/mi.2011.7

Rene de Waal Malefy, John Haanen, Hergen Spits, Maria-Grazia Koncarolo, Anje te Velde, Carl Figdor, Karen Johnson, Rob Kastelein, Hans Ysse, Jan E. de Vries, 1991. Interleukin 10 (IL-10) and Viral IL-10 Strongly Reduce Antigen-specific Human T Cell Proliferation by Diminishing the Antigen-presenting Capacity of Monocytes via Dowm'egulation of Class H Major Histocompatibility Complex Expression By Ren6 de WaalMalefyt,John Haanen, HergenSpits,. J. Exp. Med.

Ruhwald, M., Bjerregaard-Andersen, M., Rabna, P., Kofoed, K., Eugen-Olsen, J., Ravn, P., 2007. CXCL10/IP-10 release is induced by incubation of whole blood from tuberculosis patients with ESAT-6, CFP10 and TB7.7. Microbes Infect. 9, 806–812. https://doi.org/10.1016/j.micinf.2007.02.021

Sakai, S., Kauffman, K.D., Sallin, M.A., Sharpe, A.H., Young, H.A., Ganusov, V.V., Barber, D.L., 2016. CD4 T Cell-Derived IFN-γ Plays a Minimal Role in Control of Pulmonary Mycobacterium tuberculosis Infection and Must Be Actively Repressed by PD-1 to Prevent Lethal Disease. PLOS Pathog. 12, e1005667. https://doi.org/10.1371/journal.ppat.1005667

Sakai, S., Mayer-Barber, K.D., Barber, D.L., 2014. Defining features of protective CD4 T cell responses to Mycobacterium tuberculosis. Curr. Opin. Immunol. 29, 137–142. https://doi.org/10.1016/j.coi.2014.06.003

Sangster, M.Y., Riberdy, J.M., Gonzalez, M., Topham, D.J., Baumgarth, N., Doherty, P.C., 2003. An Early CD4+ T Cell–dependent Immunoglobulin A Response to Influenza Infection in the Absence of Key Cognate T–B Interactions. J. Exp. Med. 198, 1011–1021. https://doi.org/10.1084/jem.20021745

Scanga, C.A., Mohan, V.P., Yu, K., Joseph, H., Tanaka, K., Chan, J., Flynn, J.L., 2000. Depletion of CD4ƨ T Cells Causes Reactivation of Murine Persistent Tuberculosis Despite Continued Expression of Interferon ⁄⁄ and Nitric Oxide Synthase 2. J. Exp. Med.

Schoenberger, S.P., Toes, R.E.M., van der Voort, E.I.H., Offringa, R., Melief, C.J.M., 1998. T-cell help for cytotoxic T lymphocytes is mediated by CD40–CD40L interactions. Nature 393, 480–483. https://doi.org/10.1038/31002

Seiler, P., Aichele, P., Bandermann, S., Hauser, A.E., Lu, B., Gerard, N.P., Gerard, C., Ehlers, S., Mollenkopf, H.J., Kaufmann, S.H.E., 2003. Early granuloma formation after aerosolMycobacterium tuberculosis infection is regulated by neutrophils via CXCR3-signaling chemokines. Eur. J. Immunol. 33, 2676–2686. https://doi.org/10.1002/eji.200323956

1160 Shedlock, D.J., Shen, H., 2003. Requirement for CD4 T Cell Help in Generating Functional CD8
1161 T Cell Memory. Science 300, 337–339. https://doi.org/10.1126/science.1082305
1162 Shen, X., Yang, C., Wu, J., Lin, S., Gao, X., Wu, Z., Tian, J., Gan, M., Luo, T., Wang, L., Yu,
1163 C., Mei, J., Pan, Q., DeRiemer, K., Yuan, Z., Gao, Q., 2017. Recurrent tuberculosis in an
1164 urban area in China: Relapse or exogenous reinfection? Tuberculosis 103, 97–104.
1165 https://doi.org/10.1016/j.tube.2017.01.007
1166 Sikkema, L., Ramírez-Suástegui, C., Strobl, D.C., Gillett, T.E., Zappia, L., Madissoon, E.,
1167 Markov, N.S., Zaragosi, L.-E., Ji, Y., Ansari, M., Arguel, M.-J., Apperloo, L., Banchero,
1168 M., Bécavin, C., Berg, M., Chichelnitskiy, E., Chung, M., Collin, A., Gay, A.C.A., Gote-
1169 Schniering, J., Hooshiar Kashani, B., Inecik, K., Jain, M., Kapellos, T.S., Kole, T.M.,
1170 Leroy, S., Mayr, C.H., Oliver, A.J., Von Papen, M., Peter, L., Taylor, C.J., Walzthoeni,
1171 T., Xu, C., Bui, L.T., De Donno, C., Dony, L., Faiz, A., Guo, M., Gutierrez, A.J.,
1172 Heumos, L., Huang, N., Ibarra, I.L., Jackson, N.D., Kadur Lakshminarasimha Murthy, P.,
1173 Lotfollahi, M., Tabib, T., Talavera-López, C., Travaglini, K.J., Wilbrey-Clark, A.,
1174 Worlock, K.B., Yoshida, M., Lung Biological Network Consortium, Chen, Y., Hagood,
1175 J.S., Agami, A., Horvath, P., Lundeberg, J., Marquette, C.-H., Pryhuber, G., Samakovlis,
1176 C., Sun, X., Ware, L.B., Zhang, K., Van Den Berge, M., Bossé, Y., Desai, T.J.,
1177 Eickelberg, O., Kaminski, N., Krasnow, M.A., Lafyatis, R., Nikolic, M.Z., Powell, J.E.,
1178 Rajagopal, J., Rojas, M., Rozenblatt-Rosen, O., Seibold, M.A., Sheppard, D., Shepherd,
1179 D.P., Sin, D.D., Timens, W., Tsankov, A.M., Whitsett, J., Xu, Y., Banovich, N.E.,
1180 Barbry, P., Duong, T.E., Falk, C.S., Meyer, K.B., Kropski, J.A., Pe'er, D., Schiller, H.B.,
1181 Tata, P.R., Schultze, J.L., Teichmann, S.A., Misharin, A.V., Nawijn, M.C., Luecken,
1182 M.D., Theis, F.J., 2023. An integrated cell atlas of the lung in health and disease. Nat.
1183 Med. 29, 1563–1577. https://doi.org/10.1038/s41591-023-02327-2
1184 Silveira-Mattos, P.S., Narendran, G., Akrami, K., Fukutani, K.F., Anbalagan, S., Nayak, K.,
1185 Subramanyam, S., Subramani, R., Vinhaes, C.L., Souza, D.O., Antonelli, L.R.,
1186 Satagopan, K., Porter, B.O., Sher, A., Swaminathan, S., Sereti, I., Andrade, B.B., 2019.
1187 Differential expression of CXCR3 and CCR6 on CD4+ T-lymphocytes with distinct
1188 memory phenotypes characterizes tuberculosis-associated immune reconstitution
1189 inflammatory syndrome. Sci. Rep. 9, 1502. https://doi.org/10.1038/s41598-018-37846-3
1190 Smillie, C.S., Biton, M., Ordovas-Montanes, J., Sullivan, K.M., Burgin, G., Graham, D.B.,
1191 Herbst, R.H., Rogel, N., Slyper, M., Waldman, J., Sud, M., Andrews, E., Velonias, G.,
1192 Haber, A.L., Jagadeesh, K., Vickovic, S., Yao, J., Stevens, C., Dionne, D., Nguyen, L.T.,
1193 Villani, A.-C., Hofree, M., Creasey, E.A., Huang, H., Rozenblatt-Rosen, O., Garber, J.J.,
1194 Khalili, H., Desch, A.N., Daly, M.J., Ananthakrishnan, A.N., Shalek, A.K., Xavier, R.J.,
1195 Regev, A., 2019. Intra- and Inter-cellular Rewiring of the Human Colon during
1196 Ulcerative Colitis. Cell 178, 714-730.e22. https://doi.org/10.1016/j.cell.2019.06.029
1197 Srivastava, S., Ernst, J.D., 2013. Cutting Edge: Direct Recognition of Infected Cells by CD4 T
1198 Cells Is Required for Control of Intracellular *Mycobacterium tuberculosis* In Vivo. J.
1199 Immunol. 191, 1016–1020. https://doi.org/10.4049/jimmunol.1301236
1200 Stephen, T.L., Payne, K.K., Chaurio, R.A., Allegrezza, M.J., Zhu, H., Perez-Sanz, J., Perales-
1201 Puchalt, A., Nguyen, J.M., Vara-Ailor, A.E., Eruslanov, E.B., Borowsky, M.E., Zhang,
1202 R., Laufer, T.M., Conejo-Garcia, J.R., 2017. SATB1 Expression Governs Epigenetic
1203 Repression of PD-1 in Tumor-Reactive T Cells. Immunity 46, 51–64.
1204 https://doi.org/10.1016/j.immuni.2016.12.015

1205 Sun, J., Cardani, A., Sharma, A.K., Laubach, V.E., Jack, R.S., Müller, W., Braciale, T.J., 2011.
1206 Autocrine Regulation of Pulmonary Inflammation by Effector T-Cell Derived IL-10
1207 during Infection with Respiratory Syncytial Virus. PLoS Pathog. 7, e1002173.
1208 https://doi.org/10.1371/journal.ppat.1002173
1209 Sun, J., Madan, R., Karp, C.L., Braciale, T.J., 2009. Effector T cells control lung inflammation
1210 during acute influenza virus infection by producing IL-10. Nat. Med. 15, 277–284.
1211 https://doi.org/10.1038/nm.1929
1212 Sun, K., Xu, R., Ma, F., Yang, N., Li, Y., Sun, X., Jin, P., Kang, W., Jia, L., Xiong, J., Hu, H.,
1213 Tian, Y., Lan, X., 2022. scRNA-seq of gastric tumor shows complex intercellular
1214 interaction with an alternative T cell exhaustion trajectory. Nat. Commun. 13, 4943.
1215 https://doi.org/10.1038/s41467-022-32627-z
1216 Suzuki, M., Tachibana, I., Takeda, Y., He, P., Minami, S., Iwasaki, T., Kida, H., Goya, S.,
1217 Kijima, T., Yoshida, M., Kumagai, T., Osaki, T., Kawase, I., 2009. Tetraspanin CD9
1218 Negatively Regulates Lipopolysaccharide-Induced Macrophage Activation and Lung
1219 Inflammation. J. Immunol. 182, 6485–6493. https://doi.org/10.4049/jimmunol.0802797
1220 Szabo, P.A., Levitin, H.M., Miron, M., Snyder, M.E., Senda, T., Yuan, J., Cheng, Y.L., Bush,
1221 E.C., Dogra, P., Thapa, P., Farber, D.L., Sims, P.A., 2019. Single-cell transcriptomics of
1222 human T cells reveals tissue and activation signatures in health and disease. Nat.
1223 Commun. 10, 4706. https://doi.org/10.1038/s41467-019-12464-3
1224 Terekhova, M., Swain, A., Bohacova, P., Aladyeva, E., Arthur, L., Laha, A., Mogilenko, D.A.,
1225 Burdess, S., Sukhov, V., Kleverov, D., Echalar, B., Tsurinov, P., Chernyatchik, R.,
1226 Husarcikova, K., Artyomov, M.N., 2023. Single-cell atlas of healthy human blood
1227 unveils age-related loss of NKG2C+GZMB−CD8+ memory T cells and accumulation of
1228 type 2 memory T cells. Immunity S1074761323004533.
1229 https://doi.org/10.1016/j.immuni.2023.10.013
1230 Thomas, M.F., Slowikowski, K., Manakongtreecheep, K., Sen, P., Tantivit, J., Nasrallah, M.,
1231 Smith, N.P., Ramesh, S., Zubiri, L., Tirard, A., Arnold, B.Y., Nieman, L.T., Chen, J.H.,
1232 Eisenhaure, T., Pelka, K., Xu, K.H., Jorgji, V., Pinto, C.J., Sharova, T., Glasser, R., Chan,
1233 E.P., Sullivan, R.J., Khalili, H., Juric, D., Boland, G.M., Dougan, M., Hacohen, N.,
1234 Reynolds, K.L., Li, B., Villani, A.-C., 2021. Altered interactions between circulating and
1235 tissue-resident CD8 T cells with the colonic mucosa define colitis associated with
1236 immune checkpoint inhibitors (preprint). Immunology.
1237 https://doi.org/10.1101/2021.09.17.460868
1238 Van Rie, A., Warren, R., Richardson, M., Victor, T.C., Gie, R.P., Enarson, D.A., Beyers, N.,
1239 Van Helden, P.D., 1999. Exogenous Reinfection as a Cause of Recurrent Tuberculosis
1240 after Curative Treatment. N. Engl. J. Med. 341, 1174–1179.
1241 https://doi.org/10.1056/NEJM199910143411602
1242 Vargas, R., Freschi, L., Marin, M., Epperson, L.E., Smith, M., Oussenko, I., Durbin, D., Strong,
1243 M., Salfinger, M., Farhat, M.R., 2021. In-host population dynamics of Mycobacterium
1244 tuberculosis complex during active disease. eLife 10, e61805.
1245 https://doi.org/10.7554/eLife.61805
1246 Verver, S., Warren, R.M., Beyers, N., Richardson, M., Van Der Spuy, G.D., Borgdorff, M.W.,
1247 Enarson, D.A., Behr, M.A., Van Helden, P.D., 2005. Rate of Reinfection Tuberculosis
1248 after Successful Treatment Is Higher than Rate of New Tuberculosis. Am. J. Respir. Crit.
1249 Care Med. 171, 1430–1435. https://doi.org/10.1164/rccm.200409-1200OC

1250 Vignali, P.D.A., DePeaux, K., Watson, M.J., Ye, C., Ford, B.R., Lontos, K., McGaa, N.K.,
1251 Scharping, N.E., Menk, A.V., Robson, S.C., Poholek, A.C., Rivadeneira, D.B., Delgoffe,
1252 G.M., 2023. Hypoxia drives CD39-dependent suppressor function in exhausted T cells to
1253 limit antitumor immunity. Nat. Immunol. 24, 267–279. https://doi.org/10.1038/s41590-
1254 022-01379-9
1255 Weisberg, S.P., Ural, B.B., Farber, D.L., 2021. Tissue-specific immunity for a changing world.
1256 Cell 184, 1517–1529. https://doi.org/10.1016/j.cell.2021.01.042
1257 White, A.G., Maiello, P., Coleman, M.T., Tomko, J.A., Frye, L.J., Scanga, C.A., Lin, P.L.,
1258 Flynn, J.L., 2017. Analysis of ^{18}FDG PET/CT Imaging as a Tool for Studying
1259 Mycobacterium tuberculosis Infection and Treatment in Non-human Primates. J. Vis.
1260 Exp. 56375. https://doi.org/10.3791/56375
1261 Witney, A.A., Bateson, A.L.E., Jindani, A., Phillips, P.P.J., Coleman, D., Stoker, N.G., Butcher,
1262 P.D., McHugh, T.D., 2017. Use of whole-genome sequencing to distinguish relapse from
1263 reinfection in a completed tuberculosis clinical trial. BMC Med. 15, 71.
1264 https://doi.org/10.1186/s12916-017-0834-4
1265 Wollenberg, K., Harris, M., Gabrielian, A., Ciobanu, N., Chesov, D., Long, A., Taaffe, J., Hurt,
1266 D., Rosenthal, A., Tartakovsky, M., Crudu, V., 2020. A retrospective genomic analysis of
1267 drug-resistant strains of M. tuberculosis in a high-burden setting, with an emphasis on
1268 comparative diagnostics and reactivation and reinfection status. BMC Infect. Dis. 20, 17.
1269 https://doi.org/10.1186/s12879-019-4739-z
1270 Wong, E.A., Evans, S., Kraus, C.R., Engelman, K.D., Maiello, P., Flores, W.J., Cadena, A.M.,
1271 Klein, E., Thomas, K., White, A.G., Causgrove, C., Stein, B., Tomko, J., Mattila, J.T.,
1272 Gideon, H., Lin, P.L., Reimann, K.A., Kirschner, D.E., Flynn, J.L., 2020. IL-10 Impairs
1273 Local Immune Response in Lung Granulomas and Lymph Nodes during Early
1274 *Mycobacterium tuberculosis* Infection. J. Immunol. 204, 644–659.
1275 https://doi.org/10.4049/jimmunol.1901211
1276 Xie, X., Shi, Q., Wu, P., Zhang, X., Kambara, H., Su, J., Yu, H., Park, S.-Y., Guo, R., Ren, Q.,
1277 Zhang, S., Xu, Y., Silberstein, L.E., Cheng, T., Ma, F., Li, C., Luo, H.R., 2020. Single-
1278 cell transcriptome profiling reveals neutrophil heterogeneity in homeostasis and infection.
1279 Nat. Immunol. 21, 1119–1133. https://doi.org/10.1038/s41590-020-0736-z
1280 Xu, W., Snell, L.M., Guo, M., Boukhaled, G., Macleod, B.L., Li, M., Tullius, M.V., Guidos,
1281 C.J., Tsao, M.-S., Divangahi, M., Horwitz, M.A., Liu, J., Brooks, D.G., 2021. Early
1282 innate and adaptive immune perturbations determine long-term severity of chronic virus
1283 and Mycobacterium tuberculosis coinfection. Immunity 54, 526-541.e7.
1284 https://doi.org/10.1016/j.immuni.2021.01.003
1285 Yao, S., Huang, D., Chen, C.Y., Halliday, L., Wang, R.C., Chen, Z.W., 2014. CD4+ T Cells
1286 Contain Early Extrapulmonary Tuberculosis (TB) Dissemination and Rapid TB
1287 Progression and Sustain Multieffector Functions of CD8+ T and CD3− Lymphocytes:
1288 Mechanisms of CD4+ T Cell Immunity. J. Immunol. 192, 2120–2132.
1289 https://doi.org/10.4049/jimmunol.1301373
1290 Yao, Y., Jeyanathan, M., Haddadi, S., Barra, N.G., Vaseghi-Shanjani, M., Damjanovic, D., Lai,
1291 R., Afkhami, S., Chen, Y., Dvorkin-Gheva, A., Robbins, C.S., Schertzer, J.D., Xing, Z.,
1292 2018. Induction of Autonomous Memory Alveolar Macrophages Requires T Cell Help
1293 and Is Critical to Trained Immunity. Cell 175, 1634-1650.e17.
1294 https://doi.org/10.1016/j.cell.2018.09.042

Yost, K.E., Satpathy, A.T., Wells, D.K., Qi, Y., Wang, C., Kageyama, R., McNamara, K.L., Granja, J.M., Sarin, K.Y., Brown, R.A., Gupta, R.K., Curtis, C., Bucktrout, S.L., Davis, M.M., Chang, A.L.S., Chang, H.Y., 2019. Clonal replacement of tumor-specific T cells following PD-1 blockade. Nat. Med. 25, 1251–1259. https://doi.org/10.1038/s41591-019-0522-3

Zander, R., Schauder, D., Xin, G., Nguyen, C., Wu, X., Zajac, A., Cui, W., 2019. CD4+ T Cell Help Is Required for the Formation of a Cytolytic CD8+ T Cell Subset that Protects against Chronic Infection and Cancer. Immunity 51, 1028-1042.e4. https://doi.org/10.1016/j.immuni.2019.10.009

Zheng, L., Qin, S., Si, W., Wang, A., Xing, B., Gao, R., Ren, X., Wang, L., Wu, X., Zhang, J., Wu, N., Zhang, N., Zheng, H., Ouyang, H., Chen, K., Bu, Z., Hu, X., Ji, J., Zhang, Z., 2021. Pan-cancer single-cell landscape of tumor-infiltrating T cells. Science 374, abe6474. https://doi.org/10.1126/science.abe6474

TABLE 1

T cell subset	Cluster defining genes
Naïve, central memory-like ($T_{Naïve/CM\text{-}like}$) T cells	*CCR7, SELL, LEF1, S1PR1, PECAM2*
T1-T17-like	*IFNG, IL23R, BHLHE40, RORA*
Memory-like ($T_{M\text{-}like}$) T cells	*CD28, IL7R, CAPG, SAMSN1*
FURIN^{hi} Memory-like ($T_{M\text{-}like}$) T cells	*FURIN, SPOCK2, RBPJ*
Regulatory (T_{reg})	*FOXP3*, *TIGIT, BATF*
Effector-like ($T_{Eff\text{-}like}$) T cells	*GZMA, GZMB, PRF1*
Innate-like cells (ILCs)	*XCL1, CD69, EGR1*
Natural killer-like (NK-like)	*FCGR3A*, *TYROBP*, *NKG2C*
Effector memory cells re-expressing CD45RA ($T_{EMRA\text{-}like}$)	*CX3CR1, GZMH, GZMB, PRF1, KLF3*
Effector memory/Precursor to exhausted-like ($T_{EM/EX\text{-}like}$)	*GZMK, GPR183, EOMES, CXCR4, TOX, TIGIT*
Cytotoxic T-17-like cells (Tc17-like)	*ZBTB16, KLRG1, CCR6, RORA, NR4A1*

KEY RESOURCES TABLE

REAGENT or RESOURCE	**SOURCE**	**IDENTIFIER**
Antibodies		
Mouse anti-human CD3, clone SP34-2	BD Biosciences	
Mouse anti-human CD4, clone L200	BD Biosciences	
Rabbit anti-human CD20, polyclonal	ThermoFisher	
Bacterial and virus strains		
Mycobacterium Tuberculosis: Erdman strain	Flynn Lab	N/A
Biological samples		
Cynomolgus macaque granulomas	This study	N/A
Chemicals, peptides, and recombinant proteins		
2-Mercaptoethanol	Sigma	Cat# M3148-25ML
RLT Buffer	QIAGEN	Cat#79216
dNTP	New England BioLabs	Cat#N0447L
RNase Inhibitor	Fisher Scientific	Cat#AM2696
Maxima RNaseH-minus RT Enzyme	Fisher Scientific	Cat#EP0753
AMPure RNAClean XP RNA-SPRI beads	Beckman Coulter	Cat#A63987
AMPure XP SPRI beads	Beckman Coulter	Cat#A63881

Guanidinium thiocynate	Sigma	Cat#AM9422
Sarkosyl	Sigma	Cat#L7414
Exonuclease I	New England BioLabs	Cat#M0293S
Klenow Fragment	New England BioLabs	Cat# M0212L
Accutase	Sigma	Cat#A6964
Dithiothreitol (DTT)	Sigma	Cat#43816
Polycarbonate membrane filters 62x22	Fisher Scientific/Sterlitech Corporation	Cat#NC0927472
Critical commercial assays		
Nextera XT DNA Library Prepartation Kit	Illumina	Cat#FC-131-1096
Kapa HiFi HotStart ReadyMix	Kapa Biosystems	Cat#KK2602
MACOSKO-2011-10 mRNA Capture Beads	ChemGenes	Cat#NC0927472
High Sensitivity D5000 ScreenTape	Agilent	Cat#5067-5592
Qubit dsDNA High-Sensitivity kit	Thermo Fisher	Cat#Q32854
Deposited data		
Processed and raw scRNA-seq data from primary infection, reinfection, and CD4-depletion animals	This study	Broad Single Cell Portal: SRA: PRJNA900256 https://dataview.ncbi.nlm.nih.gov/object/PRJNA900256?reviewer=slod9p79svi7p1sdcpskshjs1g
Experimental models: Organisms/strains		
Cynomolgus macaques	Valley Biosystems	N/A

Oligonucleotides		
Seq-Well ISPCR: AAG CAG TGG TAT CAA CGC AGA GT	Integrated DNA Technologies	N/A
Custom Read 1 Primer: GCC TGT CCG CGG AAG CAG TGG TAT CAA CGC AGA GTA C	Integrated DNA Technologies	N/A
Seq-Well 5' TSO: AAG CAG TGG TAT CAA CGC AGA GTG AAT rGrGrG	Integrated DNA Technologies	N/A
Seq-Well Custom P5-SMART PCR hybrid: AAT GAT ACG GCG ACC ACC GAG ATC TAC ACG CCT GTC CGC GGA AGC AGT GGT ATC AAC GCA GAG TAC	Integrated DNA Technologies	N/A
Seq-Well dN-SMRT oligo: AAG CAG TGG TAT CAA CGC AGA GTG ANN NGG NNN B	Integrated DNA Technologies	N/A
Software and Algorithims		
Python Progamming Language	Python	https://www.python.org/
Python package – Scanpy v1.9.5	Github Wolf et al.	https://github.com/scverse/scanpy
Python package – gseapy	Fang etl al., 2023	https://gseapy.readthedocs.io/en/latest/introduction.html
R package – Seurat v4.1.1	Browaeys et al., 2023	https://github.com/saeyslab/multinichenetr
R package – Seurat v4.1.1	Github	https://github.com/satijalab/seurat

CellBender	Fleming et al., 2019	https://github.com/broadinstitute/CellBender
Source code	This study	https://github.com/ShalekLab/scRNA_Reinfection_CD4_depletion/tree/main
R package – DESeq2 v1.30	Bioconductor	https://bioconductor.org/packages/release/bioc/html/DESeq2
Prism	GraphPad Software	https://www.graphpad.com/scientific-software/prism/E/

RESOURCE AVAILABILITY

Further information and requests for resources and reagents should be directed to and will be fulfilled by the lead contact Dr. JoAnne L Flynn (joanne@pitt.edu).

Data and Code Availability

scRNA-seq data is publicly available for download and visualization via the Alexandria and Broad Institute Single Cell Portal upon publication. Accession numbers and links are listed in the key resources table. All original code has been deposited at GitHub (https://github.com/ShalekLab) and is publicly available as of the date of publication. Any additional information required to reanalyze the data from this study is available from the lead contact upon request. All the data generated in support of the reported findings can be found at: https://fairdomhub.org/studies/1239 by the time of publication, including scRNASeq, barcoding, flow cytometry and PET-CT imaging data

EXPERIMENTAL MODEL AND SUBJECT DETAILS

Research Animals

All experimental manipulations, protocols, and care of the animals were approved by the University of Pittsburgh School of Medicine Institutional Animal Care and Use Committee (IACUC). The protocol assurance number for our IACUC is A3187-01. Our specific protocol approval number for this project is 15066174. The IACUC adheres to national guidelines established in the Animal Welfare Act (7 U.S.C. Sections 2131–2159) and the Guide for the Care

and Use of Laboratory Animals (8th Edition) as mandated by the U.S. Public Health Service Policy.

All macaques used in this study were housed at the University of Pittsburgh in rooms with autonomously controlled temperature, humidity, and lighting. Animals were singly housed in caging at least 2 square meters apart that allowed visual and tactile contact with neighboring conspecifics. The macaques were fed twice daily with biscuits formulated for nonhuman primates, supplemented at least 4 days/week with large pieces of fresh fruits or vegetables. Animals had access to water *ad libitem*. Because our macaques were singly housed due to the infectious nature of these studies, an enhanced enrichment plan was designed and overseen by our nonhuman primate enrichment specialist. This plan has 3 components. First, species-specific behaviors are encouraged. All animals have access to toys and other manipulata, some of which will be filled with food treats (e.g., frozen fruit, peanut butter, etc.). These are rotated on a regular basis. Puzzle feeders foraging boards, and cardboard tubes containing small food items also are placed in the cage to stimulate foraging behaviors. Adjustable mirrors accessible to the animals stimulate interaction between animals. Second, routine interaction between humans and macaques are encouraged. These interactions occur daily and consist mainly of small food objects offered as enrichment and adhere to established safety protocols. Animal caretakers are encouraged to interact with the animals (by talking or with facial expressions) while performing tasks in the housing area. Routine procedures (e.g., feeding, cage cleaning, etc) are done on a strict schedule to allow the animals to acclimate to a routine daily schedule. Third, all macaques are provided with a variety of visual and auditory stimulation. Housing areas contain either radios or TV/video equipment that play cartoons or other formats designed for children for at least 3 hours each day. The videos and radios are rotated between animal rooms so that the same enrichment is not played repetitively for the same group of animals.

All animals are checked at least twice daily to assess appetite, attitude, activity level, hydration status, etc. Following *M. tuberculosis* infection, the animals are monitored closely for evidence of disease (e.g., anorexia, weight loss, tachypnea, dyspnea, coughing). Physical exams, including weights, are performed on a regular basis. Animals are sedated prior to all veterinary procedures (e.g., blood draws, etc.) using ketamine or other approved drugs. Regular PET CT imaging is conducted on most of our macaques following infection and has proved very useful for monitoring disease progression. Our veterinary technicians monitor animals especially

closely for any signs of pain or distress. If any are noted, appropriate supportive care (e.g. dietary supplementation, rehydration) and clinical treatments (analgesics) are given. Any animal considered to have advanced disease or intractable pain or distress from any cause is sedated with ketamine and then humanely euthanatized using sodium pentobarbital.

METHOD DETAILS

Necropsy Procedures

Procedures done during necropsy have been previously described (Lin et al., 2009, 2006). Briefly, 1-3 days prior to necropsy, a PET CT scan was taken and used to identify the location and metabolic activity (FDG avidity) of granulomas and lymph nodes; this scan was used as a map to aid in the individual identification and excision of these samples during necropsy. On the day of necropsy, macaques were humanely sacrificed with sodium pentobarbital and terminally bled. Individual granulomas, thoracic and peripheral lymph nodes, lung tissue, spleen and liver were all excised and homogenized separately into single cell suspensions. New granulomas determined by PET-CT and uninvolved lung lobes (no granuloma present in the lobe) were enzymatically homogenized using a human tumor dissociation kit (Miltenyi Biotec) and a gentleMACS Dissociator (MiltenyiBiotec) following manufacturer's protocols. Homogenates were aliquoted for plating on 7H11 agar for bacterial burden, freezing for DNA extraction and staining for flow cytometry analysis. Any remaining samples were frozen for future use. Homogenates were plated in serial dilutions on 7H11 medium and incubated at 37°C/5% CO_2 for 3 weeks before enumeration of CFU.

Isolation of genomic DNA from bacteria

DNA extraction was performed on granuloma and lymph node homogenates, as well as their scrapates (scraped colonies that grew on 7H11 agar plates) for library identification as described previously (Lin et al., 2014). Briefly, a small aliquot of the homogenate or scrapate were vortexed with 0.1mm zirconia-silica beads (BioSpec Products, Inc.) and subsequently extracted twice with phenol chloroform isoamyl alcohol (25:24:1, Sigma-Aldrich) before precipitating DNA with molecular grade 100% isopropanol (Sigma-Aldrich) and 3M sodium acetate (Sigma-Aldrich) and resuspending in nuclease-free water (Invitrogen).

Library identification

Identification of library DNA tags have been previously described (Cadena et al., 2018). Briefly, DNA was amplified by PCR for 24-36 cycles before using in the NanoString nCounter assay (NanoString Technologies) with custom designed probes (Martin et al., 2017). New granulomas after reinfection were identified by PET-CT scan comparing pre- and post-reinfection scans and verified by presence of Library S barcodes.

Intracellular cytokine staining and flow cytometry

Because of the abundance of *Mtb* antigens already present in granulomas and involved lymph nodes (Gideon et al., 2015), these samples were not further stimulated with *Mtb* peptides (Gideon et al., 2015). Due to low number of cells, uninvolved lung lobes were also not stimulated. All samples were incubated in the presence of Brefeldin A (GolgiPlug, BD Biosciences) at 37°C/5% CO_2 for 3.5-4 hours prior to staining. Cells were stained with a viability marker (LIVE/DEAD fixable blue dead cell stain kit, Invitrogen) and surface and intracellular markers. Surface markers include CD3 (clone SP34-2, BD Pharmingen), CD4 (Clone L200, BD Horizon), CD8 (Clone SK1, BD Biosciences) and CD20 (Clone 2H7, eBioscience).

Animals, infections, CD4 depletion and disease tracking by PET CT

Nineteen cynomolgus macaques (*Macaca fasicularis*) with age range of 5.8-9.1 years were obtained from Valley Biosystems (Sacramento, California). Animals were placed in quarantine for 1 month where they were monitored to ensure good physical health and no prior *Mtb* infection. All animals were infected with Library P DNA-tagged *Mtb* Erdman via bronchoscopic instillation as previously described (Capuano et al., 2003; Lin et al., 2009). Thirteen macaques received *Mtb* library P as the first infection. Granuloma formation, lung inflammation and overall disease was tracked using ^{18}F-fluorodeoxyglucose (FDG) PET-CT every 4 weeks throughout infection. PET-CT scans were analyzed using OsiriX viewer as previously described with a detection limit of 1mm (White et al., 2017). The first infection was followed for 9 weeks before drug-treating all 13 macaques. Based on our previous study (Lin et al., 2012b), exacerbation of TB disease occurs after $CD4^+$ T cell depletion, thus to facilitate identification of new granulomas arising from the second infection we opted to treat all macaques with anti-TB drugs. Macaques were given anti-TB drugs orally once daily for 4-5 months (RIF 20mg/kg; INH

15mg/kg; ETH 50mg/kg; PZA 150mg/kg) (Lin et al., 2012a). Compliance ranged from 97-100%. The 13 macaques were matched by PET CT for disease status and randomized into 2 cohorts: $CD4^+$ T cell depletion (n=7) and IgG control (n=6). After resting for 4 weeks after drug treatment, CD4R1 (50mg/kg, NHP Reagent Resource), a rhesus recombinant $CD4^+$ T cell-depleting antibody, was administered subcutaneously in 4 animals and intravenously in 3 animals 1 week before the second infection with *Mtb* Library S and then was administered intravenously every 2 weeks until necropsy. $CD4^+$ T cell depletion was monitored by flow cytometry in the blood and complete blood count weekly. To measure $CD4^+$ T cell depletion in tissues, a peripheral lymph node biopsy was performed before $CD4^+$ T cell depletion and the $CD4^+$ T cell level was compared with a peripheral lymph node from the same macaque obtained at necropsy. Macaques from the IgG control group received rhesus recombinant IgG1 control antibody (50mg/kg, NHP Reagent Resource) following the same timeline of the $CD4^+$ T cell-depletion group. Six macaques were included as naïve controls infected with *Mtb* Library S only.

Macaques received 4-12 CFU of *Mtb* Library P for the first infection and 8-22 CFU of *Mtb* Library S for the second infection (or the first infection for the naïve monkeys). Dose was calculated from colony counts after plating an aliquot of the infection inoculum on 7H11 agar plates and incubating for 3 weeks at 37ºC/5% CO_2.

Antibody validation

To test whether the anti-$CD4^+$ depletion antibody masks CD4 receptors, peripheral blood mononuclear cells (PBMC) were incubated with 1X (0.77 mg/ml, the calculated concentration of αCD4 antibodies in blood of macaques given a dose of 50mg/kg), 0.25X and 4X concentration of CD4 T cell-depleting antibody for 30 minutes at 37ºC before surface staining with CD3 (clone SP34-2, BD Pharmingen), CD4 (Clone L200, BD Horizon) and CD8 (Clone RPA-T8, BD Biosciences) surface markers. PBMCs that were not incubated with the αCD4 antibody were included as a control. Data was acquired using the LSR II (BD) and analyzed using FlowJo software v10.6.1 (BD).

Single-cell RNA-sequencing (scRNA-seq) and alignment

Massively parallel scRNA-seq was performed using the Seq-Well S^3 platform, as previously described (Gierahn et al., 2017; Hughes et al., 2020). Approximately 15,000-20,000 cells were loaded onto Seq-Well arrays equipped with uniquely barcoded mRNA capture beads (ChemGenes). Cells were allowed to settle by gravity into wells for 10 minutes, after which the arrays were washed with PBS and serum-free RPMI. Arrays were then sealed with a semi-permiable polycarbonate membrane and incubated at 37°C for 30 minutes. Cell lysis was achieved by incubating the sealed arrays in a lysis buffer (5 M guanidine thiocyanate, 10 mM EDTA, 0.1% BME, and 0.1% sarkosyl) for 20 minutes. Subsequently, the arrays were rocked in hybridization buffer (2M NaCl, 8% v/v PEG8000) for 40 minutes. After membrane removal, the arrays were washed with in Seq-Well wash buffer (2M NaCl, 3 mM MgCl2, 20 mM Tris-HCl, and 8% v/v PEG8000) to collect the mRNA capture beads. Reverse transcription was conducted at 52°C using Maxima H Minus Reverse Transcriptase (ThermoFisher), and excess primers were removed with an Exonuclease I digestion (New England Biolabs). Whole transcriptome amplification (WTA) was achieved via PCR using KAPA Hifi PCR Mastermix (Kapa Biosystems). The WTA product was purified using Agencourt Ampure beads (Beckman Coulter). For sequencing, dual-indexed 3' DGE libraries were prepared using Nextera XT (Illumina) and sequenced to depth on the NovaseqS4 platform with a paired-end read structure (R1: 20 bases; I1: 8 bases; I2: 8 bases; R2: 50 bases) using custom sequencing primers. Transcript reads were tagged for cell barcode and UMI utilizing DropSeqTools v1.12 (Macosko et al., 2015). These tagged sequencing reads were subsequently aligned to the *Macaca fascicularis* v5 genome (https://useast.ensembl.org/Macaca_fascicularis/Info/Index) using the Dropseq-tools pipeline on the Terra platform (app.terra.bio). By collapsing the aligned reads based on barcode and UMI sequences, we derived digital gene expression matrices for each array, covering 10,000 barcodes.

QUANTIFICATION AND STATISTICAL ANALYSIS

Statistical analysis on macaque samples (depletion and CFU)

Test for normality was conducted with a Shapiro-Wilk test. For assessment of depletion over time, mixed effects model with Dunnett's multiple comparison test adjusted for the comparison of IgG vs anti-CD4 and IgG vs naïve. For pre- and post-PET data, two-way ANOVA with Bonferroni multiple comparisons test. For paired analyses, Wilcoxon matched-pairs signed rank

tests were used. For comparison of three groups (IgG vs naïve and IgG vs αCD4), either one-way ANOVA with Dunnett's multiple comparisons or Kruskal-Wallis with Dunn's multiple comparisons were used dependent on normality.

Data processing and quality control

For individual granuloma, collapsed gene expression matrices containing 10,000 barcodes were subject to CellBender to estimate the fraction of ambient RNA contaminating cell transcriptomes. The CellBender "remove-background" function was then applied using default parameters. Individual CellBender "corrected" matrices were then subject to Scrublet, using default parameters, to identify putative doublets. Transcriptomes with a doublet_score >0.30 were removed from downstream analyses. Sample-specific gene expression matrices were then combined and analyzed using Scanpy (version 1.8.2). Transcriptomes were filtered using min_genes > 300, min_counts>500, mitochondrial_threshold=0.05, and genes expressed in fewer than 10 cells were removed. Gene expression counts were normalized using default Scanpy parameters (i.e., $\log_2$(TP10K+1)).

Dimensionality reduction and batch correction

Following preliminary filtering processes, we performed coarse-level cell type clustering and iterative sub-clustering to annotate cell types and identify low-quality transcriptomes (e.g., doublets) not identified or removed during preliminary quality control processing, respectively. The top 2,000 highly-variable genes – identified using the Scanpy "highly_variable_genes function" – were used for dimensionality reduction. Following variable gene selection, these data were subject to scaling, principal component analysis (PCA), integration to mitigate sample-specific batch effects, and Leiden-based clustering. More specifically, data were scaled to 10, and the top 19 principal components (PCs) were used for dimensionality reduction. PCs were used to construct a neighborhood graph using the scanpy.pp.neighbors function, setting n_neighbors=40 and using the top 19 PCs. Leiden-based clustering was then implemented, setting the resolution= 1.0, which identified 26 distinct clusters.

Cell clustering and annotation

From these 26 clusters we identified 14 coarse cell types. The Leiden resolution=1.0 failed to distinguish between several cell types (e.g., cDCs 1 and pDCs; alveolar type-1 and alveolar type 2 cells). As a result, these preliminary coarse-level cell types were not used as the final reference but instead used to inform sub-clustering. All coarse-level cell types (e.g., T, NK cells, macrophages) were subject to sub-clustering to remove low-quality cells. Transcriptomes classified as doublets featured elevated expression of genes derived from distinct cell ontologies. These doublets were excluded from downstream analyses.

Following quality control processing, our data set comprised 88,360 high-quality transcriptomes, which were annotated as 15 distinct cell types, including: alveolar type-1 cells, alveolar type 2 cells, B cells, ciliated cells, endothelial cells, eosinophils, fibroblasts, macrophages, mast cells, neutrophils, plasma cells, T, NK cells, cDCs 1, cDCs 2, and pDCs. Among cDCs 1, cDCs 2, pDCs, and plasma cells additionally subset diversity was not found, as such these coarse-level annotations are equivalent to cellular subsets. The major cell populations alveolar type-1 cells, alveolar type 2 cells, B cells, ciliated cells, endothelial cells, eosinophils, fibroblasts, macrophages, mast cells, neutrophils, and T, NK cells underwent further sub-clustering to discern cellular subtypes. Sub-clustering resolution was determined by selecting the most stable/robust silhouette score that uncovered biologically relevant and/or known cell subsets (e.g., Tregs).

Differential abundance analysis of scRNA-seq cell type and subset frequencies

To identify differential cell type frequencies across naïve, IgG, and αCD4 granuloma, we implemented three distinct statistical frameworks: (1) scCODA, (2) the Mann-Whitney U-test, and (3) Fischer's exact test.

One inherent challenge in scRNA-seq data is the compositional nature of cell proportions – they are not mutually exclusive. Illustratively, the elevation of one cell subset's proportion inherently diminishes the proportions of others due to the requirement that all proportions sum to one (e.g., antibody-mediated $CD4^+$ T cell depletion results in elevated frequencies of $CD8A^+$ T cells among T, NK cells). To address these limitations, we implemented scCODA, a statistical framework rooted in a Bayesian hierarchical model, which is adept at dissecting cell type co-dependencies and the low inputs typically associated with scRNA-seq data, thus ensuring that observed shifts in cell type or subset frequencies are biologically significant. In addition to

scCODA, we employed the Mann-Whitney U-test and Fischer's exact test. Differentially abundant cell types and subset had to be identified as significant by at least two of the aforementioned methods.

Differential expression analysis

Pairwise (i.e., naïve vs IgG; αCD4 vs IgG) differential expression (DE) analyses were conducted using MAST, on log2(TP10K+1) normalized gene expression data (Finak et al., 2015; Kotliar et al., 2020); **Figures 4, 5, 6**). The covariates mitochondrial reads and number of genes we included when performing DE.

Pseudobulk differential expression analysis

To robustly identify DE genes among cell subsets, we performed pseudobulk DE analysis. For cell subsets of interest, we generated pseudobulk counts from scRNA-seq gene expression matrices. Psuedobulk counts and associated metadata (e.g., sample, NHP identity) were imported into R and subject to DE analysis using the DESeq2 package. DE was performed using the Wald statistical test and highlighted genes where selected using the threshold pvalue<0.05 and $\log_2(|\text{fold change}|)>0.3785$.

Differential cell-cell and receptor-ligand analyses

To discern putative differential cell-cell interactions from our scRNA-seq dataset, we adopted MultiNicheNet. Distinct from conventional interaction cell-cell interaction methods, MultiNicheNet can identify differential, context-dependent cellular communications, leveraging 'pseudobulk' profiles from scRNA-seq data.

Using MultiNicheNet, we assessed the interaction strength between cell types and identified putative differential cell-cell and ligand-receptor (L-R) pairs – derived from MultiNicheNet's 50 top-prioritized links (i.e., top 50 predictions across contrasts, senders, and receivers). To highlight highly interconnected cellular populations, we focused on the top 10 (five per experimental group) – as identified in MultiNicheNet's 50 top-prioritized links – differential interactions per experimental group. To identify cellular subsets underlying differential coarse-level cell-cell L-R among reinfection granulomas (IgG vs naïve, and IgG vs αCD4), we removed all nonimmune cell subsets to identify putative "senders" and "receiver" subsets modulating

immune tone in the reinfection granuloma. The top 50 prioritized links among all *IL10*+ T, NK cell sender subsets were queried to identify putative receivers (among all immune cell subsets). The same strategy was employed in determining putative receivers of neutrophil- and monocyte-senders. Interaction matrices were visualized in Python.

FIGURE LEGENDS

Figure 1. Experimental design. (A) Overview of cynomolgus macaque sample processing for clinical, microbiologic, and immunologic data (created with BioRender.com). **(B)** PET-CT scan of representative NHPs pre- and post-HRZE treatment. Old granulomas shown with blue arrows; new granulomas shown with green arrows. Left panel: IgG; middle panel: αCD4; right panel: naïve. **(C)** Fraction of CD3 expressing the cell surface marker CD4 post-antibody infusion in peripheral blood. Median and range shown (****, $p<0.0001$; mixed-effects model with Dunnett's multiple comparisons test). **(D)** $CD3^+$, $CD4^+$ cells derived from TB granulomas. **(E)** $CD3^+$, $CD4^+$ cells from uninvolved lung tissue from *Mtb* infected macaques. **(F)** $CD3^+$, $CD4^+$ cells from the spleen of *Mtb* infected macaques **(G)** $CD3^+$, $CD4^+$ cells from CFU^+ LNs of *Mtb* infected macaques. (D-G) Transparent smaller dots represent granulomas, colored by animal. Larger dots represent mean per animal and lines represent medians. One-way ANOVA with Dunnett's multiple comparisons test.

Figure 2. Reinfection with *Mtb* reduces granuloma formation, as well as bacterial burden and dissemination in a $CD4^+$ T cell dependent manner

(A) Number of new granulomas identified using PET-CT following infection with *Mtb* library S. Lines represent medians. One-way ANOVA with Dunnett's multiple comparison test, adjusted p-values reported. **(B)** Median number of viable *Mtb* colony forming units (CFU) per macaque (Kruskal-Wallis with Dunn's multiple correction). Solid dots represent the median CFU per animal; lines represent medians. Transparent dots represent the median CFU of individual granulomas. **(C)** Median number of chromosomal equivalents (CEQ) per macaque (Kruskal-Wallis with Dunn's multiple correction). Solid dots represent the median CFU per animal; lines represent medians. Transparent dots represent the median CFU of individual granulomas. **(D)** CFU:CEQ ratio, a proxy for bactericidal activity (Kruskal-Wallis with Dunn's multiple correction). Solid dots represent the median CFU per animal; lines represent medians.

Transparent dots represent the median CFU of individual granulomas. **(E)** Total CFU from granuloma, uninvolved lung tissue, and thoracic lymph nodes tissue. **(F)** Lung CFU from granuloma and uninvolved lung tissue. **(G)** Thoracic lymph node CFU. (E – G) Lines represent medians. One-way ANOVA with Dunnett's multiple comparisons test. **(H)** Individual granuloma *Mtb* CFU. Individual dots represent single granuloma subject to Seq-Well S^3 scRNA-seq (Mann-Whitney U Test). **(I)** Fraction of tissues (lymph node, spleen, lung) sharing library S barcodes (Kruskal Wallis with Dunn's multiple comparison test).

Figure 3. Cellular remodeling of the TB granuloma microenvironment following *Mtb* reinfection. (A) UMAP embedding of Seq-Well S^3 derived granuloma transcriptomes colored by coarse cell type. **(B)** Coarse cell type frequencies colored by experimental group. Individual dots represent single granuloma. Differentially abundant IgG vs naïve (purple) and IgG vs αCD4 (green) marked with colored square. Cell types are differentially abundant if significant using two of three methods: Mann-Whitney U test; scCODA Bayesian model, and Fishers exact test. **(C)** Fraction of granuloma T, NK cells expressing *CD4* from Seq-Well S^3 derived transcriptomes (Mann-Whitney U Test). **(D)** Fraction of granuloma T, NK cells expressing *CD8A* from Seq-Well S^3 derived transcriptomes (Mann-Whitney U Test).

Figure 4. $CD4^+$ T cells regulate T cell cellularity, cytokine flux, and immune tone in in the TB granulomas following *Mtb* reinfection. (A) UMAP embedding depicting T, NK cell subpopulations identified by sub-clustering. **(B)** Heatmap depicts gene expression levels (mean z-score) of T cell lineage markers *CD4, CD8A,* and *CD8B*. Columns represent gene expression in individual NHP groups – Naïve (light blue), IgG (yellow), αCD4 (red). Bar plot of T, NK subpopulation frequencies among all granuloma cellular subpopulations colored by experimental group. Differentially abundant IgG vs naïve (purple) and IgG vs αCD4 (green) marked with colored square. Cell types are differentially abundant if significant using two of three methods: Mann-Whitney U test; scCODA Bayesian model, and Fishers exact test. **(C-D)** T, NK cell pseudobulk Log_2CPM for naïve (light blue), IgG (yellow), and αCD4 (red) NHP granulomas (*** $p<0.001$,** $p<0.01$, *$p<0.05$; Wilcoxon rank-sum test). Heatmap depicting $log_{10}FC$ of lineage markers, cytolytic molecules, select transcription factors, immunoregulatory molecules, and chemokines, and cytokines (rows) for each cell type (columns) in NHP granulomas IgG vs

naïve (C) or IgG vs αCD4 lesions (D). White circles indicate >$\log_{10}$|1.3| fold change, relative to naïve or αCD4 granulomas. Black rectangles indicate 0.05 FDR and >$\log_{10}$|1.3| fold change, relative to naïve or αCD4 granulomas.

Figure 5. Attenuated type-1 immunity among monocyte-derived transcriptomes in *Mtb* reinfection granulomas. (A) UMAP embedding depicting Monocyte-derived cell identified by sub-clustering. UMAP embeddings depicting Monocyte-derived cell subpopulation densities, split by NHP cohort **(B)** Bar plot of Monocyte-derived progenitor frequencies, among all granuloma cell subpopulations, colored by experimental group. Individual dots represent single granuloma. Differentially abundant IgG vs naïve (purple) and IgG vs αCD4 (green) marked with colored square. Cell types are differentially abundant if significant using two of three methods: Mann-Whitney U test; scCODA Bayesian model, and Fishers exact test. **(C, D)** Enriched pathways from identified using differentially expressed genes (Mann-Whitney U test (Wilcoxon rank-sum) (p value<0.05)) from naïve, IgG, and αCD4 Sizes. Circles size represent to the number of genes in Hallmark Geneset, and color (Red-Blue) represents the geneset enrichment score. Genesets that are "up" (x-axis) are enriched among IgG granulomas, whereas "down" genesets are enriched among naïve **(C)** and αCD4 **(D)** granulomas, respectively. **(E-F)** Monocyte-derived pseudobulk Log_2CPM for naïve (light blue), IgG (yellow), and αCD4 (red) NHP granulomas (*** p<0.001, ** p<0.01, *p<0.05; Wilcoxn rank-sum test). Heatmap depicting $\log_{10}$FC of select transcription factors, immunoregulatory molecules, and chemokines, and cytokines (rows) for each cell type (columns) in NHP granulomas IgG vs naïve (E) or IgG vs αCD4 lesions (F). White circles indicate >$\log_{10}$|1.3| fold change, relative to naïve or αCD4 granulomas. Black rectangles indicate 0.05 FDR and >$\log_{10}$|1.3| fold change, relative to naïve or αCD4 granulomas.

Figure 6. Neutrophil heterogeneity in the TB granuloma. (A) UMAP embedding depicting neutrophil cell subpopulations identified by sub-clustering **(B)** Bar plot of neutrophil subset frequencies, among all granuloma cell subpopulations, colored by experimental group. Individual dots represent single granuloma. Differentially abundant IgG vs naïve (purple) and IgG vs αCD4 (green) marked with colored square. Cell types are differentially abundant if significant using two of three methods: Mann-Whitney U test; scCODA Bayesian model, and

Fishers exact test. **(C)** Volcano plot depicting pseudobulk differential gene expression (DESeq2) *ICAM1*^{hi}, *NBN*^{hi} vs , *SORL1*^{hi}, *CFD*^{hi} neutrophils (for all NHP experimental groups). Volcano plot x-axis indicates the log_2FC and y-axis indicates the -log10(pvalue). Vertical dashed lines represent log_2FC threshold >|1.3|. Horizontal line indicates -log10(pvalue)>|0.05| threshold. **(D-E)** Neutrophil pseudobulk Log_2CPM for naïve (light blue), IgG (yellow), and αCD4 (red) NHP granulomas (*** p<0.001,** p<0.01, *p<0.05; Wilcoxon rank-sum test). Heatmap depicting log_{10}FC of select transcription factors, immunoregulatory molecules, and chemokines, and cytokines (rows) for each cell type (columns) in NHP granulomas IgG vs naïve (D) or IgG vs αCD4 lesions (E). White circles indicate >log_{10}|1.3| fold change, relative to naïve or αCD4 granuloma. Black rectangles indicate 0.05 FDR and >log_{10}|1.3| fold change, relative to naïve or αCD4 granulomas. **(F)** Violin plots of IFN-inducible neutrophil module scores, split by NHP group. Significance by Mann-Whitney U test.

Figure 7. Differential cell-cell interactions in immunologically primed granulomas. (A) **(A)** Heatmap depiction of differential (naïve vs IgG) cell-cell interaction pairs among coarse cell types. Columns represent cell-cell interactions from the top-prioritized links – "sender" ligands and receptors differential L-R pairs specific to IgG or naïve granulomas. Heat map and dot size represent L-R interactions from the 50 top-prioritized links. Black rectangles indicate the top 5 interactions, based on number of interactions between two cell types, per NHP group. Green rectangles depict putative T, NK-T, NK interactions. **(B)** Cartoon depiction of (A) with differential L-R (i.e., top-prioritized linkages) specific to naïve granulomas. **(C)** Barplot depiction of differential cell-cell interactions among naïve granulomas. Left barplot depicts *IL10*$^{+}$sender cellular subpopulations; right barplot represents *IL10RA/RB*$^{+}$ cell subpopulations. Receptor-ligand and inferred interaction pairs are derived from the top 200 top-prioritized linkages. **(D)** Similar heatmap to that of (A), highlighting linkages specific to IgG (vs naïve) granulomas. **(E)** Schematic representation of the differential L-R pairs unique to IgG granulomas from (D). **(F)** Barplot representation of differential *IL10-IL10RA/RB* interactions among IgG lesions, similar to that of (C). **(G)** Heatmap of αCD4 (vs IgG) granulomas**.** **(H)** Schematic representation of the differential L-R pairs unique to αCD4 granulomas from (G). **(I)** Heatmap of IgG (vs αCD4) granulomas. **(J)** Schematic representation of the differential

L-R pairs unique to IgG granulomas from (I). **(K)** Barplot representation of differential *IL10-IL10RA/RB* interactions among IgG lesions, similar to that of (C).

SUPPLEMENTAL FIGURE LEGENDS

Figure S1. Cellular frequencies across anatomic compartments, related to Figure 1. (A) Total lung FDG activity pre- and post-HRZE drug treatment. Two-way ANOVA with Bonferroni's multiple comparisons test. Dots with connected lines represent individual animals. **(B)** Absolute counts (count/uL) of $CD4^+$ T cells, $CD8^+$ T cells, $CD20^+$ B cells, monocytes, and neutrophils post-antibody infusion in peripheral blood. Median and range shown; mixed-effects model with Dunnett's multiple comparisons test (** $p<0.01$, ***, $p<0.001$, **** $p<0.0001$). **(C)** Fraction of $CD3^+$, $CD4^+$ cells from peripheral lymph nodes resected pre- and post-Ab infusion. Dots with connected lines represent individual animals. Wilcoxon matched-pairs signed rank test. **(D)** Absolute counts (count/μL) of $CD4^+$ T cells in new granuloma, uninvolved lung, CFU^+ and CFU^- thoracic lymph nodes, peripheral lymph nodes, and spleen. **(E)** Absolute counts (count/μL) of $CD8^+$ T cells in new granuloma, uninvolved lung, CFU^+ and CFU^- thoracic lymph nodes, peripheral lymph nodes, and spleen. **(F)** Absolute counts (count/μL) of $CD20^+$ B cells in new granuloma, uninvolved lung, CFU^+ and CFU^- thoracic lymph nodes, peripheral lymph nodes, and spleen. **(G)** Fraction of $CD3^+$, $CD4^+$ cells from CFU^- thoracic lymph nodes resected at necropsy. One-way ANOVA with Dunnett's multiple comparisons test. (D-F) Transparent smaller dots represent granulomas, colored by animal. Larger dots represent mean per animal and lines represent medians. Kruskal-Wallis with Dunn's multiple comparisons test adjusted p-values reported.

Figure S2. *Mtb* CFU, CEQ, CFU:CEQ, and dissemination, related to Figure 2. (A) CEQ (left), and CFU (right). Individual dots represent individual TB granulomas. Linkages depict CEQ and CFU within the same lesion. Wilcoxon matched-pairs signed rank test. **(B)** *Mtb* CFU per granuloma. Integers on the x-axis represent an individual macaque. Colored dots are individual granuloma. Lines represent median per animal. **(C)** *Mtb* CEQ per granuloma. Integers on the x-axis represent an individual macaque. Colored dots are individual granuloma. **(D)** CFU:CEQ per granuloma. Integers on the x-axis represent an individual macaque. Colored dots are individual granuloma. Lines represent median per animal. **(E-G)** Circos plots depicting *Mtb*

strains shared between anatomical sites in naïve (E), reinfected (F) or reinfected with CD4 depletion (G) animals. Individual circos plots represent a single macaque, labeled with their study ID. In the plots, each wedge represents a distinct tissue site that was sampled and/or sequenced for barcodes. There are three tracks in each plot. The outer ring defines tissue samples as being from lungs (red), thoracic lymph nodes (blue) or distal extrapulmonary sites (green). Lighter shades represent tissues that were plated for *Mtb* but were sterile. The middle ring represents lesions that were detected by PET-CT during primary infection with the first *Mtb* library ('old lesion'), new lesions detected by PET-CT after re-infection ('new lesion'), or new lesions (as defined by Library S barcode sequencing) that were also found at sites where old lesions had previously formed (detected by PET-CT). The innermost ring represents distinct barcodes found in each tissue, where each unique barcoded *Mtb* strain (from the secondary *Mtb* library) is given a different color. Tissues that share the same *Mtb* strain by sequencing are linked by ribbons. Lung tissues are further grouped by lobe, abbreviated as follows: RUL, right upper lobe; RML, right middle lobe; RLL, right lower lobe; LUL, left upper lobe; LML, left middle lobe; LLL, left lower lobe; Acc, accessory lobe.

Figure S3. Coarse-level cell types and T, NK cell diversity in the TB granuloma, related to Figures 3, 4. (A) Heatmap depicting gene expression profiles (mean z-score) of coarse cell-type markers. Marker genes are depicted on the x-axis, and coarse-cell types on the y-axis. **(B)** Coarse-level cell type frequencies in the TB granuloma (naïve (left), IgG (middle), αCD4 (right)). Individual bars represent a single TB granuloma profiled using Seq-Well S^3. **(C)** Heatmap depicting gene expression profiles (mean z-score) of T,NK subpopulation markers, as well as select transcription factors, cytokine and chemokine receptors, co-inhibitory and co-activation markers. **(D)** T, NK cell pseudobulk Log_2CPM for naïve (light blue), IgG (yellow), and αCD4 (red) NHP granulomas (*** $p<0.001$,** $p<0.01$, *$p<0.05$; Wilcoxon rank-sum test). Heatmap depicting $log_{10}FC$ of lineage markers, cytolytic molecules, select transcription factors, immunoregulatory molecules, and chemokines, and cytokines (rows) for each cell type (columns). White circles indicate $>log_{10}|1.3|$ fold change, relative to naïve or αCD4 granulomas. Black rectangles indicate 0.05 FDR and $>log_{10}|1.3|$ fold change, relative to naïve or αCD4 granulomas. **(F)** Number of differentially expressed genes among T, NK cell subpopulations with 0.05 FDR< and $>log_{10}|1.3|$ fold change, naïve (light blue), IgG (yellow), and αCD4 (red).

Figure S4. Monocyte-derived gene programming and neutrophil heterogeneity, related to Figures 5, 6. (A) Heatmap depicting gene expression profiles (mean z-score) of monocyte-derived subpopulation markers. **(B)** Number of differentially expressed genes among monocyte-derived subpopulations with 0.05 FDR< and >$\log_{10}$|1.3| fold change, naïve (light blue), IgG (yellow), and αCD4 (red). **(C-D)** Monocyte-derived pseudobulk Log_2CPM for naïve (light blue), IgG (yellow), and αCD4 (red) NHP granulomas (*** p<0.001,** p<0.01, *p<0.05; Wilcoxon rank-sum test). Heatmap depicting $\log_{10}$FC of select chemokines and cytokines, bacterial response genes (Yao et al., 2018), adipogenesis, and reactive oxygen species (rows) for each cell type (columns) in NHP granulomas, IgG vs naïve (C) or IgG vs αCD4 lesions (D). White circles indicate >$\log_{10}$|1.3| fold change, relative to naïve or αCD4 granulomas. Black rectangles indicate 0.05 FDR and >$\log_{10}$|1.3| fold change, relative to naïve or αCD4 granulomas. **(E)** Heatmap depicting neutrophil subpopulation marker gene expression profiles (mean z-score). **(F)** Number of differentially expressed genes among neutrophil subpopulations with 0.05 FDR< and >$\log_{10}$|1.3| fold change, naïve (light blue), IgG (yellow), and αCD4 (red).

Figure S5. Cell-cell and ligand-receptor interactions during *Mtb* reinfection, related to Figure 7. (A) Circos plot depicting differential network interactions among coarse-level cell type annotations in naïve granulomas (naïve vs IgG). Ribbon arrows indicate directionality (sender to receiver) populations. The outer edge color among senders denotes the sender cell type, with the inner edge color representing the receiver cell type. Circos plot depicts the 50 top-prioritized linkages. **(B)** Differential cell-cell interactions among IgG lesions (IgG vs naïve). **(C)** Heatmap depicting type 1 interferon ligand-activity among coarse cell types. **(D)** Heatmap (left) depiction of scaled ligand-receptor expression among the top 50 prioritized linkages among T, NK cells from IgG granulomas, relative to naïve. Columns represent individual granulomas. Heatmap split by NHP group. Heatmaps (right) are representations of the scaled ligand activity among putative receiver populations. **(E)** Heatmap similar to (D) but depicting the top 50 prioritized linkages among all coarse-level cell types. **(F)** Circos plot showing differential network interactions among immune cell subpopulations in naïve granulomas (naïve vs IgG). Top 100 prioritized linkages are plotted. **(G)** Differential cell-cell interactions among all immune cell subpopulations IgG vs naïve. **(H)** Differential cell-cell interactions among αCD4 lesions (αCD4 vs

IgG). **(I)** Differential cell-cell interactions among IgG lesions (IgG vs αCD4). **(J)** Heatmap depicting type 1 interferon ligand-activity among coarse cell types, IgG vs αCD4. **(K)** Heatmap similar to (D) but displaying the top 50 prioritized linkages among T, NK cells from IgG granulomas, relative to αCD4. **(L)** Heatmap similar to (D) but depicting the top 50 prioritized linkages among all coarsely annotated cell types from IgG granulomas relative to αCD4. **(M)** Circos plot depicting differential network interactions among immune cell subpopulations in αCD4 granulomas (αCD4vs IgG). Top 100 prioritized linkages are plotted. **(N)** Differential cell-cell interactions among all immune cell subpopulations IgG vs αCD4.

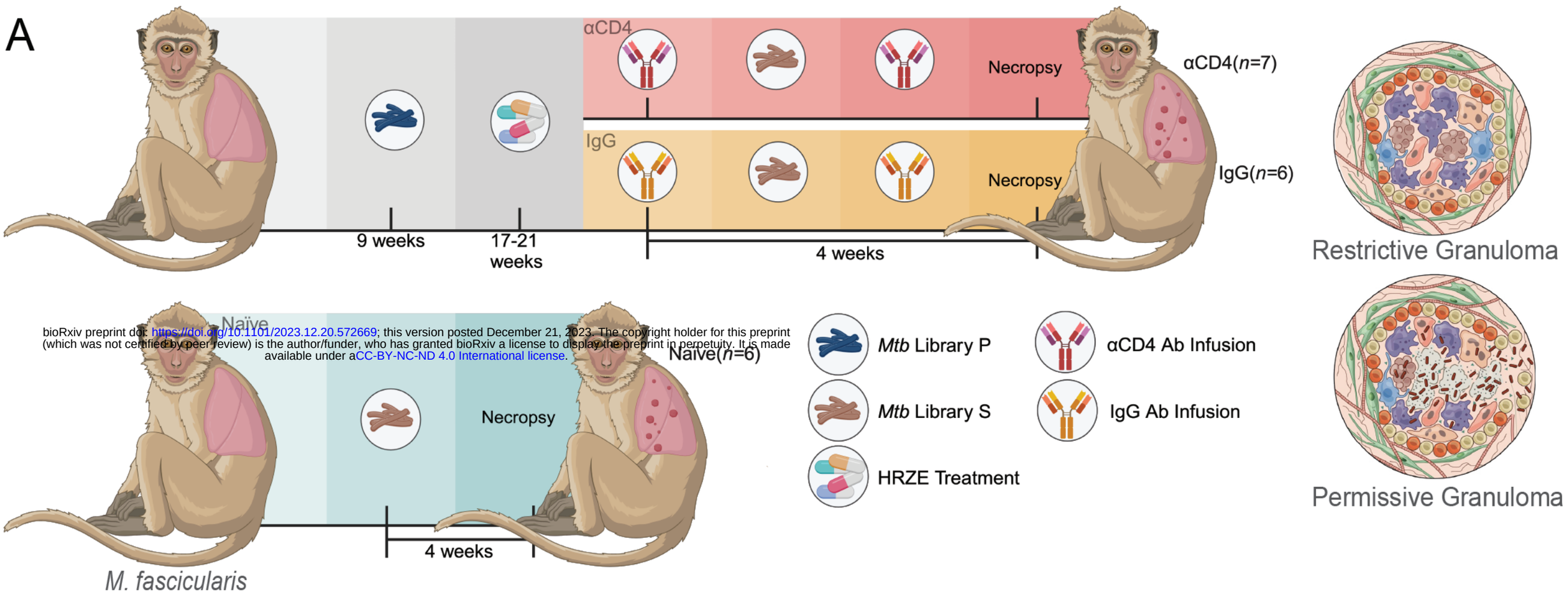

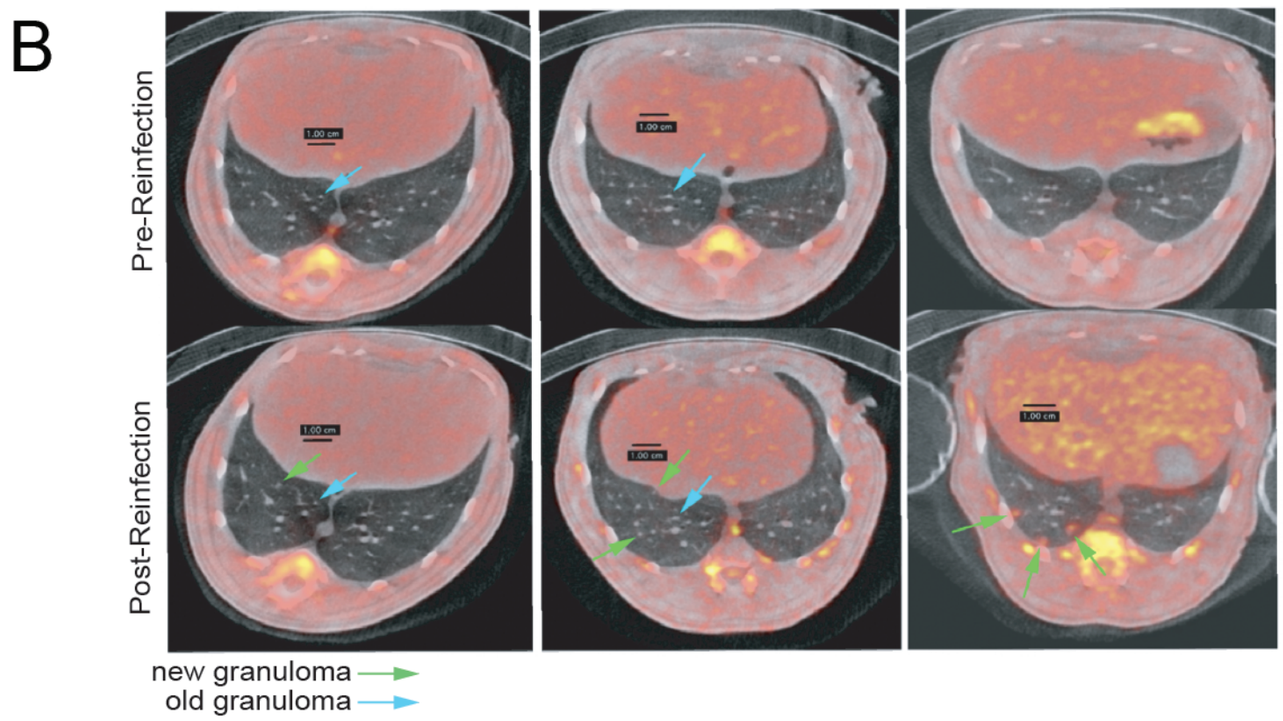

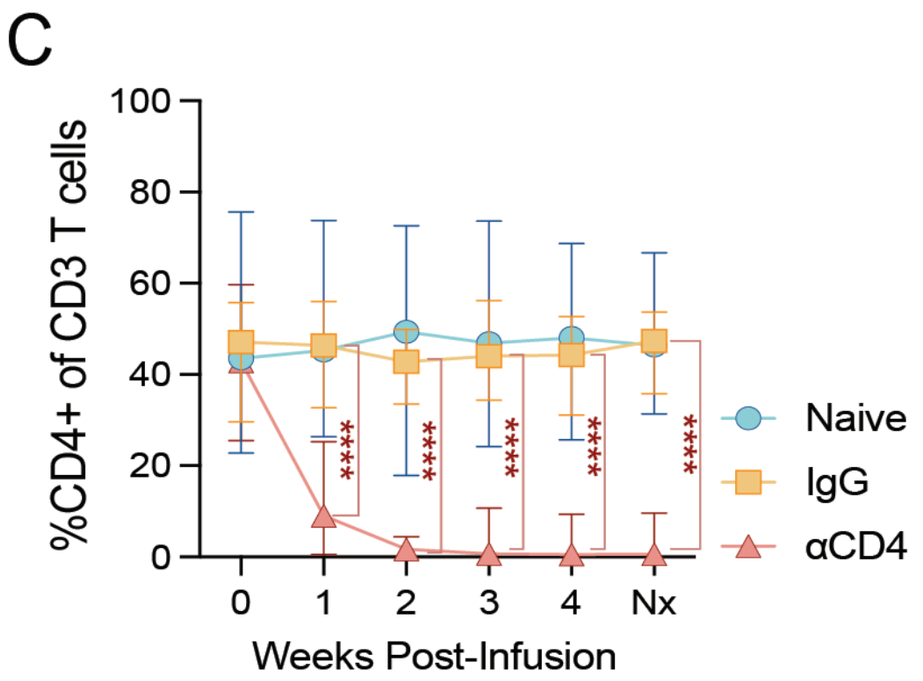

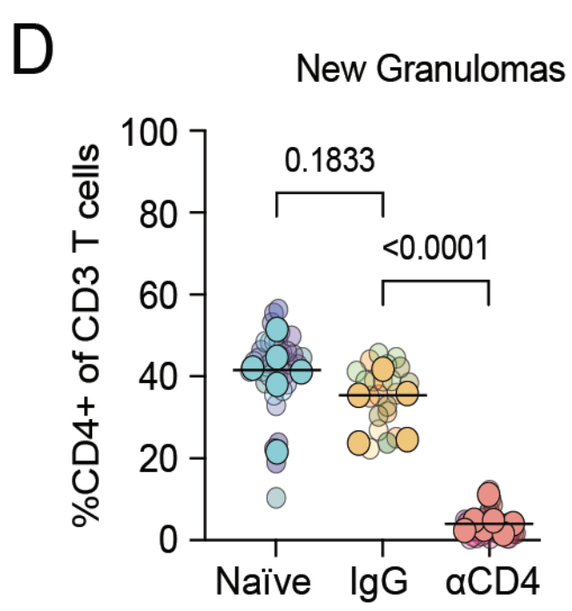

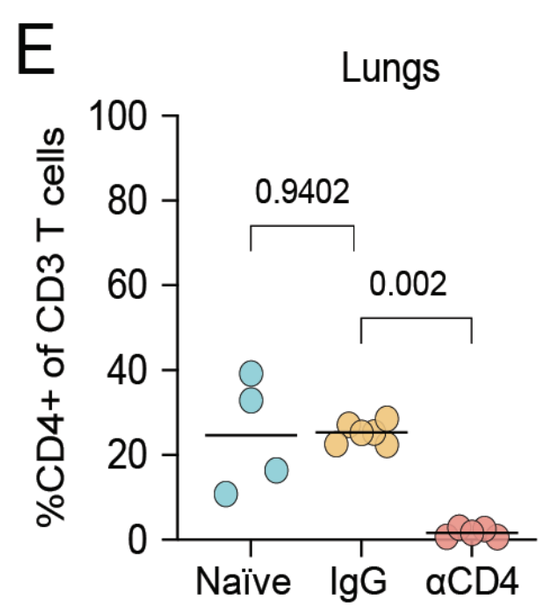

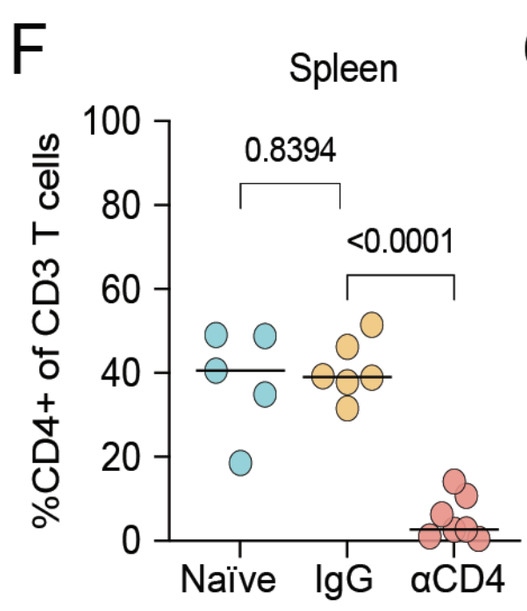

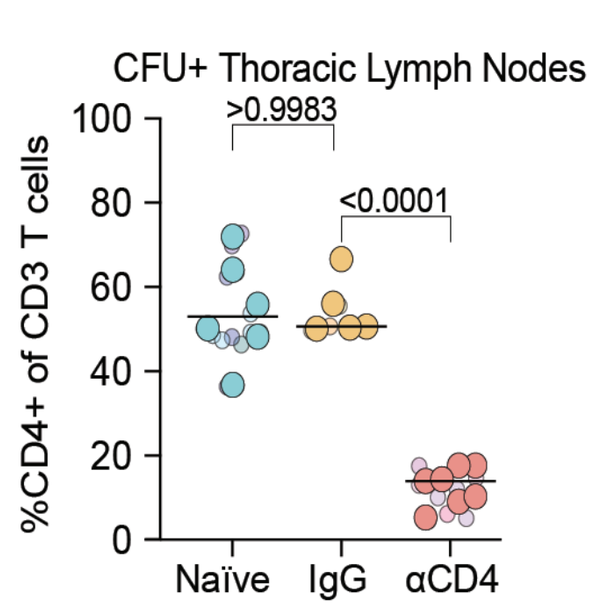

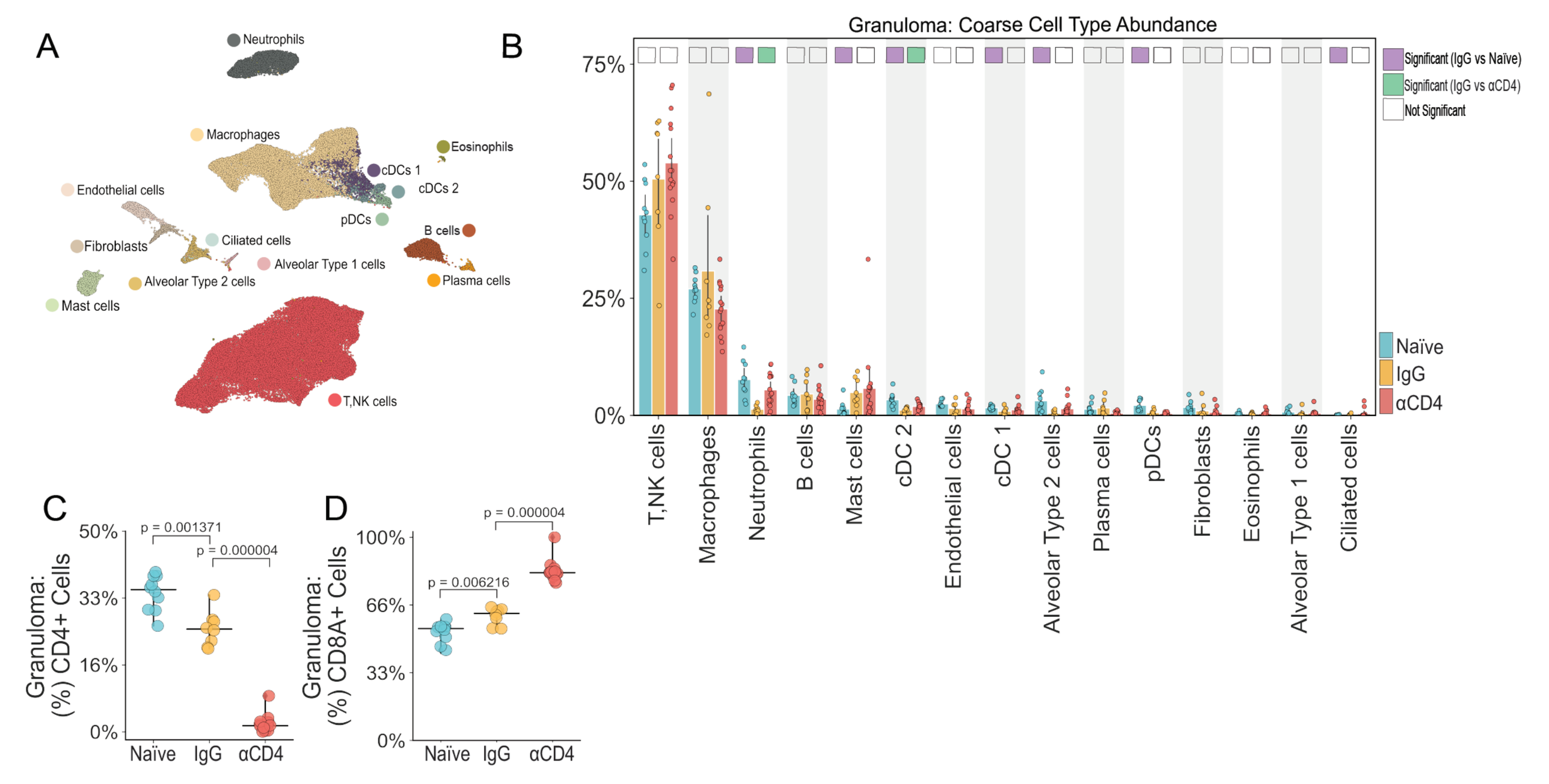
A
Neutrophils
Macrophages
Eosinophils
cDCs 1
cDCs 2
Endothelial cells
pDCs
B cells
Fibroblasts
Ciliated cells
Alveolar Type 1 cells
Alveolar Type 2 cells
Plasma cells
Mast cells
T,NK cells
B
Granuloma: Coarse Cell Type Abundance
75%
50%
25%
0%
Significant (IgG vs Naïve)
Significant (IgG vs αCD4)
Not Significant
Naïve
IgG
αCD4
T,NK cells
Macrophages
Neutrophils
B cells
Mast cells
cDC 2
Endothelial cells
cDC 1
Alveolar Type 2 cells
Plasma cells
pDCs
Fibroblasts
Eosinophils
Alveolar Type 1 cells
Ciliated cells
C
Granuloma: (%) CD4+ Cells
50%
33%
16%
0%
p = 0.001371
p = 0.000004
Naïve
IgG
αCD4
D
Granuloma: (%) CD8A+ Cells
100%
66%
33%
0%
p = 0.000004
p = 0.006216
Naïve
IgG
αCD4

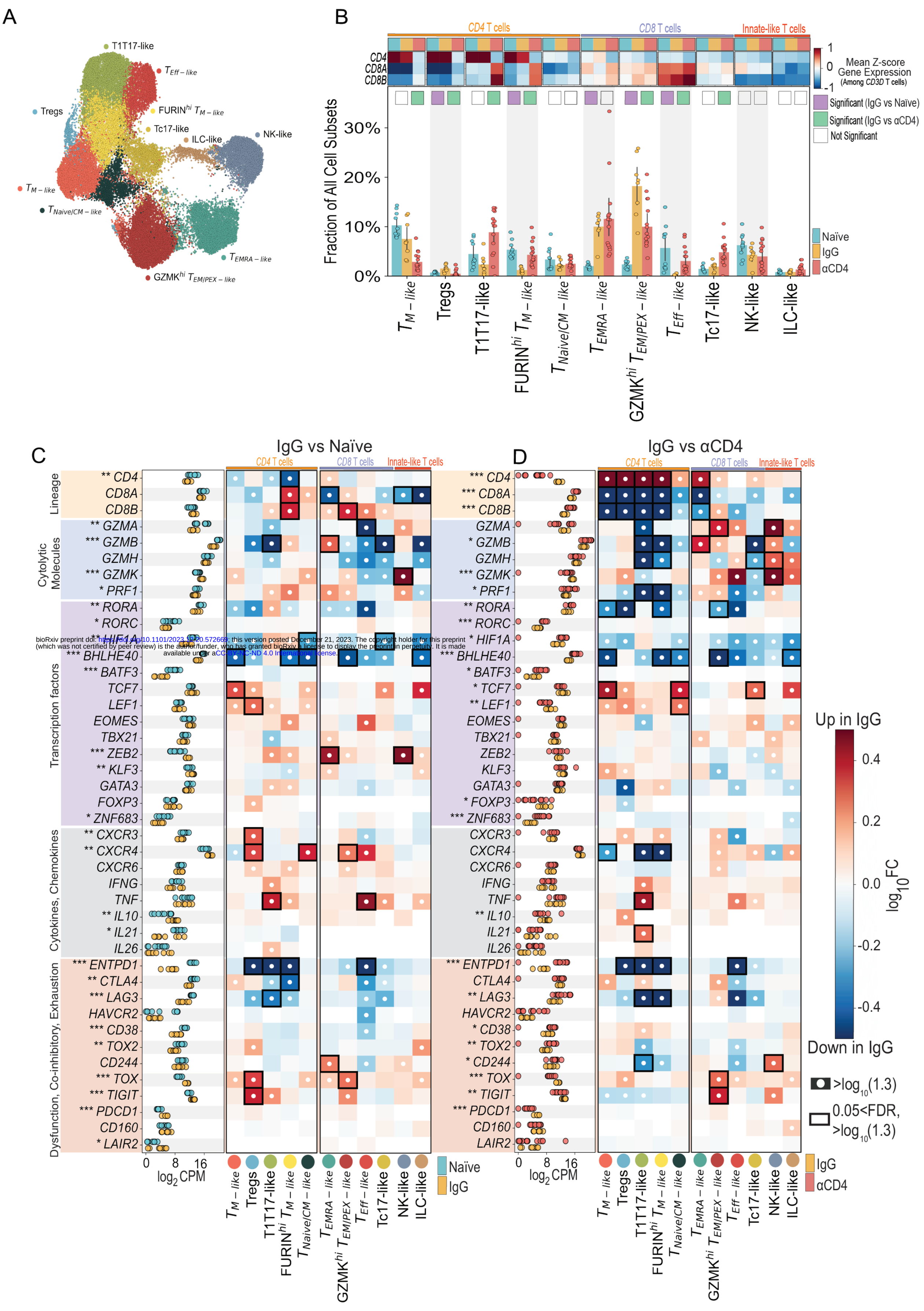

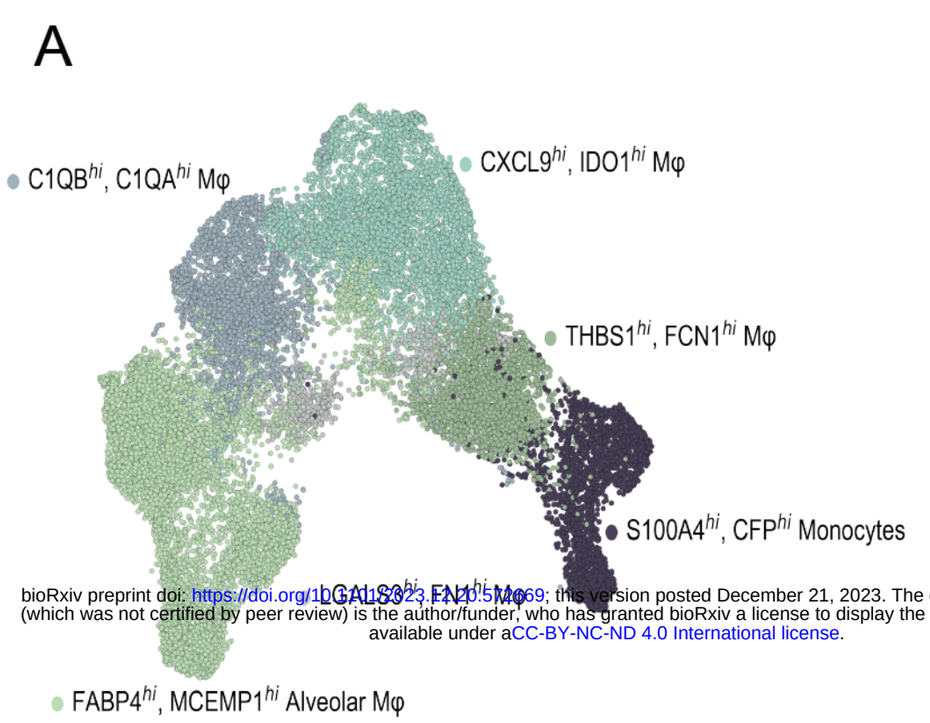

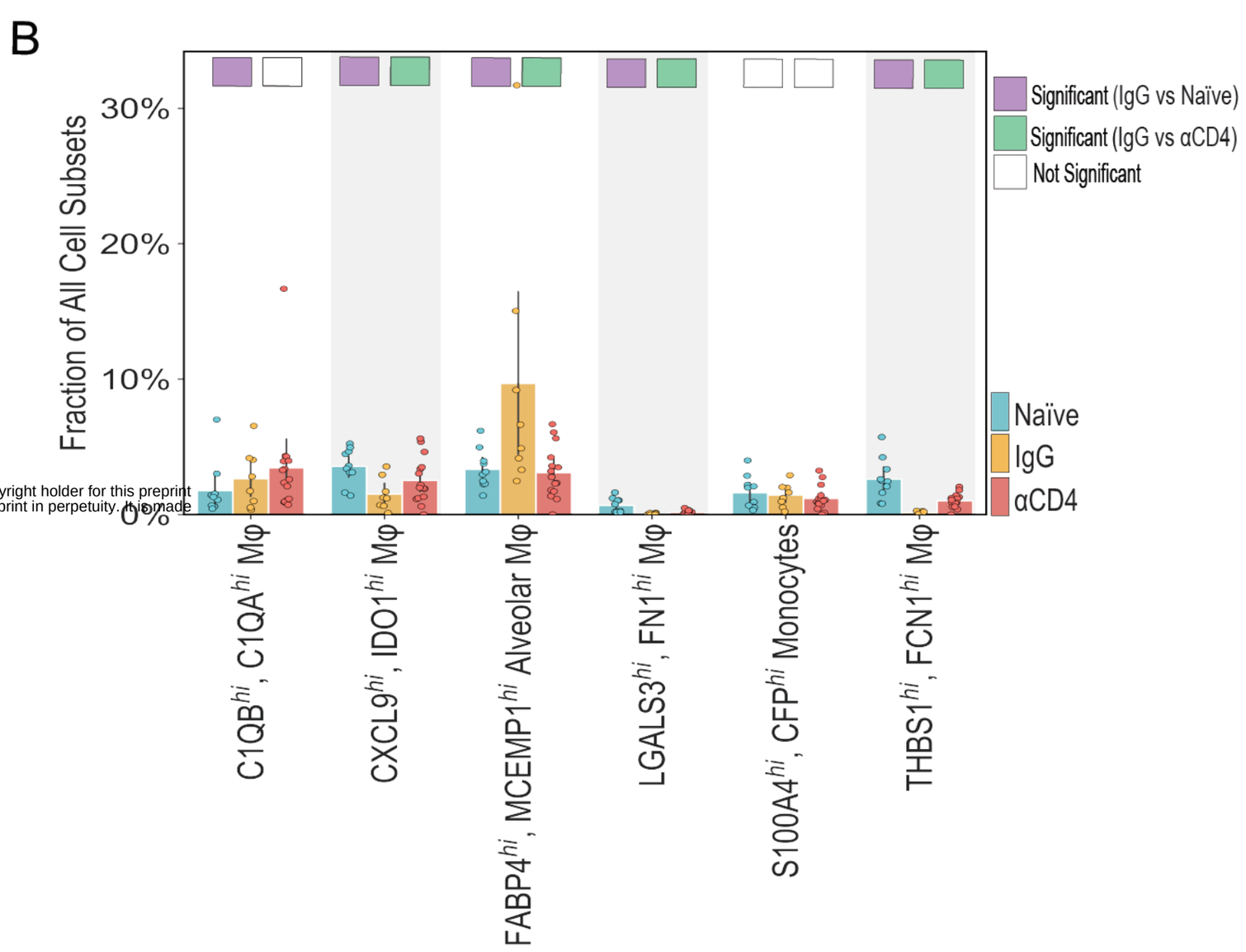

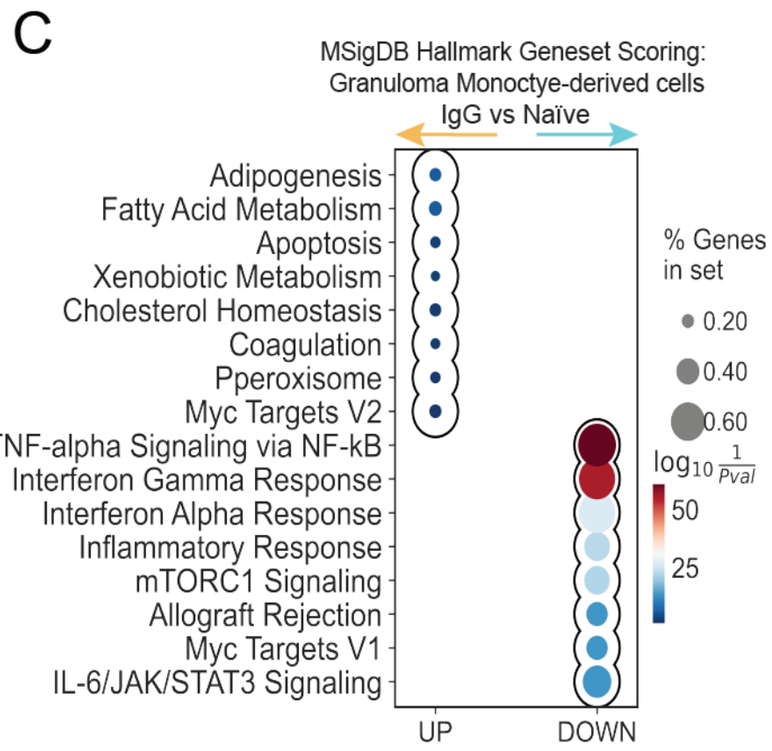

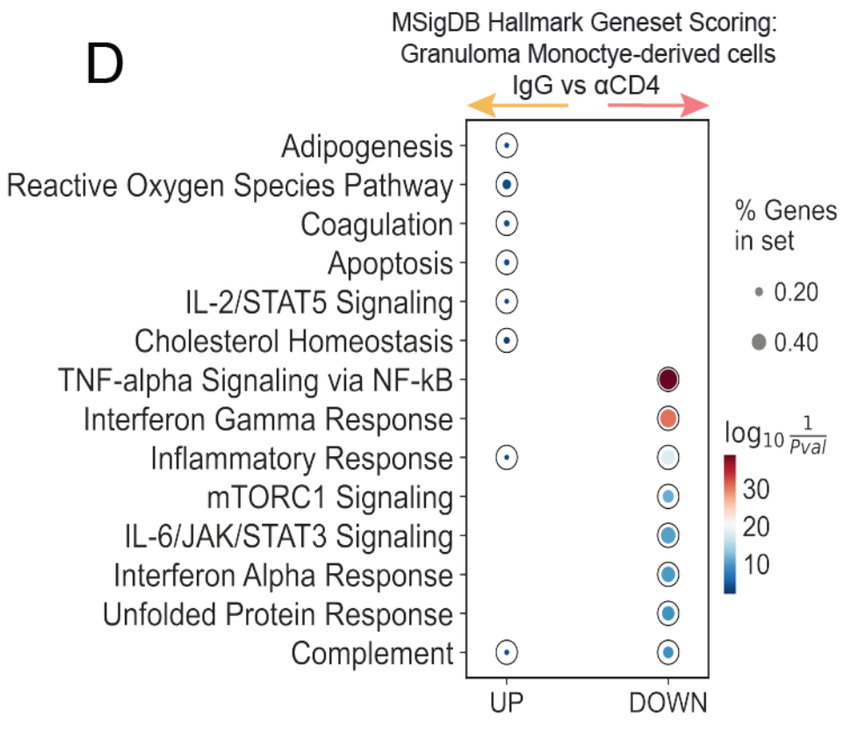

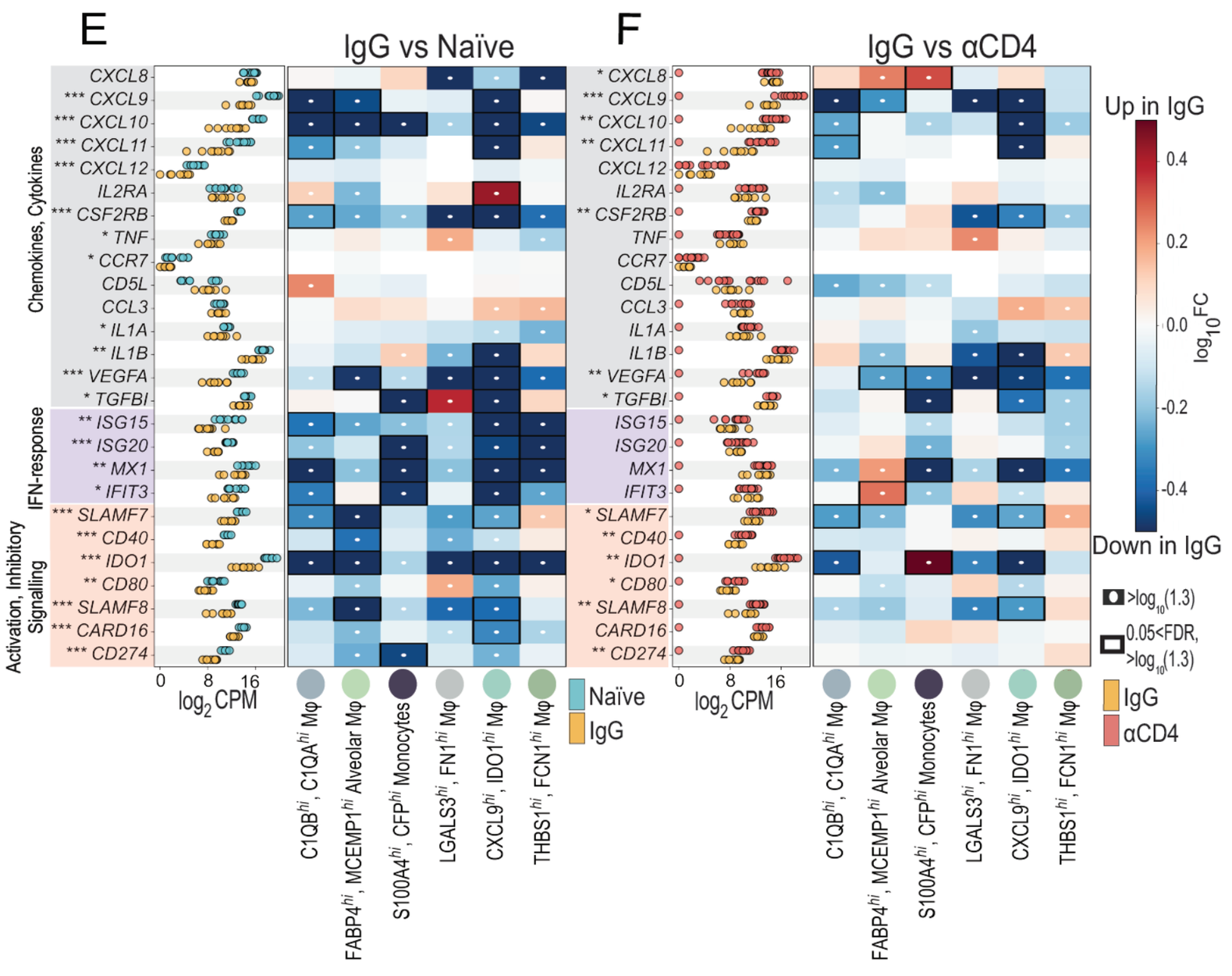

A

● SORL1^{hi}, CFD^{hi} Neutrophils
● ICAM1^{hi}, NBN^{hi} Neutrophils

B

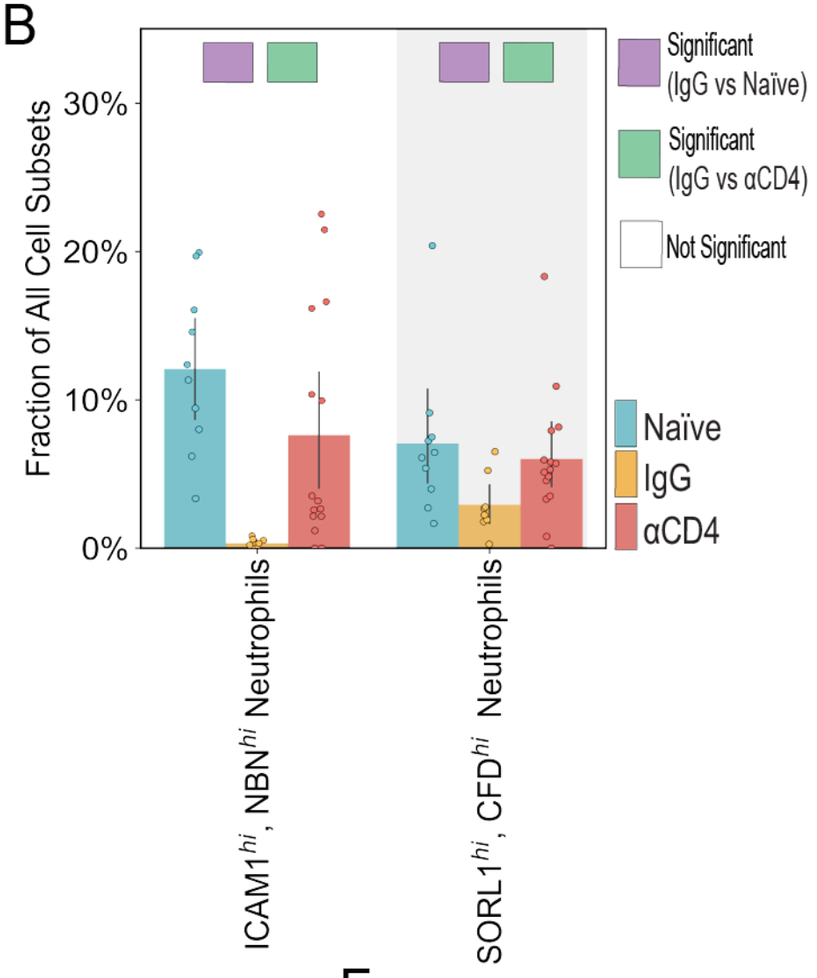

C

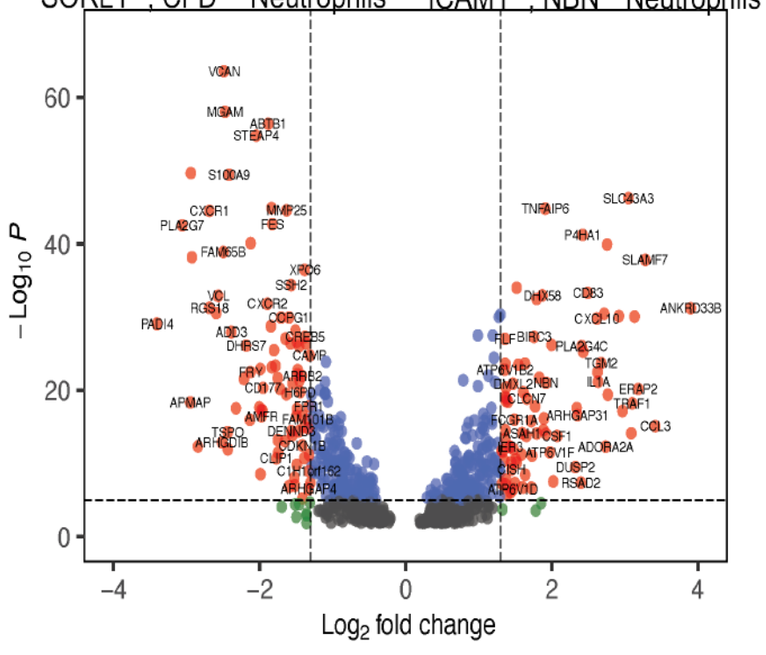

D

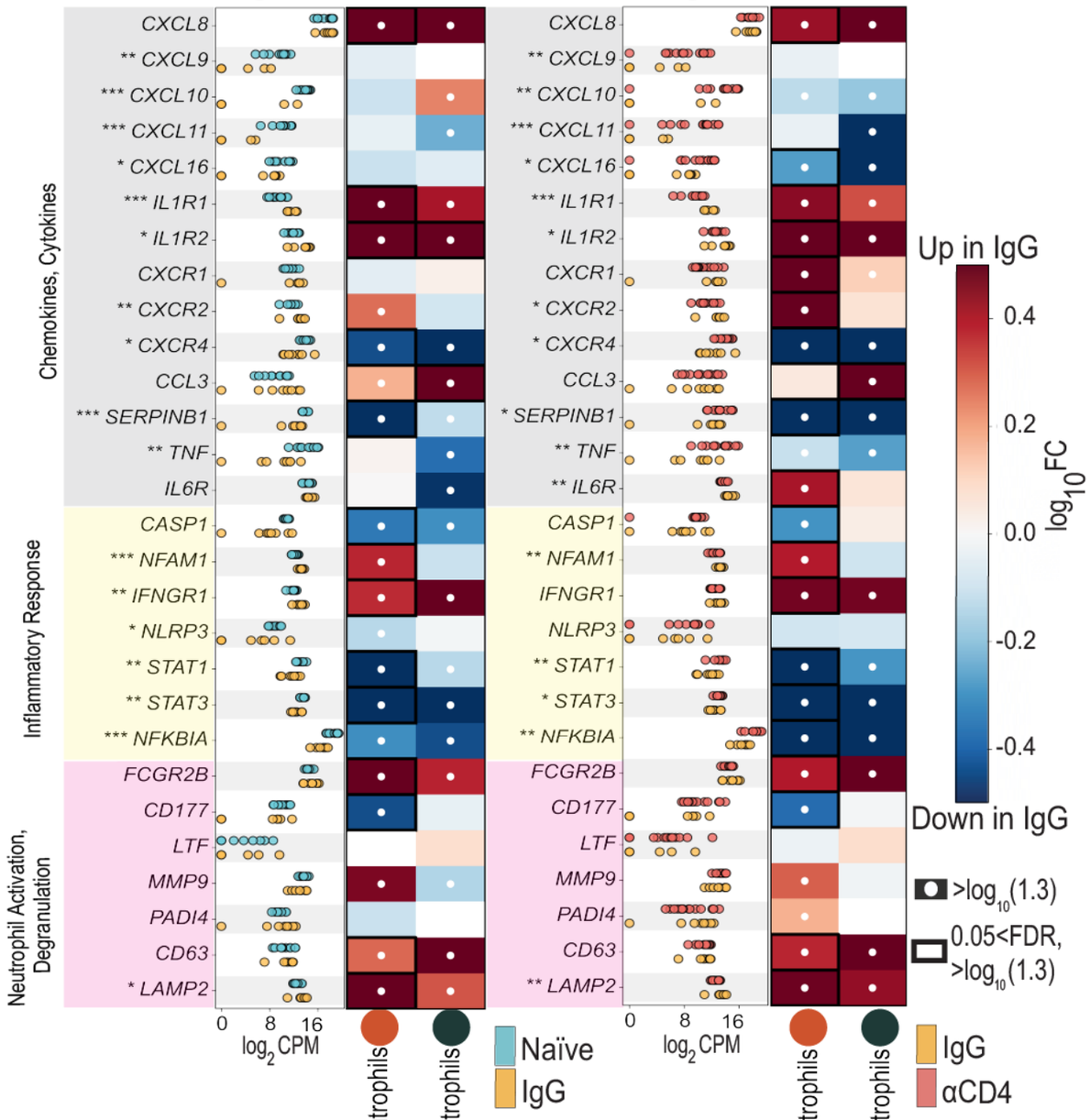

F

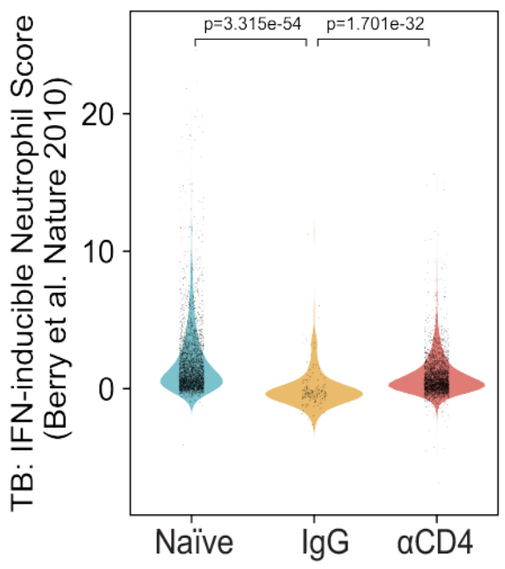

Cell-Cell Interactions (IgG vs Naïve)

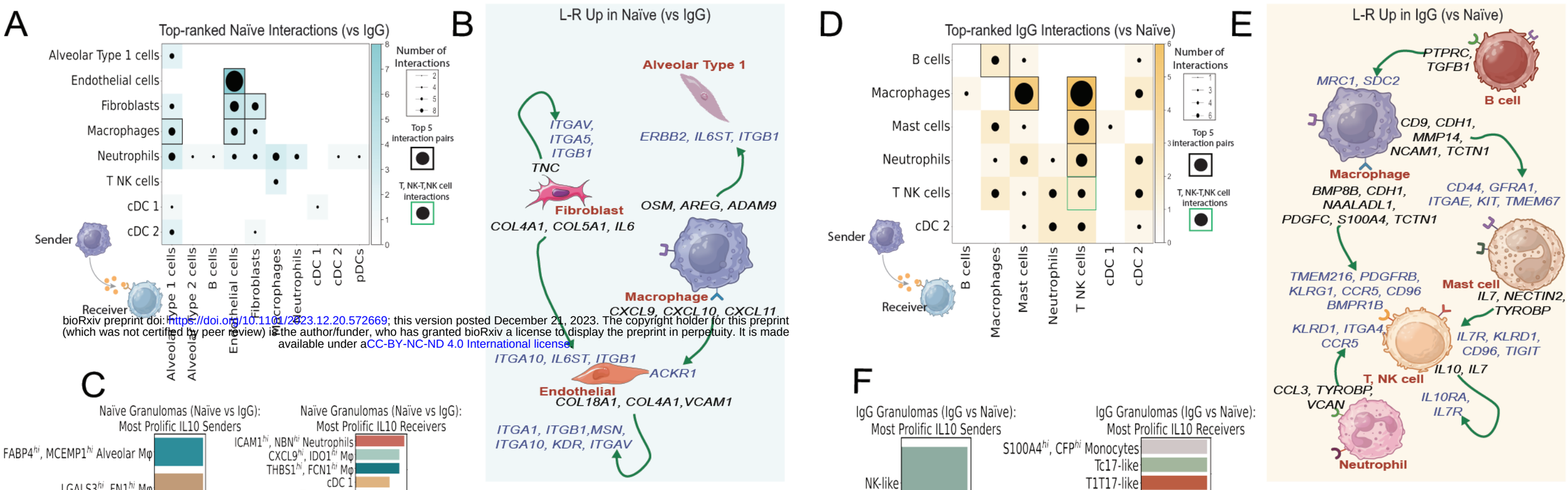

Cell-Cell Interactions (IgG vs αCD4)